FUNCTIONAL ANALYSIS OF THE SEX RELATED GENE *DMRT1* IN *XENOPUS*

MECHANISTIC INVESTIGATION OF THE SEX RELATED GENE *DMRT1* IN AFRICAN CLAWED FROGS (*XENOPUS*) EVIDENCES BOTH NEOFUNCTIONALIZATION AND SUBFUNCTIONALIZATION

By LINDSEY KUKOLY, HONOURS B.Sc.

A Thesis Submitted to the School of Graduate Studies in Partial Fulfilment of the Requirements for the Degree of Master of Science

McMaster University MASTERS OF SCIENCE (2023) Hamilton, Ontario (Biology)

TITLE: Mechanistic investigation of the sex related gene *dmrt1* in African clawed frogs (*Xenopus*) evidences both neofunctionalization and subfunctionalization

AUTHOR: Lindsey Kukoly (McMaster University)

SUPERVISOR: Dr. Ben Evans NUMBER OF PAGES: ix, 99

Lay abstract

In many species sexual differentiation is a crucial developmental event. Surprisingly, however, the systems orchestrating sexual differentiation are highly variable among species. The *doublesex* and *mab-3* related transcription factor 1 (*dmrt1*) gene plays a role in sexual differentiation in many groups, but its specific roles in this process are incompletely characterized and potentially diverse. We used genetic engineering in two species of African clawed frog (*Xenopus*) to disable function of *dmrt1* in order to explore effects on gonadal development and the development of secondary sex characteristics. We found that *dmrt1* is required for normal ovary or testis development in both *Xenopus* species, and that functional divergence occurred following duplication of *dmrt1* by whole genome duplication. Taken together, these findings identify previously uncharacterized roles of *dmrt1* in *Xenopus* and provide evidence of dynamic functional evolution of this important gene.

Abstract

Sex determination is a key developmental process in several species regulated by sex-related transcription factors. In many species a gene called *doublesex and mab-3 related transcription factor 1* (*dmrt1*), plays an important role in sexual differentiation. I used African clawed frogs (*Xenopus*) to examine function of *dmrt1* in two species: a diploid species, *X. tropicalis,* and an allotetraploid species, *X. laevis*. In both species, *dmrt1* is an autosomal gene; *Xenopus tropicalis* has one copy of *dmrt1* and *X. laevis* has two homeologous copies that by definition are derived from whole genome duplication: *dmrt1.L* and *dmrt1.S* in *X. laevis*. We generated knockouts of each of these genes to further examine their function in sexual differentiation. Histological examination showed testicular dysgenesis in *X. tropicalis dmrt1* and *X. laevis dmrt1.L* null males whereas *dmrt1.S* null males presented no obvious difference in sperm density compared to wildtype males. *X. tropicalis dmrt1* and *X. laevis dmrt1.L* null females were found to completely lack reproductive organs and are infertile whereas *dmrt1.S* null females appeared unaffected. The contrasting results between *dmrt1.L* and *dmrt1.S* in *X. laevis* provides evidence of both neofunctionalization and subfunctionalization following gene duplication and suggest that gene duplication is a major contributor to evolutionary change.

Additional investigation of the transcriptome of these frogs and the role of *dmrt1* in the secondary sex characteristic vocalization provides further evidence of the role of *dmrt1* in development. Comprehensively, this investigation provides further knowledge of the role of *dmrt1* and homeologs of this gene in sexual differentiation and introduces a novel aspect of this gene in female development. Future efforts are focused on generating double knockouts for *dmrt1.L* and *dmrt1.S,* further examining the role of *dmrt1.S* in somatic cell function and developing additional mutant lines in other *Xenopus* for comparative analysis.

Acknowledgements

I would like to start by thanking my friends and family for their continuous support, not only throughout my Master's degree, but along the entire journey that has led me to where I am today. I would like to thank my parents for their support and assistance through the countless reports my mom would proofread, and by listening to me give the same presentation over and over again. Even if they did not always understand what I was talking about, I know they were paying attention as when my dad's crossword puzzle clue read "African clawed frog", he immediately knew the answer was *Xenopus*.

I would also like to thank my lab mates Tharindu Premachandra, Jianlong Zhu, Emmanuela Anele and Martin Knytl for all the help and learning opportunities they gave me as well as all the laughs we shared together in lab. Thank you to Tharindu for teaching me various lab techniques at the start of my program and for always being there to help me troubleshoot when things go wrong. Thank you to Jianlong for helping me out when I would become frustrated because I could not get R to do what I wanted it to. Thank you to Emmanuela for giving me the opportunity to learn new things about frog parasites that I never expected would be a topic with so many interesting components. I will always remember the excitement we shared every time we got a new frog to dissect, hoping something cool would crawl out of it.

Next, I would like to thank my committee members Dr. Ian Dworkin and Dr. Joanna Wilson for always providing new insights and ideas of how to improve my research. Thank you to Dr. Dworkin for helping my take my histological analysis to the next level, first by training me to use your microscope to take high resolution images of my tissues and by teaching me how to complete computational analysis for these images.

I would also like to give a tremendous thanks to my supervisor, Dr. Ben Evans for giving me this educational opportunity and allowing me to achieve the next step towards the career goals I have been dreaming of since I first started to learn about Biology. Thank you, Dr. Evans, for the continuous support you gave me throughout this program. For teaching me so many different skills and techniques that I know will stick with me throughout my career. Thank you for being the first to teach be the importance of bioinformatics and for taking so much time to walk me through the steps of these analyses. Bioinformatics and coding are not things that come very easily to me, and I am incredibly grateful for your help and patience as I started to learn them. In addition, thank you for always encouraging me to take part in opportunities outside of the lab. As someone who was always a little nervous about standing in front of a room full of people and sharing my work, your encouragement has allowed me to take part in amazing experiences such as travelling to give a talk at one of the largest evolution conferences in the world, an experience that I will never forget. Overall, this program has been such an amazing opportunity that has allowed me to grow in so many ways, and the two years I have spent here will always remain close to my heart.

Finally, I would like to acknowledge everyone who made this research possible. Marko Horb, Sarah Burton, Danielle Jordan, Nikko-Ideen Shaidani, William Thomas and the staff at the National *Xenopus* Resource (NXR), Carl Anderson, Leanna Herrick and Jacek Kwiecien have each been essential in the completion of this research and I am incredibly thankful of their assistance and contributions.

Contents

Lay Abstract iii
Abstract iv
Acknowledgments v
List of Abbreviations viii
Declaration of Academic Achievement ix

1 Chapter 1 1
1 Introduction 1
1.1 Sex determining systems 1
1.2 Triggers for sex determination 1
1.3 Other conserved components of sex-determining pathways 2
1.4 Sex determination in *Xenopus* 2
1.5 Gene duplication 3
1.6 Testes anatomy and histology 4
1.7 Secondary sex characteristics 4
2 Materials and Methods 5
2.1 *Xenopus laevis* and *Xenopus tropicalis* knockout lines 5
2.2 Phenotypic analysis 5
i) Internal anatomy and histology 5
ii) Fertility 7
iii) Gene expression in the developing gonad 8
iv) Vocalizations 9
3 Results 10
3.1 Sex and genotypes 10
3.2 Gonadal histology 11
3.3 Fertility 12
3.4 RNAseq analysis 12
3.5 Impact on laryngeal morphology and function 13
4 Discussion 14
4.1 Sex reversal 14
4.2 Gonadal development and fertility 15
4.3 Transcriptome analysis 16
4.4 Subfunctionalization and neofunctionalization 17
4.5 Secondary sexual differentiation 18
5 Conclusion 18
6 Figures 20
7 Supplementary Information 31

List of Figures and Tables

1	Testis histology imaged at 10X and 40X.	20
2	Key stages of development from oocyte to tadpole.	20
3	Sanger sequences of *X. laevis dmrt1.S* from individuals with the following genotypes: wildtype, homozygous null, and heterozygous.	21
4	Sanger sequences of *X. laevis dmrt1.L* from individuals with the following genotypes: wildtype, homozygous null, and heterozygous.	21
5	Sanger sequences of *X. tropicalis* dmrt*1* from individuals with the following genotypes: wildtype, homozygous null, and heterozygous.	22
6	Example female-specific amplifications of individuals from the *dmrt1.L* line.	22
7	Testis histology of *X. laevis* wildtype and *dmrt1.L* heterozygous individuals.	23
8	Testis histology from a wildtype male and a stage-matched *dmrt1.S* knockout male.	23
9	Testis histology from a wildtype male and a stage-matched *dmrt1.L* knockout male.	24
10	Microscopy of sperm cells taken at 40X with phase contrast for *X. laevis* wildtype and *dmrt1.L* null individuals.	24
11	Testis histology from *X. tropicalis* wildtype and *dmrt1* null individuals.	25
12	Proportions of whitespace in testis histological cross sections.	25
13	Body cavity of *X. tropicalis* females that are wildtype or *dmrt1* knockout.	26
14	Venn diagrams illustrating the results of the EdgeR analysis using STAR counts data.	27
15	Results of the transcriptome masculinization analysis using EdgeR with STAR counts data.	28
16	Larynx histology of a wildtype male, a *dmrt1.S* null male, and a *dmrt1.L* null male.	29
17	Larynx histology of a wildtype female, a *dmrt1.S* null female, and a *dmrt1.L* null female.	29
18	Inter-click intervals (ICI) coloured by each individual.	30
S1	Summary of histological findings for *dmrt1.S* and *dmrt1.L* null males.	31
S2	Testis histology from each null male tested compared to a wildtype male.	31
S3	Results of the thresholding checks comparing three different threshold values.	32
S4	Significantly differentially expressed transcripts in the mesonephros/gonad.	33
S5	Gene ontology analysis of differentially expressed genes in the developing gonads.	65
S6	"Functional dissection and assembly of a small, newly evolved, female-specific genomic region of the W chromosome of the African clawed frog *Xenopus laevis*" Cauret et al. submitted to PLOS Genetics July 19th, 2023.	68
S7	Additional research on androgen-receptor null frogs.	92

List of Abbreviations

DGE differential gene expression

Dmrt1 *doublesex* and *mab-3*-related transcription factor 1

DNA deoxyribonucleic acid

GO gene ontology

hCG human chorionic gonadotropin

NA numerical aperture

PCR polymerase chain reaction

PMSG pregnant mare serum gonadotropin

RNAseq ribonucleic acid sequencing

X. laevis *Xenopus laevis*

X. tropicalis *Xenopus tropicalis*

Declaration of Academic Achievement

I, Lindsey Kukoly, declare this thesis and the work presented within it as my own. This thesis is an original report of the research I have completed during my Master of Science degree unless otherwise indicated by citations. The work in this document entitled "Mechanistic investigation of the sex related gene *dmrt1* in African clawed frogs (*Xenopus*) evidences both neofunctionalization and subfunctionalization" has not been submitted for publication or to any other academic institution.

Additional work that I have completed is detailed in supplementary sections 5&6. This includes the paper "Functional dissection and assembly of a small, newly evolved, female-specific genomic region of the W chromosome of the African clawed frog *Xenopus laevis*" by Cauret et al. submitted for publication in PLOS Genetics on July 19th, 2023.

My work includes original research I completed under Dr. Ben Evans' supervision with assistance from my committee members Dr. Ian Dworkin and Dr. Joanna Wilson, as well as the staff at the National *Xenopus* Resource (NXR) in Woodshole, Massachusetts. Additionally, the results and figures pertaining to the transcriptome analysis portion of this thesis were generated by Dr. Ben Evans.

The research presented in this thesis will be developed into a manuscript for submission to be published in a peer-reviewed journal in the future.

Chapter 1

1 Introduction

1.1 Sex determining systems

Sexual differentiation is a key aspect of development of anisogamous species, i.e., species with two differently sized gametes. In these species, sexual differentiation results in the formation of (usually) two sexes, with the sex with the larger gamete generally considered to be female. The development of different sex phenotypes is generally achieved even though most of the genome (the autosomes) are shared between the sexes, which highlights the pivotal roles of sex-specific triggers for sex determination and sex-specific regulation of autosomal loci. Despite the shared outcome of this process, the systems that trigger sex are often quite variable, including between closely related species. Sexual differentiation can be divided into gonadal, or primary sexual differentiation, and non-gonadal, or secondary sexual differentiation. Examples of secondary sex characteristics include facial hair in human males, differences in male and female plumage in birds, and the presence or absence of horns or antlers in other species (Owens & Short, 1995).

1.2 Triggers for sex determination

In mammals, including humans, the XX/XY system of sex determination occurs where the males are the heterogametic sex (XY). However, this is not the only sex determining system that exists in nature. In order to fully understand these sex determining systems and how they evolved, it is important to investigate the mechanisms that regulate this process. In placental and marsupial mammals, there is a male-specific gene on the Y chromosome called sex-determining region Y protein (*SRY*) that triggers male development (Koopman et al., 1991; Sinclair et al., 1990). Studies conducted in mice have attributed this role of *SRY* to interactions with the autosomal *Sox9* gene, which is known to play a vital role in testis development as it drives the production of the Sertoli cells (Koopman et al., 1991; Sekido & Lovell-Badge, 2009). This role of *SRY* in the development of the testes suggests that *SRY* is crucial in the differentiation of a male individual and without this transcription factor, female primary sexual differentiation is triggered. But this gene is absent in monotremes and sex-differences in dosage of an X-linked gene called *doublesex* and *mab-3*-related transcription factor 1 (*dmrt1*) likely triggers sexual differentiation (Alam et al., 2018; El-Mogharbel et al., 2007; Maier et al., 2021; Veyrunes et al., 2008) and this may also be the way sex is determined in birds (Ioannidis et al., 2021; C. Raymond, 1999; Smith et al., 2003). Only a handful of triggers for sex determination have been identified in other vertebrate species (Kubiak et al., 2020; Nagahama et al., 2021). In medaka fish (*Oryzias latipes*), a male-specific duplicate of *dmrt1* called *DMY* is the trigger for sex determination (Masuyama et al., 2012; Matsuda et al., 2002). However, in rainbow trout, a gene called *sdY* is required for testis differentiation and is the probable trigger for sex determination (Yano et al. 2012). Unlike many other triggers for sex determination that tend to be derived from

sex-related autosomal genes, *sdY* shares similarities with interferon 9 (Irf9) proteins which are involved in the immune response, and it is hypothesized that this gene evolved from a specific *irf9* paralog (Yano et al. 2012). Examples of such genes demonstrate the complexity of sex determining systems which makes this an important area of study for investigating the evolution of a species.

1.3 Other conserved components of sex-determining pathways

Along with the among species variation in triggers for sex determination, there is also variation in the genetic components and interactions that form the downstream pathways that orchestrate sexual determination. Usually, these pathways are driven by specific genes or transcription factors and many sex determining genes have conserved function, meaning they influence the same features or have similar genetic roles in a diversity of species (Reaume & Sokolowski, 2011). In vertebrates, *Sox9* has a broadly conserved involvement with development of specialized cells associated with sperm maturation called Sertoli cells (Da Silva et al., 1996). Likewise, anti-mullerian hormone (amh) and forkhead box protein L2 (*foxl2*) are typically involved with testis and ovarian development and function, respectively. The *Amh* gene has been identified as playing a major role in testis development as it is responsible for the regression of the Müllerian ducts which marks the start of male differentiation in vertebrates (Josso et al., 2001; Zhou et al., 2019). In comparison, mutations in *Wnt4* resulted in masculinization of females (Vainio et al., 1999) and knockouts of *foxl2* in mice were found to impact the maturation of the ovaries (Ottolenghi et al., 2007; Pisarska et al., 2011)

Another sex-related gene with broadly conserved functions that is studied here is the *doublesex* and *mab-3*-related transcription factor 1 (*dmrt1*) which exists in the DM binding domain and has been found to play a role in male differentiation across metazoans including humans and other mammals, birds, reptiles, nematodes, and insects (C. S. Raymond et al., 2000). Biological roles of *dmrt1* have been revealed in several species. In humans, *dmrt1* is located within the 9p chromosomes where deletions of this region resulted in 46,XY gonadal dysgenesis that can lead to partial sex reversal (Inui et al., 2017; C. Raymond, 1999; Veitia et al., 1997). In mice, *dmrt1* is considered necessary for the differentiation of the testis at later stages of development as a knockout of *dmrt1* resulted in improper differentiation of Sertoli and germ cells (Herpin & Schartl, 2011; Kim et al., 2007). In *Drosophila* fruit flies, sex-specific splicing of the *doublesex* gene triggers sexual differentiation based on the presence or absence of expression of a protein called transformer which also undergoes sex specific splicing (Rideout et al., 2010). In *Caenorhabditis* nematodes, the *dmrt1* ortholog of the *male abnormal* gene (*mab-3*) plays a major role in male differentiation through the prevention of expressing yolk proteins and regulating the morphology of tails in males (Shen & Hodgkin, 1988). The current knowledge of various sex determining genes and the species they are present in serves as a strong basis for further investigation of the sex determining systems working in other species.

1.4 Sex determination in Xenopus

The African Clawed Frog (*Xenopus laevis*) and other amphibian species use an entirely different sex determining system compared to mammals where females are the heterogametic sex (WZ) and males are homogametic (ZZ) (Chang & Witschi, 1956) and there is a female-specific gene/allele called *dm-w* (Yoshimoto et al., 2008). In these frogs, substantial variation in triggers

for sex-determination is evidenced by among species variation in (i) the presence or absence of *dm*-w, (ii) female-specificity of *dm-w*, and (iii) the genomic locations of the sex chromosomes which suggests that *dm-w* evolved from a duplication *dmrt1.S* but resides in the L subgenome. PCR-assays, capture sequencing, and whole genome sequencing indicate that *dm-w* evolved recently in an ancestor of 2n=4s=36 allotetraploid African clawed frogs in the subgenus *Xenopus* after divergence of subgenus Silurana, which includes the diploid species *X. tropicalis* (Bewick et al., 2011; Cauret et al., 2020). In *X. laevis* a DM-domain gene called *dm-w* is sex specific and resides on Chromosome 2L (Cauret et al., 2020; Yoshimoto et al., 2008). But this gene was then lost several times (Cauret et al., 2020), including in the allotetraploid *X. borealis* where Chromosome 8L are the sex chromosomes, at least in the population in east Kenya (Evans et al., 2022; Furman et al., 2018; Furman & Evans, 2016).The closely related species *X. tropicalis* lacks *dm-w* and instead determines sex using a combination of pairs of three different sex chromosomes – W, Y, and Z – where females have either WZ or WW chromosomes and males can have ZZ, ZY or WY chromosomes (Roco et al., 2015; Furman et al., 2020). The sex determining gene has not yet been identified in *X. tropicalis*. Divergence of *X. laevis* and *X. tropicalis* occurred approximately 48 million years ago (Session et al., 2016).

Current research has identified a few key factors that may play a role in the sex determining systems of *Xenopus* species. One transcription factor that is of particular interest is the *doublesex* and *mab-3*-related transcription factor 1 (*dmrt1*) which exists in all *Xenopus* species including *X. tropicalis* (Yoshimoto et al., 2006). This transcription factor exists in two copies in *X. laevis*, *dmrt1.L* and *dmrt1.S*. These two gene copies originally diverged as a result of a gene duplication event occurring approximately 34 million years ago (Session et al., 2016). Each of these homeologs have been identified as having a male biased expression due to their role in testis development (Yoshimoto et al., 2010).

1.5 Gene duplication

How might sex determination pathways evolve rapidly? One possibility is that gene or genome duplication are major catalysts for evolutionary change, because these processes are frequently associated with rapid functional evolution. In many cases, one of the gene copies will be lost (nonfunctionalization). However, both of the duplicated genes may also persist, and function of each individual copy may or may not acquire functional differences. One possible outcome is neofunctionalization where one of the gene copies holds the original gene function while the other develops an entirely different function after the occurrence of specific mutations (Birchler & Yang, 2022; Teshima & Innan, 2008; Voordeckers & Verstrepen, 2015). Another possible outcome is when the original function is divided between the two gene copies through the process of subfunctionalization (Birchler & Yang, 2022; Lynch & Conery, 2000; Voordeckers & Verstrepen, 2015). In each of these cases, both of the gene copies obtain functions that are essential to the development or survival of the organism and thus, both copies are likely to persist in the population.

With the current knowledge of the gene duplication event leading to the production of *dmrt1.L* and *dmrt1.S* in *X. laevis* which have become fixed in this species, this investigation hopes to develop a complete understanding of the independent functions of each gene copy and the overall importance to the evolution of the species. In addition, by studying the functions of each of these copies in *X. laevis* compared to the single *dmrt1* gene present in *X. tropicalis*,

further insights to the importance of this gene can be developed to provide a comprehensive overview of how such genes regulate sexual differentiation in these species.

1.6 Testes anatomy and histology

The testis is a complex organ consisting of multiple cell types and structures. To complete the histological analysis for this investigation, a thorough understanding of testis anatomy and function was crucial. Apparent in the histology images were spermatocytes which lead to the production of spermatids through the process of meiosis as well as the maturing spermatids that ultimately give rise to sperm (Figure 1B). In addition to these cell types, Sertoli cells can also be seen in the histology images (Figure 1B). These are very large cells that can be classified as eosinophiles to which the spermatids remain attached until they become fully matured (Wiechmann & Wirsig-Wiechmann, 2003). The testes also consist of other structures called tubules which can be categorized into two types. First, are the seminiferous tubules (Figure 1A) in which the spermatids are produced. The seminiferous tubules merge with the straight tubules (Figure 1A) which then carry the spermatids towards the mediastinum where they exit the testis (Wiechmann & Wirsig-Wiechmann, 2003). Lastly, one additional cell type that can be viewed through histology are the Leydig cells (Figure 1B) which are responsible for producing the male androgens (Wiechmann & Wirsig-Wiechmann, 2003).

1.7 Secondary Sex Characteristics

As a complement to understanding the role of *dmrt1* on primary sex characteristics such as gonadal development and function, this research also aims to identify any impact this transcription factor has on secondary sex characteristics. In *Xenopus* species, the most obvious secondary sex characteristic involves vocalization. During a vocalization, an initial stimulus of the vocal nerve initiates the call by causing the muscles of the larynx to contract which forces the AD disks to separate, thus creating an opening for air to pass through towards the glottis which remains closed during a vocalization but then opens again for normal respiration (Kelley et al., 2017; Wiechmann & Wirsig-Wiechmann, 2003). Variations in the size of the larynx and its morphology can lead to differences in the pitch of a call which is one of the factors believed to cause diversity in calls between sexes and species (Tobias et al., 2011). There are clear structural differences within the laryngeal tissue based on the sex of the frog. Males generally have a larger and wider shaped larynx with thicker areas of cartilage in the bottom region of the organ whereas females typically have much thinner segments of cartilage resulting in a thin, triangular shaped larynx (Sassoon & Kelley, 1986). Based on this understanding, questions arise on what factors may be controlling such characteristics and if these factors overlap with those regulating primary sex characteristics. As a result, this investigation will also study the impact of *dmrt1* on vocalization with the hopes of further understanding the role of this gene in development of these frogs.

2 Materials and Methods

2.1 Xenopus laevis and X. tropicalis knockout lines

We used CRISPR-Cas9 to introduce deletions and frameshift mutations in the 5' portion of the coding regions of *dmrt1.S* and *dmrt1.L* in *X. laevis* and *dmrt1* in *X. tropicalis* (Figure 3, 4 & 5). F0 mosaic individuals were crossed with wildtypes to generate non-mosaic F1 individuals with germline transmission; F1s were then intercrossed to generate homozygous null and heterozygous F2 individuals for each locus. Genotypes were determined by Sanger sequencing using DNA extracted from samples of foot webbing from each individual using the DNeasy kit (Qiagen, Hilden, Germany) following the manufacturer's protocol. For the *X. laevis* knockout lines, four pairs of primers specific to *dm-w* and the upstream untranslated region of this gene were used for PCR amplification including dmw_5pr_for_71 & dmw_5pr_rev_810, dmw_5pr_for_2762 & dmw_5pr_rev_3122, dmw_5pr_for_1300 & dmw_5pr_rev_2131(SI, Bewick et al., 2011), and dmw_intron1_for1 & dmw_intron2_rev1 (Table S7 of Cauret et al. submitted July 19 to PLOS Genetics). These amplifications were used to determine the genetic sex of each individual by comparing the amplifications between each primer set to increase the accuracy of the results. The *dmrt1.L* and *dmrt1.S* genes were amplified and Sanger sequenced to genotype individuals. In total, 24 F2 individuals from the *dmrt1.L* line were sampled and 51 F2 individuals from the *dmrt1.S* line were sampled. Because individuals from each line were parented by two heterozygous F1 parents, there were three possible F2 genotypes: homozygous knockout, homozygous wildtype, and heterozygous individuals. The sequences were analyzed using the Geneious Prime software version 2023.0.1 (Biomatters Ltd., Auckland, New Zealand) to identify which individuals contained the deletions.

For the *X. tropicalis* line, *dmrt1* knockout individuals were generated at the National Xenopus Resource (NXR), Woods Hole, Massachusetts (Figure 5). The sex of each frog was determined based on external morphology and was later confirmed through dissections. In total, five *dmrt1* knockout individuals (one male and four females) and two wildtype individuals were compared. The two wildtype individuals consisted of one male and one female taken from a cross between two *X. tropicalis* individuals collected from Ankasa West, Ghana.

2.2 Phenotypic analysis

The phenotypes of wildtype and knockout individuals from each line were determined through a series of analyses. These phenotypes were then compared based on the investigation of internal anatomy and histology (i), fertility testing (ii), investigating gene expression within the developing gonads (iii) and studying the vocalizations of males (iv).

i) Internal anatomy and histology

A sample of wildtype and mutant frogs were euthanized for anatomical and histological analysis from each of the knockout lines. In total, 19 *X. laevis* frogs were dissected including three *dmrt1.L* homozygous null males, two *dmrt1.L* heterozygous null males, six *dmrt1.S* null males, four *dmrt1.S* heterozygous null males and four wildtype males, which included F2 siblings from each mutant line that were raised in the same tank as the other individuals from

each line. In addition, one *X. tropicalis dmrt1* knockout male was also prepared for histological examination. Each individual was euthanized by transdermal overdose of MS-222 (Sigma-Aldrich, St. Louis, MO, USA). Following euthanasia, internal anatomy of each animal was inspected, and any missing or abnormal organs (especially gonads) were noted. To prepare tissues for histology, cardiac perfusion was performed using a 50 ml syringe that was filled with phosphate-buffered saline (PBS) with pH of 7.4, followed by fixation by perfusion with 10% formalin. The PBS was injected into the bottom of the heart after clipping of the veinous vessels of the heart, until the fluid exiting these vessels was clear, usually around 25 ml. Next, approximately 25 ml of the formalin was injected into the bottom of the heart as a first step towards fixation of tissues.

Following the perfusion, tissues were dissected and placed into plastic histology containers. The testes or oviduct were removed first and were kept separate from other tissues. For each individual, a sample of liver, heart, kidney, stomach, intestine, spleen, skin, muscle, lung, eyes and brain were removed. The brain was extracted by removing the entire top half of the skull and placing the skull in decalcification solution for a minimum of two weeks before completing histology. The decalcification solution was prepared consisting of 200 gm of EDTA disodium salt, 950 ml of distilled water and 50 ml of 10N NaOH adjusted to a pH of 7.4. The rest of the tissues were first fixed in 10% formalin for minimum of 48 hours, then were transferred to 70% ethanol for a minimum of 48 hours before submitting for histology. Once tissues had been properly fixed, they were embedded in paraffin, sectioned, and stained at the core histology facility at the McMaster Immunology Research Centre (Hamilton, Ontario). Four µm sections were stained with hematoxylin and eosin stain following the protocol recommended by Leica Biosystems for use with Leica's SelecTech stains Hematoxylin 260MX, Eosin 515LT on the Leica Autostainer XL.

As a complement to this histological analysis, live sperm samples were collected in order to view sperm cells and determine sperm count under the microscope. Testes were taken from a *dmrt1.L* null male and a wildtype male which were both masticated in 100 µl of 1.2x Marc's Modified Ringer solution (MMR). This solution consisted of sodium chloride, potassium chloride, magnesium sulfate heptahydrate, HEPES free acid and calcium chloride dihydrate diluted to the appropriate concentration (Shaidani et al., 2021). Samples were then diluted by 10 µl of the *dmrt1.L* null solution to 20 µl of 1.2x MMR and 1 µl of the wildtype samples to 99 µl of 1.2x MMR. A total of four dilutions were completed for each sample and sperm cells were counted using the full grid of the hemacytometer. From the sperm cell count, the total concentration of sperm was calculated for each sample.

To further analyze the histological results collected, slides were imaged using the ZIESS Axioscan 7 slide scanner (10X; 0.45 NA). Images were taken by scanning across the testis using specified regions of interest to produce a collection of 10X images that could be stitched together to form a comprehensive image of the entire testis. Each image file was opened in FIJI version 2.9.0 (Schindelin et al., 2012) using the Bio-formats plugin. Images were then converted to RGB image format then finally 8-bit image format to display the image in grey scale for thresholding.

We then quantified and compared the amount of white space in the slides from each genotype for each line in FIJI. Because the images contained the entire testis on a white background, we next needed to remove the background so only white space within the tissue was quantified. To accomplish this, a Gaussian Blur filter was applied to the image where sigma was set to 75. A threshold function was used to identify the area occupied by tissue; the "analyze particles feature" was then used to create an outline of the testis. This outline was applied to the

original 8-bit image, allowing us to section out the testis from the background. From here, the Otsu built-in threshold feature (Otsu, 1979) was applied and using the measure function provided the percentage of area that was occupied by tissue. From here, this value was subtracted from 100 to get the final percentage of the image that was covered by white space. To determine if the threshold value had a large effect on the results, we then tested this procedure by manually adjusting threshold values five higher and five lower than the Otsu threshold value. The percentage of area covered by white space for each analysis was organized in a table and the means and standard deviations were compared in RStudio (RStudio Team, 2022, Boston, MA). Once the area containing white space had been determined for each image, the results were input to RStudio (RStudio Team, 2022) which was used to compare wildtype to knockout individuals by first fitting a linear model using the function area of whitespace ~ genotype of the frog, random = ~1|Individual, where the differences in area occupied by whitespace was determined between genotypes while differences between individuals were included as a random factor. From here, the emmeans function was used to obtain confidence intervals, and to test whether there was a statistically significant difference between the genotypes within each line (Lenth 2023).

ii) Fertility

Fertility was assessed for *X. laevis dmrt1.L* and *dmrt1.S* knockout males and females using in vitro fertilization (IVF). For each mutant line, we attempted to generate embryos *in vitro* using a wildtype male with a homozygous null female, or a wildtype female with a homozygous null male. For each fertility assay, we concurrently performed a cross between a wildtype pair using the same solutions and wildtype gametes (eggs or sperm depending on the assay) as a control. Briefly, the protocol for IVF followed that outlined by Shaidani et al., 2021, which began by priming females with 300 international units (IU) of pregnant mare serum gonadotropin (PMSG; BioVendor, Asheville, NC, USA). A minimum of 24 hours later, females were injected with 500 IU of human chorionic gonadotropin (HCG; BioVendor R&D, Asheville, NC, USA) and left overnight. The next morning, attempts were made to extrude eggs from the female into a petri dish by holding the frog with the index finger between the legs of the frog, pulling back on one leg with the other hand, and carefully applying pressure to the abdomen of the frog with the thumbs. Once the eggs had been collected in the petri dish, any excess water was removed with a pipette. Next, the selected male was euthanized with transdermal overdose of MS-222 and the testis were removed and masticated in 1x MMR. The sperm mixture was then pipetted over the eggs and was left for 5 minutes. The plate was then flooded with 0.1x MMR for 15 minutes. From here, eggs were kept in 0.1x MMR and were monitored to determine if fertilization took place. Fertilization was first perceived by the appearance of the oocytes rotating so the dark coloured animal pole was facing upward in the petri dish. When viewed under the dissection microscope, cell division was observed through the formation of blastulas that had undergone multiple cleavage events (Figure 2A). Figure 2 B&C shows the further development from embryos to tadpoles as additional confirmation that this cross achieved successful fertilization.

In total, the fertility assay was performed on three *dmrt1.L* knockout females, one *dmrt1.S* knockout female, two *dmrt1.L* knockout males and three *dmrt1.S* knockout males. In the event that no eggs were released by the female, this was noted, and the remaining steps of this protocol were halted for that individual. Additionally, six *dmrt1.L* females were dissected to

further investigate the lack of fertility achieved. Four of the *X. tropicalis dmrt1* knockout females were also dissected for analysis of reproductive organs.

iii) Gene expression in the developing gonad

Complete transcriptome sequencing (RNAseq) data were collected from mesonephros/gonad tissue at tadpole at stage 50, which is when the gonads begin sexual differentiation (Yoshimoto et al., 2008). In total, this analysis consisted of a sample size of 42 tadpoles (five wildtype males, three wildtype females, six null males and six null females from the *dmrt1.L* line and three wildtype males, seven wildtype females, three null males and six null females from the *dmrt1.S* line). For the *dmrt1.L* mutant line, we compared expression among siblings that were raised in the same tank. This included six knockout females, six knockout males, three wildtype females, and five wildtype males. For the *dmrt1.S* mutant line, we compared expression among siblings reared in the same tank that were sequenced in two separate runs. The first run included four knockout females, one knockout male, three wildtype females, and three wildtype males. The second run included three knockout females, two knockout males, three wildtype females, and three wildtype males. Normalized counts were obtained through STAR 2.7.9a (Dobin et al., 2013) by mapping to the *X. laevis* version 10.1 genome assembly which was obtained from Xenbase (Fisher et al., 2023). Counts were analyzed in RStudio using EdgeR version 3.40.0 (Chen et al. 2016, McCarthy et al. 2012, Robinson et al. 2010), and for *dmrt1.S*, the lane effects were controlled for by including this variable in the design. For each mutant line, separate analyses were performed that compared wildtype to mutant individuals within each sex. Significantly differentially expressed genes were classified as those with a false detection rate (FDR) less than 0.10.

To further characterize the function of differentially expressed genes, a gene ontology (GO) analysis was completed. Because many transcripts of *X. laevis* are not annotated, we relied on putative orthologous annotations from the human transcriptome GRCh38.p13 release 42 (Frankish et al. 2021). This was completed by using the discontiguous blast algorithm to obtain annotations for each differentially expressed gene using the original gene sequences and estimating putative orthologs based on the best bit score within BLAST (Cauret et al. submitted July 19 to PLOS Genetics; Altschul et al. 1997). From here, the GO analysis was completed using a false discovery rate of 0.05 through Fisher's exact test by listing the corresponding gene acronyms in an online tool provided at http://geneontology.org/.

As a complement to the gene ontology analysis of differentially expressed genes, an additional analysis that focuses on a set of 74 previously identified sex-related genes was also performed (Piprek et al. 2018). For these 74 genes, expression ratios were determined for wildtype males:wildtype females and knockout females:wildtype females or knockout males:wildtype males within three different clutches (one each from the *dmrt1.L* and *dmrt1.S* lines and a third from a separate line). For these 74 genes, the correlation between the female:male expression ratios and the null:wildtype expression ratio for each sex and each mutant line was assessed. A permutation test with 1000 replications was used to assess whether the observed correlation departed from our expectation based on correlations between 74 randomly selected genes.

iv) Vocalizations

Similar to most frogs, the vocal organ (larynx) of *Xenopus* species is sexually dimorphic (Kelley et al., 2020). We therefore explored whether knockouts of *dmrt1.L* or *dmrt1.S* had any effect on secondary sexual differentiation of this organ in terms of morphology (histology) and function (sound production in males). For histological analysis of *X. laevis*, four wildtype males, four wildtype females, three *dmrt1.S* knockout males, two *dmrt1.S* knockout females, one *dmrt1.L* knockout males and three *dmrt1.L* knockout females were analyzed. Each frog was euthanized by transdermal overdose of MS-222 prior to dissection, which followed the procedure outlined above. For histological analysis, excess tissue was left attached to the larynx to ensure the entire organ was removed. The extracted tissues were fixed in formalin for a minimum of 48 hours, and then transferred to 70% ethanol for a minimum of 48 hours prior to paraffin embedding, four µm sectioning, and hematoxylin and eosin staining as detailed above. Slides were then imaged using the Zeiss slide scanner at 10X magnification for analysis.

We analyzed vocalizations from two *dmrt1.L* knockout males, three *dmrt1.S* knockout males, and four wildtype males that were reared separately from the knockout individuals. Recordings were completed for one frog at a time. First, the male was isolated into a container of approximately 16 L of tank water. The male was then injected with HCG, where 250µl was injected for smaller juvenile frogs and 400µl was used for adult frogs. The container was covered with cloth to minimize visual disturbances, and the injected male was left isolated for 6-8 hours. Then a non-injected, wildtype female was added into the container and the recording was started. The recording was completed by submerging a hydrophone (High Tech, Gulfport, MI, USA) into a container of water and recording using a laptop connected to the PreSonus AudioBox 22VSL (Baton Rouge, LA, USA). The microphone sensitivity was set by adjusting the input gain dial slightly past the midpoint. The recording was completed through the computer program Audacity. Sound activated recording was achieved by setting the program parameters to -34 dB and leaving the system to record overnight. The next morning, the water temperature was recorded, and the recording was stopped

Recordings were then analyzed using Audacity software version 3.2.1 (Muse Group, Limassol, Limassol, Cyprus) and RStudio version 4.2.2 (RStudio Team, 2022). The inter-click interval (ICI) (Tobias et al. 2014) was measured from the start of one click to the start of the subsequent click by carefully placing time markers directly onto the recording file. Markers were added for each click within a call for a total of 20 calls per individual. The start of a click was identified by the presence of the first peak with amplitude above background. Due to variations between clicks and the potential for background noise, there were some cases where the start of the click differed in structure. In the case that there were above background sounds immediately preceding the first peak, these were included as part of the click only if there was a clear gap of a minimum of 0.003 seconds from the end of the previous click. If it was not possible to clearly differentiate between the end of one click and start of the next, ICI was set to begin at the start of the first peak. ICI durations were exported to RStudio where we tested for a difference between the ICI of wildtype and knockout individuals using the emmeans function (Lenth 2023). To achieve this, we fit a linear model using the function ICI ~ genotype, random = ~1|Individual, in order to analyze the ICI by taking into account the difference between genotypes while keeping the difference between individuals as a random factor.

3 Results

3.1 Sex and genotypes

We generated knockout lines for *dmrt1.S* and *dmrt1.L* in *X. laevis* and *dmrt1* in *X. tropicalis* using CRISPR/Cas9. Figure 3 shows Sanger sequences of *X. laevis dmrt1.S* for a homozygous wildtype, homozygous knockout, and heterozygous individual. Homozygous knockouts were generated by a seven bp frameshift deletion in the coding region located within the 11th codon that changed this codon from an arginine to a proline in this codon and introduced a premature stop codon downstream of this. Heterozygous individuals from this line were identified by the presence of double peaks in Sanger sequences of the start of the region where the deletion was located (Figure 3C). Figure 4 shows Sanger sequences of *X. laevis dmrt1.L* for a homozygous wildtype, homozygous knockout, and heterozygous individual. Similar to the *dmrt1.S* line, knockouts were identified by a (different) seven bp frameshift deletion in the coding region that occurred after the tenth codon and changed the subsequent codon from a proline to an arginine and introduced a premature stop codon downstream of this. As expected, heterozygous individuals from this line had double peaks near the start of the deletion (Figure 4C). For *X. tropicalis*, a knockout mutation was achieved by introducing a one bp frameshift deletion in the coding region within the 26th codon that changed this codon from a leucine to a tyrosine and introduced a premature stop codon downstream of this. The normal length of this protein is around 300 amino acids in length, so provided that the mutations occur early in the sequence, these are considered null mutations. Figure 5 shows Sanger sequences of *X. tropicalis dmrt1* for a knockout, a wildtype, and heterozygous individual.

To determine the genetic sex of each individual in our two mutant lines for *X. laevis*, we used four independent PCR amplifications, each with a different pair of primers that targeted portions of the coding region of exon 2 of *dm-w* and three different portions of the 5' upstream untranslated region of this gene. Independent successful amplification of each of these four regions identified genetic females and unsuccessful amplifications of each of these four regions identified genetic males; wildtype females were amplified in tandem as a positive control.

The genetic sex was then compared to the phenotypic sex of each frog as determined based on external morphology (n = eight, four, five, 13 for female and male *dmrt1.L* and *dmrt1.S* knockouts, respectively) and internal morphology (n = six, three, two, and six for female and male *dmrt1.L* and *dmrt1.S* knockouts, respectively). Sex was also determined for 11, 13, five and three heterozygous null males and females from the *dmrt1.S* and *dmrt1.L* lines, respectively. These assays demonstrated that all phenotypic females were genetically female and that all phenotypic males were genetically male. Figure 6 shows an example of female-specific amplifications for eight females and eight males taken from the *dmrt1.L* line. Multiple amplifications were completed for each of the individuals from the *dmrt1.L* and *dmrt1.S* lines in order to accurately determine genetic sex. In the *X. tropicalis dmrt1* line, we analyzed a total of two wildtype individuals (one male and one female), three *dmrt1* null females and one *dmrt1* null male for comparison between external and internal anatomy. As discussed below, there is not a reliable sex-specific genetic marker for sex in *X. tropicalis,* so we were unable to assess this for this line.

3.2 Gonadal histology

We performed histological analysis on adult testes of heterozygous males from the *dmrt1.S* and *dmrt1.L* lines. A total of four *dmrt1.S* heterozygotes and two *dmrt1.L* heterozygotes were considered. No pronounced differences were detected between the *dmrt1.S* heterozygous males and the wildtype males. However, qualitative differences were detected between the *dmrt1.L* heterozygotes and the wildtype individuals in that spermatocytes appear to be more dispersed in the heterozygote compared to the wildtype (Figure 7). In addition, sperm in the *dmrt1.L* heterozygote appear in general to be more immature compared to the wildtype; this is evidenced by an increased abundance of small, darkly stained dots, which represent earlier stages of spermatogenesis. However, it is important to note that some of the sperm present in the *dmrt1.L* heterozygous null have developed past the immature stage described above.

We also performed histology on adult testes from four wildtypes, six *X. laevis dmrt1.S* knockouts, three *X. laevis dmrt1.L* knockouts, and one *X. tropicalis* knockout. Figure 8 shows an example of adult testis histology from a *dmrt1.S* knockout and a wildtype. Qualitative inspection suggests these individuals have similar densities of mature spermatids and this observation was consistent across all six *dmrt1.S* knockout males we inspected (Figure S1&S2). In contrast, in the adult *dmrt1.L* knockout individuals no mature spermatids were observed; instead, we observe darkly stained dots towards to center of the seminiferous tubules that may be late spermatocytes that failed to mature into spermatids (Figure 9). In addition, one of the three *dmrt1.L* knockout males sampled had only one testis (Figure S1&S2).

To further investigate the presence of mature sperm in *dmrt1.L* null males, live sperm samples were tested. Through this analysis, very few mature sperm were seen; however, a small number of sperm were detected that appeared to be mature (Figure 10). The final concentration of sperm detected in the *dmrt1.L* null sample was approximately 230,700 sperm/ml, which was a much lower concentration compared to the wildtype male with approximately 183,500,000 sperm/ml. Taking into account the weight difference between the two testes, the wildtype male was found to have approximately 842 times more sperm than the *dmrt1.L* null male.

Histological analysis of testis from the *X. tropicalis dmrt1* knockout male identified mature spermatids, albeit in lower densities compared to the wildtype male (Figure 11).

We used a computational approach to quantify the area of each testis occupied by white space within FIJI version 2.9.0 (Schindelin et al., 2012). We tested whether results were substantially affected by three different threshold values that define whitespace in our histological images. The first threshold value was assigned by the Otsu threshold feature, and two other analyses were performed using values that were five values higher or five values lower than the Otsu threshold values. Using these different threshold values, positive correlations were observed for the proportions of white space from images of *dmrt1.S* and also *dmrt1.L* histological sections of testis tissue (Figure S3). These results suggest that while the proportion of white space changes with different threshold values, the correlations indicate that these changes are consistent between comparisons of each image. Based on this result, we selected the Otsu threshold feature for subsequent analysis.

Each testis image was analyzed individually to quantify the percentage of area occupied by white space for each image. For the *X. laevis dmrt1.S* knockout males a total of nine *dmrt1.S* and eight wildtype testes were analyzed. Figure 12A shows a box plot comparing the means of these two groups with error bars showing the 95% confidence interval of the mean computed using the R package emmeans (Lenth 2023). The mean proportion of whitespace for the *dmrt1.S*

knockout individuals had a 95% confidence interval of 44.2–49.1% whereas that for the wildtype individuals was 37.9–43.1%. These confidence intervals do not overlap and are significantly different (P = 0.0042).

For the *X. laevis dmrt1.L* knockout males a total of four *dmrt1.L* images were compared to the same eight wildtype testes. Figure 12B shows a box plot of the compared means for these two groups with error bars showing the confidence intervals. The *dmrt1.L* knockout group had a 95% confidence interval of 29.2–48.0%, whereas that for the wildtype was 32.8–48.1%. These confidence intervals overlap and are not significantly different (P = 0.71).

3.3 Fertility

Male and female heterozygotes for either the *dmrt1.L* or the *dmrt1.S* null allele were fertile; these individuals were successfully crossed to generate the homozygous nulls we studied. In vitro fertilization with an opposite sex (test) wildtype individual was used to test fertility of homozygous null individuals; crosses between the tested wildtype individual and another opposite sex wildtype individual was used as a positive control. When a wildtype female and a *dmrt1.S* knockout male were crossed, fertilization was not detected in the positive control cross; but it was detected in the experimental pairing. Failure of the positive control could reflect poor sperm quality of the wildtype male. When a *dmrt1.S* knockout female was crossed with a wildtype male, fertilization was also successful (no positive control was performed for this cross). Together these crosses demonstrate fertility of *dmrt1.S* null males and null females.

When a wildtype female was crossed with a *dmrt1.L* knockout male, fertilization did not occur. Unfortunately, however, fertilization also was not observed in the positive control cross. Thus, while we suspect that males of this genotype are sterile based on the analysis of testis histology and sperm concentration, we were not able to confirm this in our fertility assay. We also tested fertility of *dmrt1.L* knockout females. A total of three *dmrt1.L* knockout females were injected but no eggs were released from any of these individuals. Thus, the remaining steps for determining fertility could not be completed; however, information presented next conclusively demonstrates that *X. laevis dmrt1L* null females are sterile.

To further examine the fertility of the *X. laevis dmrt1.L* knockout females, six adult individuals were dissected. In adult wildtype females, oviducts full of eggs are readily observed upon dissection and ovulation is elicited by injection of human chorionic gonadotropin. However, in all six *dmrt1L* null females, no reproductive organs, male or female, or eggs were observed. These null females were normal in size and healthy based on large fat pads. Three *X. tropicalis* females containing the *dmrt1* knockout were also examined for the presence of reproductive organs through dissection. Consistent with the results from *X. laevis*, there was no ovulation induced by injection of human chorionic gonadotropin in any of these three individuals, and dissection demonstrated the complete absence of reproductive organs. Figure 13 shows an image of a dissected *X. tropicalis dmrt1* knockout and wildtype females.

3.4 RNAseq analysis

We performed an analysis of differential expression in transcriptomes from gonad/mesonephros tissue at tadpole stage 50, which is the developmental stage where sexual differentiation is triggered by transient expression of *dm-w* (Yoshimoto et al., 2008). *Dmrt1.S* males had the highest number (n = 1251) of differentially expressed genes compared to wildtype

males. The remaining groups listed from highest to lowest number of differentially expressed genes includes *dmrt1.L* female (n = 337), *dmrt1.S* females (n = 20) and *dmrt1.L* males (n = 5). Figure S4 includes a complete list of the significantly differentially expressed genes discovered from this analysis.

A summary of shared differentially expressed genes between sex-biased transcripts from each of three wildtype batches (MF1, MF2 and MF3) and same-sex mutant to wildtype comparisons for *dmrt1.L* females or males, and *dmrt1.S* females or males is provided in Figure 14. For *dmrt1.L* knockout female analysis, three differentially expressed genes were also differentially expressed in the wildtype analyses, and for the *dmrt1.S* knockout male analysis, four differentially expressed genes were also differentially expressed with the wildtype analyses. There were no differentially expressed transcripts in the *dmrt1.L* male analysis or the *dmrt1.S* female analysis that were also differentially expressed in the wildtype analysis. For comparisons between mutant analyses (Figure 14E), there were 40 differentially expressed genes in common between *dmrt1.L* knockout females and *dmrt1.S* knockout males; none of these were differentially expressed in the comparison between male and female wildtype individuals. This highlights a shared but not sex-specific effect of these knockout lines.

A gene ontology analysis was performed for the differentially expressed genes identified in each of these four analyses (Figure S5). Enrichment of differentially expressed genes from both the *dmrt1.S* males and *dmrt1.L* females identified specific gene functions falling into each of the three gene ontology categories (biological process, molecular function, and cellular component functions) included phenomena associated with methylation and mitochondria function. Differentially expressed genes for the *dmrt1.S* females and *dmrt1.L* males were not found to have significant ontology enrichments. Additionally, the small number of differentially expressed genes from the three wildtype batches were enriched for functions that did not have obvious links to sexual differentiation in the molecular function and cellular component categories but not in the biological process category.

As a complement to this analysis, 74 previously identified genes with sex related functions were used to determine the expression ratios, as detailed in the methods section 2.2 (iii), and correlations between the groups were analyzed through permutation tests. Figure 15 shows the results of these permutation tests. In total, each of the four knockout groups were compared with the three M-F batches for a total of 12 tests. None of these tests was significant as indicated by the r and p-values in Figure 15.

3.5 Impact on laryngeal morphology and function

We investigated secondary sexual differentiation of the larynx in terms of morphology and function (vocalization in males). Through comparisons of histological samples, we did not detect a substantial difference in structure of the larynx resulting from the gene knockouts. Figure 16 shows the larynx histology of wildtype, null *dmrt1.S*, null *dmrt1.L* males and Figure 17 shows histology of wildtype, null *dmrt1.S*, null *dmrt1.L* females. For females, the larynx is small relative to the males, where the purple stained cartilage can be seen to make up the main structure of the organ. Since this tissue was smaller in females, excess tissue was left during dissection to ensure the organ stayed intact, which can be seen in the pink stained regions surrounding the cartilage. For males, the general structure of the larynx is larger and takes on a more rounded shape where the cartilage is thicker. The five wildtype, three *dmrt1.S* knockout and one *dmrt1.L* knockout males all have similar morphology as outlined in Figure 16. Each of the

females examined – two wildtype, two *dmrt1.S* knockouts and four *dmrt1.L* knockouts – had similarly thinner morphology depicted in Figure 17.

Recordings were collected for *dmrt1.L* knockout, *dmrt1.S* knockout and wildtype males. These recordings were analyzed to identify any differences in inter-click intervals (ICI) between the wildtype and knockout frogs. Figure 18A includes a boxplot to compare the ICI of three *dmrt1.S* knockout males to four wildtype males used in the previous analysis. The 95% confidence interval for the wildtype males was 0.0259–0.0306. In comparison, the *dmrt1.S* knockout males had a 95% confidence interval from 0.0267–0.0324. These intervals overlap and are not significantly different (P = 0.4186). In addition, this analysis was performed for the *dmrt1.L* knockout males. Figure 18B shows a box plot illustrating the ICI of 20 calls for the same four wildtype males and two *dmrt1.L* knockout males. The mean ICI of the wildtype group had a 95% confidence interval from 0.0247–0.0319 and that of the *dmrt1.L* knockout calls was 0.0298–0.0407. Though these confidence intervals overlap, there is a significant difference between them (P = 0.0448).

4 Discussion

4.1 Sex reversal

One possible consequence of a loss of function mutation at a sex related gene is sex reversal – when the genetic sex of an individual does not correspond to the phenotypic sex. In our *X. laevis* (F2) homozygous knockout lines the genetic sex was determined based on the presence or absence of *dm-w* based on three PCR amplifications that each targeted different portions of this female-specific gene. The sex phenotype of each individual was then determined based on external and internal morphology. We found no evidence of sex reversal: *dm-w* successfully amplified in each phenotypic female and never amplified in a phenotypic male. As a result, we can conclude that sex reversal is not occurring as a result of either *dmrt1.S* or *dmrt1.L* knockouts. Because a sex-specific marker is not yet known for *X. tropicalis* we were unable to assess the genetic sex of our knockout line from this species. The external morphology of the *X. tropicalis* knockout individuals matched their gonads (an adult male had a smaller body size than adult females and had testes and a proportionately larger larynx than females; females had a larger body, no testes and proportionately smaller larynx than males). Because sex reversal was not observed in the *X. laevis* frogs, and we observed two differentiated sexes for the *X. tropicalis dmrt1* knockout line, we suspect sex reversal was also elicited by the *dmrt1* knockout in *X. tropicalis*.

A lack of sex reversal in these knockout lines contrasts to some degree with findings from *dmrt1* knockout in other species. In Nile tilapia (*Oreochromis niloticus*), for example, knockout of *dmrt1* causes male-to-female sex reversal, whereas females remain unaffected (Dai et al., 2021). Similarly, male chickens (ZZ) that carry only one allele of *dmrt1* develop ovaries rather than testes (Ioannidis et al., 2021). These results are inconsistent with our findings were neither *X. tropicalis* nor *X. laevis* experienced sex reversal when *dmrt1* knockouts were introduced.

Variation among species in the consequences of *dmrt1* knockout points to differences in the genetic networks within which *dmrt1* is embedded. In Nile tilapia disruption of *foxl3* function leads to masculinization of genetic females; and knockout of *dmrt1* had the opposite effect resulting in male-to-female sex reversal (Dai et al., 2021). Interestingly, the double knockout of

dmrt1 and *foxl3* resulted in the recovery of normal sex determination (Dai et al., 2021). This highlights an influential sex-related interaction between these two genes; whether this interaction also exists in *Xenopus* is unclear.

In chickens, *dmrt1* transcription is inhibited by epigenetic factors including long-coding RNAs and hypermethylated regions (Roeszler et al., 2012; Zhang et al., 2023). Interestingly and potentially related to this, the gene ontology analysis identified differentially expressed genes in the developing gonad/menonephros of the *X. laevis dmrt1.L* null females that were involved with methylation. This opens the possibility that *dmrt1L* in some what may regulate its own transcription via methylation.

In *X. laevis,* female differentiation is triggered by a partial duplicate of *dmrt1S* called *dm-w* (Yoshimoto et al., 2008). Knockouts of *dm-w* results in complete female-to-male sex reversal (Cauret et al., submitted July 23 to PLOS Genetics). *Dm-w* shares the same DM binding domain as *dmrt1* and thus, interactions between these two genes are also likely regulating sex determination for *X. laevis.*

4.2 Gonadal development and fertility

Histological analysis of the *dmrt1L dmrt1S* knockouts in *X. laevis* and *dmrt1* knockout in *X. tropicalis* provided insights into the role of this gene in gonadal development. In the one *X. tropicalis dmrt1* null male exampled, two testes developed but the quantity of mature sperm was far lower than in a wildtype male. In three *X. laevis dmrt1.L* knockout males a more drastic phenotype was observed where no mature spermatids were observed in the histology cross sections. Inspection of mascerated testis tissue from a *dmrt1.L* null male showed very few sperm that had developed from spermatocytes. However, in six *X. laevis dmrt1.S* knockout males no substantial difference in the densities of mature sperm compared to wildtype was observed, although there was a significantly lower tissue density in histological preparations of testis from this line. Overall, these results demonstrate that *X. tropicalis dmrt1* knockout and the *X. laevis dmrt1.L* knockout both play important roles in male germ cell development and that *dmrt1L* and *dmrt1S* have at least partially non-overlapping roles in *X. laevis*.

This is not the only case where mutating *dmrt1* did not result in sex reversal but still impacted testis development. When somatic mutations are introduced in *dmrt1* in tilapia, low expression of *dmrt1* does not result in sex reversal but most of the germ cells do not develop past the stage of secondary spermatocytes (Li et al., 2013). In Japanese eel (*Anguilla japonica*) *dmrt1* is highly expressed in spermatogonia B cells, spermatocytes, and spermatids but not in the earlier spermatogonia or Sertoli cells. This suggests that *dmrt1* may be involved in the developmental progression from spermatogonia B cells to mature spermatids (Jeng et al., 2019). These results are consistent with findings from our investigation wherein the main consequence of the *dmrt1* knockout in *X. tropicalis* and *dmrt1.L* knockout in *X. laevis* concerned production of mature spermatids.

Insights into partially non-overlapping roles in *X. laevis* can be gleaned from focused analyses of gene expression. Moreover, *dmrt1.L* has higher expression in germ cells whereas *dmrt1.S* has higher expression in somatic cell types (Mawaribuchi et al., 2017). This is consistent with our results that *dmrt1.L* knockouts impact germ cell development, and that the tissue density in *dmrt1.S* knockout testes is lower. No significant difference was seen in the quantity of white space between *dmrt1.L* null males and wildtype males. While white space in hematoxylin and eosin stained tissues could be an artefact of how the samples were sectioned and stained, this

result could possibly be indicative of the role of *dmrt1.S* in the testis. If *dmrt1.S* is more highly expressed in somatic cells such as the Sertoli cells, variation in Sertoli cell number or development could explain the increased white space seen. In order to identify the cause of increased white space for testis histology of these males, further research into the functionality of the Sertoli cells is required.

In many species, known phenotypic effects of *dmrt1* are restricted testis or sperm production. Interestingly, we found that knockouts of *X. tropicalis dmrt1* and *X. laevis dmrt1.L* failed to develop ovaries or oviducts. In Atlantic cod (*Gadus morhua*), *dmrt1* is expressed in the gonads of both sexes (albeit more highly in males) opening the possibility that this gene may influence female development in this species as well (Johnsen et al., 2010). In zebrafish, *dmrt1* is required for the down-regulation of *foxl2*, a gene involved in ovarian development (Webster et al., 2017). However, *dmrt1* is not directly influencing ovarian development in zebrafish which contrasts our results as *dmrt1* knockout females did not develop ovaries. Additionally, *dmrt1* is associated with the development of ovarian follicles in the ovaries of juvenile mice and is believed to have a similar effect in the Japanese eel (Jeng et al., 2019; Krentz et al., 2011). Although these and other studies implicate *dmrt1* in ovarian development in some species, to our knowledge, our investigation of *X. laevis* is the first to show that *dmrt1* knockout completely prevents development of oviduct and ovaries.

4.3 Transcriptome analysis

The results of the transcriptome analysis based on RNAseq data collected from tadpoles at stages 50 investigated the number of differentially expressed genes in both *dmrt1.S* and *dmrt1.L* knockout lines compared to wildtype individuals. The most differentially expressed genes were detected in the comparison between *dmrt1.S* null males and wildtype males (n = 1251), followed by the comparison between *dmrt1.L* null females and wildtype females (n = 337). Interestingly, *dmrt1.S* null males and *dmrt1.L* null females were found to share 40 significantly differentially expressed genes. Consistent with this, at tadpole stage 50 *dmrt1.S* has a higher expression in males than females whereas *dmrt1.L* has a higher expression in females than males (Mawaribuchi et al., 2017).

Gene ontology analysis identified enrichment of differentially expressed genes in the biological function, molecular function and cellular component categories for both *dmrt1.S* males and *dmrt1.L* females. Notable enrichments play roles in epigenetic phenomena and the regulation of cholesterol and testosterone. Methylation and related functions in particular were enriched all three gene ontology categories for the *dmrt1.L* knockout females. As previously discussed, epigenetics factors including hypermethylation have been found to inhibit the transcription of *dmrt1* in chickens (Roeszler et al., 2012; Zhang et al., 2023). Also consistent with the enrichment of the cholestoerol biosynthetic prosess in the biological function category that Sertoli cells within the testis regulate cholesterol metabolism, which is crutial for sperm maturation (Shi et al., 2017; Titi-Lartey & Khan, 2023).

The gene ontology analysis also detected differentially expressed genes with functions related to mitochondria in the cellular component category for the *dmrt1.S* males. Mitochondria have been found to take on a variety of roles in the testis including the production and survival of sperm as mitochondrial respiration defects have been associated with abnormal sperm structures leading to infertility (Nakada et al., 2006; Park & Pang, 2021). In addition, the ability of the Leydig cells to produce testosterone is is dependent on the function of mitochondria which

identifies a role of mitochondria in hormone production (Park & Pang, 2021; Ramalho-Santos et al., 2009). Provided that the RNAseq data collected for this investigation was taken from both the gonads and mesonephros tissues, it important to note that some of the genes from this analysis may not be directly related to gonadal function. As a result, further investigation into the genes identified in the GO analysis would be crucial to develop a complete understanding of the role of *dmrt1* in development.

We also compared expression ratios from *dmrt1.S* or *dmrt1.L* mutant to same sex wildtype individuals to wildtype male:female ratios for 74 previously identified sex-related genes. Permutation tests indicate that none of the correlations was more positive or more negative than expected by chance. This finding suggests that we found no evidence of sex reversal in the transcriptome of the developing gonad/mesonephros even though we did observe severe mutant phenotypes in the adult gonad of both sexes for *dmrt1L* null individuals and detectable differences in tissue density in testis of *dmrt1.S* null individuals.

4.4 Subfunctionalization and neofunctionalization

As discussed above, analysis of morphology, histology, fertility and transcriptomics of *X. laevis* knockout mutations for *dmrt1.L* and *dmrt1.S* demonstrate variation in function between these homeologous loci. These differences demonstrate that either subfunctionalization (degradation of ancestral function) or neofunctionalization (the origin of novel function) (Birchler & Yang, 2022; Lynch & Conery, 2000; Teshima & Innan, 2008; Voordeckers & Verstrepen, 2015) occurred following their origin by allotetraploidization in *Xenopus* about 30 million years ago (Evans et al., 2015; Session et al., 2016). Analysis of the mutant phenotype of an outgroup (*X. tropicalis*) provides insights into these changes and evidences both subfunctionalization and neofunctionalization. Moreover, the *X. tropicalis dmrt1* knockout male has a higher density of mature spermatids as compared to the *X. laevis dmrt1.L* knockout male, but lower than a wildtype individual. This suggests that *X. laevis dmrt1.L* was neofunctionalized to take on a more important role in germ cell production compared to the ancestral gene. In contrast, *dmrt1.S* knockout males produce spermatids in amounts comparable to the wildtype males. This suggests that subfunctionalization may have occurred following the gene duplication event where *dmrt1.S* has a less significant role in germ cell production as compared to the outgroup. Clearly an interesting direction for future work would involve analysis of individuals that are homozygous for null alleles for *dmrt1.S* and *dmrt1.L*.

Apart from differences in testis tissue density, we did not detect a pronounced functional phenotype associated with the *X. laevis* knockout mutations for *dmrt1.S* in either sex. However, as previously discussed, *dmrt1.S* has been shown to have higher expression levels in somatic cells compared to germ cells thus suggesting a role in Sertoli or Leydig cell functions (Mawaribuchi et al., 2017). Each of these cell types take on specific roles in male development which may not be apparent through normal hematoxylin and eosin stained histology. Sertoli cells have been identified to have multiple different functions. Sertoli cells are known to help regulate numerous aspects of spermatogenesis by supplying nutrients to developing germ cells, regulating cell cholesterol levels and assisting with the removal of foreign bodies and phagocytosis of abnormal sperm (Arandjelovic & Ravichandran, 2015; Ni et al., 2019; Titi-Lartey & Khan, 2023). However, there are other aspects of development that Sertoli cells play a role in including the secretion of androgen-binding protein which assists with the uptake of testosterone produced by the Leydig cells (Shi et al., 2017; Titi-Lartey & Khan, 2023). Provided the roles of both

Sertoli and Leydig cells in production and usage of androgens, closer investigation of hormone levels in *dmrt1.S* null males could provide further indication of how this gene impacts the functionality of somatic cells within the testis.

4.5 Secondary sexual differentiation

Secondary sexual differentiation refers to sex-specific development of non-gonadal phenotypes. In *Xenopus* the vocal organ (larynx) is sexually dimorphic and develops into a much larger organ in males, even though they are smaller than females in body size (Sassoon & Kelley, 1986). Here we did not recover evidence that *dmrt1.S* or *dmrt1.L* play a substantial role in the development of laryngeal tissue in terms of gross morphology or histology. This is consistent with findings in other species. For example, in chickens *dmrt1* knockout males which developed ovaries instead of testis, but were found to develop normal male secondary sex characteristics such as the large red coloured combs that fan out across their head in adulthood (Ioannidis et al., 2021; Zhang et al., 2023). Similarly, while *dmrt1* knockouts lead to sterility in male zebrafish, secondary sex characteristics developed normally for these males (Webster et al., 2017). However, we did detect a significant difference in laryngeal function of the *dmrt1.L* knockouts, albeit with a small number of biological replicates and overlapping confidence intervals. From the recording analysis, we found the *dmrt1.L* knockout males had longer ICIs compared to the wildtype groups whereas there was no significant difference in ICIs between *dmrt1.S* knockout and wildtype frogs. In order to fully understand any impact of *dmrt1* on the secondary sex characteristic of vocalization, further research is required.

Next steps in investigating the impact of *dmrt1* on vocalizations include both histological analysis and further analysis of call recordings. In *Xenopus*, exposure to atrazine was found to result in feminization of the larynx in males as indicated by differences in the measurement of the *dilator laryngis* muscle (Hayes et al., 2010). The comparison of this muscle was possible by sectioning the larynx perpendicular to the orientation of our tissues. This allows the muscle which wraps underneath the larynx to be clearly seen. Future work with histology of larynx tissues at different orientation could allow us to better visualize more specific features of the larynx in order to detect any changes between our treatment groups. In addition, we will also be analyzing the dominant frequency of each call within wildtype and mutant male recordings. Vocalizations of *Xenopus* males generally have one dominant frequency per call unit and these frequencies vary between species (Tobias et al., 2011). As a result, comparing the dominant frequencies between wildtype and knockout groups can provide further knowledge of how *dmrt1* impacts vocalization in males. In addition, recordings of *X. tropicalis dmrt1* knockout males will also be tested to determine if the results are consistent across these two *Xenopus* species.

5 Conclusion

In this study, I used histological analysis, transcriptome analysis, fertility testing, and the examination of secondary sex characteristics, to provide a comprehensive understanding of how the well-known *dmrt1* gene impacts development in *Xenopus* species. Generations of knockout lines of *X. tropicalis dmrt1* and *X. laevis dmrt1.S* and *dmrt1.L* allowed us to closely examine the effect of these genes have on development in both males and females. While *dmrt1* knockouts have resulted in sex reversal in other species, our histological and transcriptome analysis results

found that sex reversal was not occurring for any of our mutant lines. However, we determined that *dmrt1* in *X. tropicalis* and *dmrt1.L* in *X. laevis* are required for the normal development of the testes as null males from each of these lines failed to produce sperm in densities comparable to wildtype males. Our investigation also identified a role of these genes in female development as each of the *X. tropicalis dmrt1* and *X. laevis dmrt1.L* null females were completely lacking reproductive organs and are considered infertile. This finding offers new insights to the functionality of *dmrt1* in female development, a novel area of research that could advance our understanding of how sex determination evolved in these species.

This investigation also introduces several areas for further research in these genes. Further work towards understanding the role of *dmrt1* in somatic cell functions, interactions between *dmrt1* and other sex determining genes and the ways in which epigenetic factors influence *dmrt1* transcription promises to advance our knowledge of how sex determining systems function. Comprehensively, this work addresses key areas of evolutionary genetics by developing an understanding of how specific genes regulate the process of sexual differentiation and by providing evidence that gene duplication can be a major catalyst for evolutionary change across species.

6 Figures

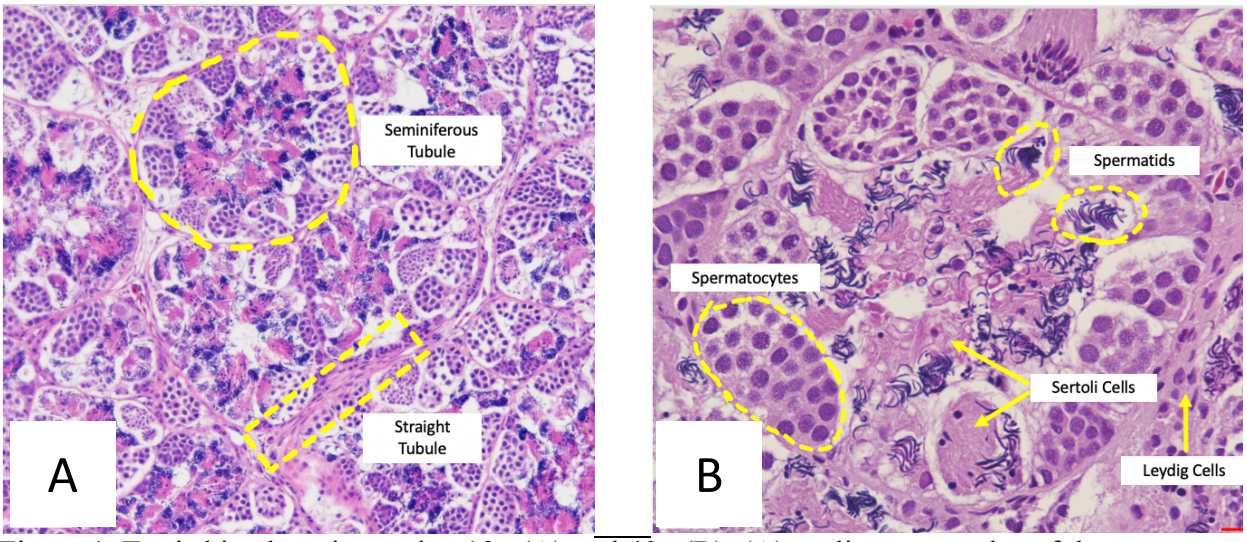

Figure 1. Testis histology imaged at 10x (A) and 40x (B). (A) outlines examples of the seminiferous and straight tubules as denoted by the yellow dotted lines. (B) shows examples of the spermatocytes, spermatids, Sertoli cells and Leydig cells represented by the yellow arrows and dotted lines.

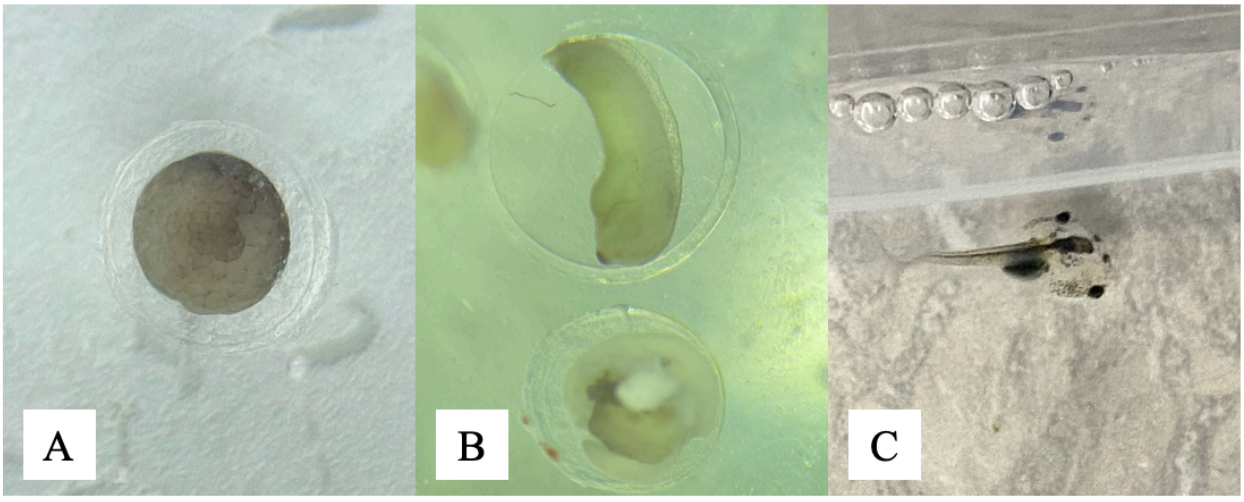

Figure 2. Key stages of development from oocyte to tadpole. The images were each taken from the cross between the *dmrt1.S* knockout female and the wildtype male. (A) shows the formation of a blastula which has undergone multiple cleavage events. (B) shows the late embryonic stage of development and (C) provides an image of a young tadpole.

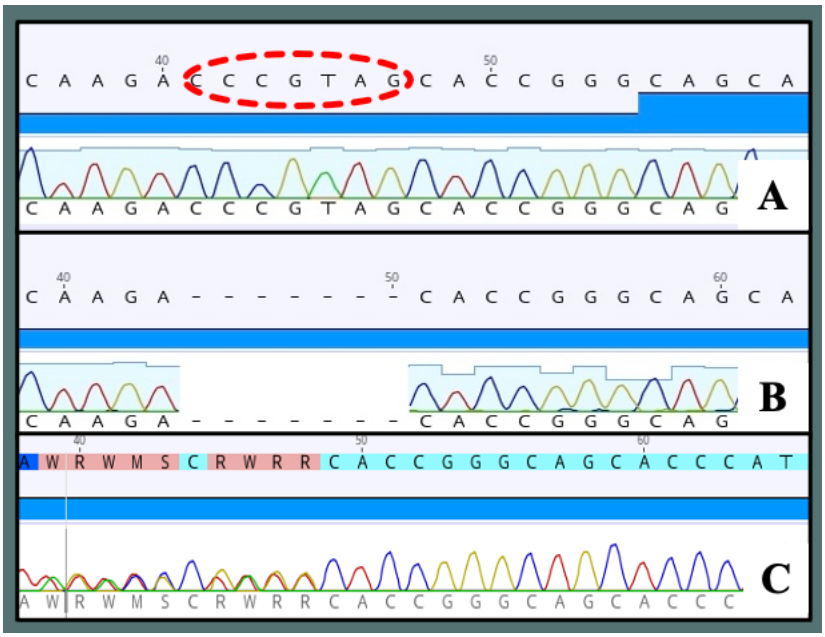

Figure 3. Sanger sequences of *X. laevis dmrt1.S* from individuals with the following genotypes: (A) wildtype (B) homozygous null, and (C) heterozygous. In the reverse sequence read in (C), double peaks can be seen following the deletion; a dotted circle demarcates the deleted region in the mutant allele.

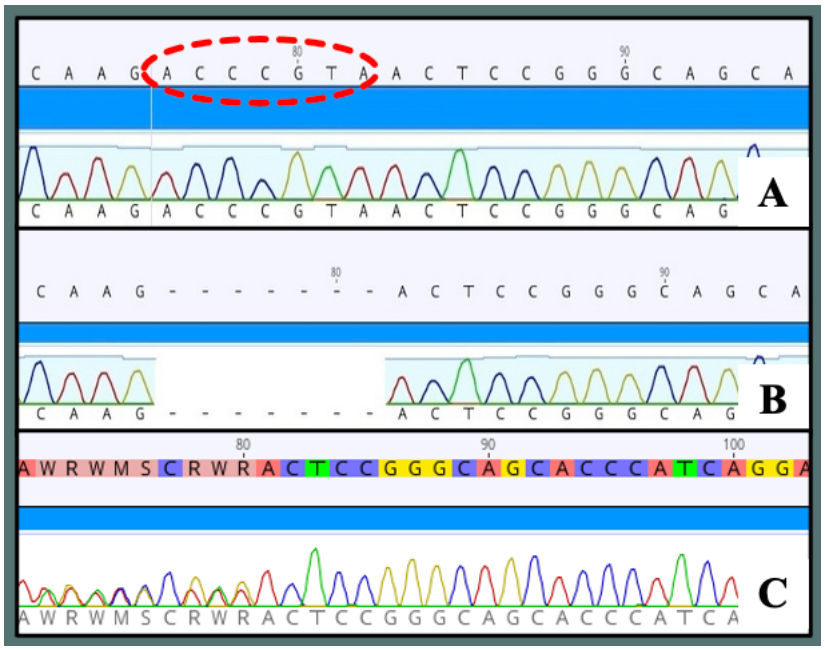

Figure 4. Sanger sequences of *X. laevis dmrt1.L* from individuals with the following genotypes: (A) wildtype (B) homozygous null, and (C) heterozygous. In the reverse read in (C), double peaks can be seen following the deletion. A dotted circle in (A) highlights the deleted region in the mutant allele.

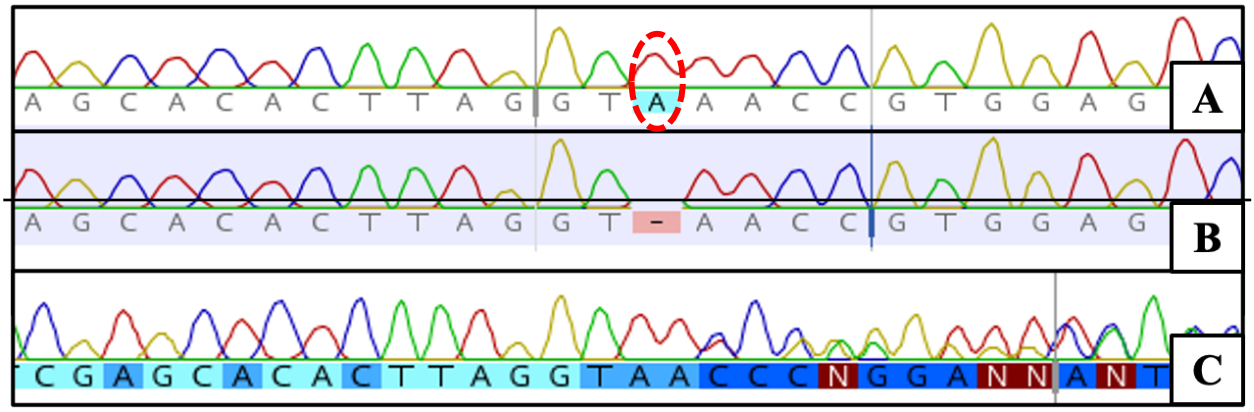

Figure 5. Sanger sequences *X. tropicalis dmrt1* from individuals with the following genotypes (A) wildtype (B) homozygous knockout, and (C) heterozygous. A dotted circle in (A) highlights a single nucleotide deletion present in the mutant allele.

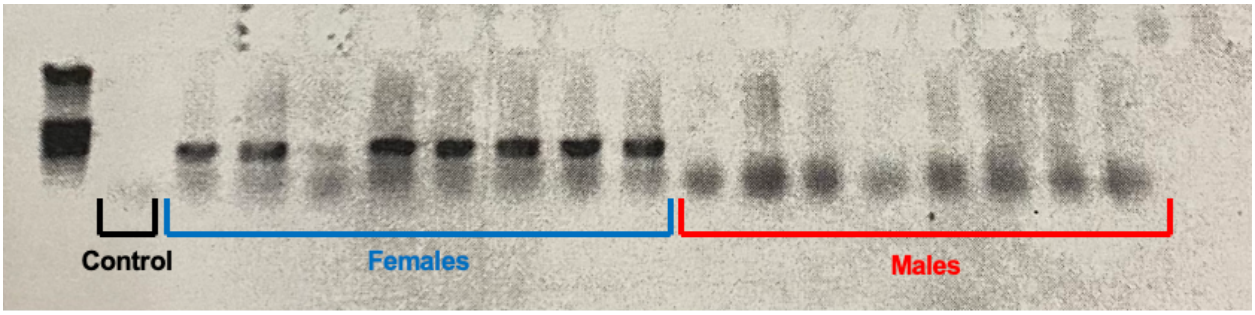

Figure 6. Example female-specific amplifications of individuals from the *dmrt1.L* line. The leftmost lane is a 100-bp ladder, the second column is a negative control with no DNA. The amplicon show here is *dm-w* exon 2.

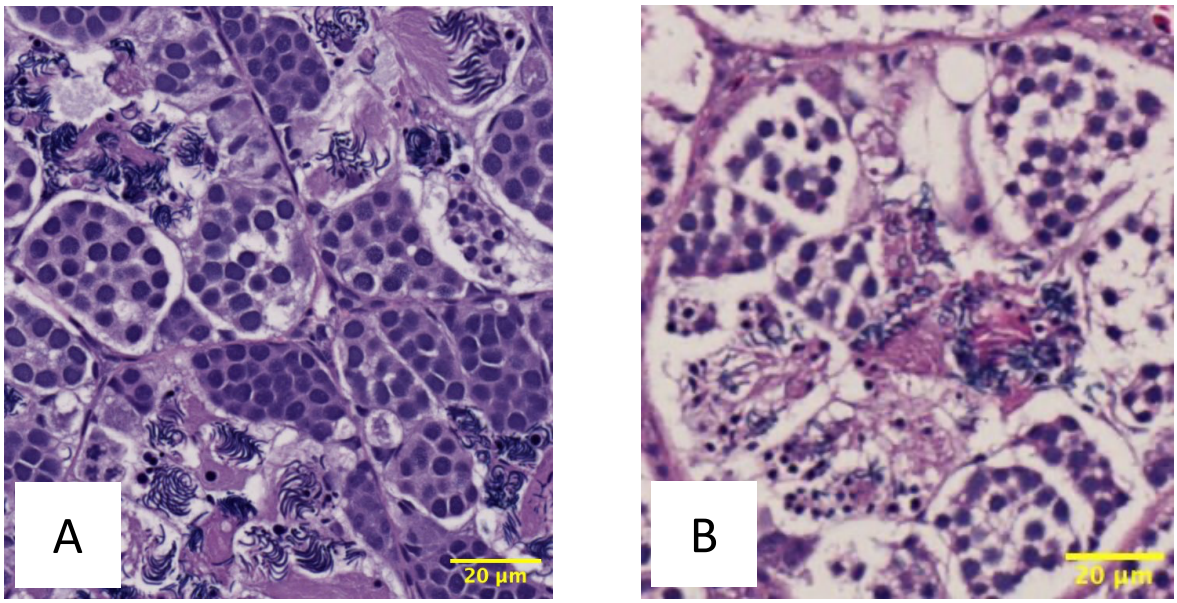

Figure 7. Testis histology of *X. laevis* (A) wildtype and (B) *dmrt1.L* heterozygote individuals. Each image was taken under the 10X objective as indicated by the yellow scale bars representing 20 µm.

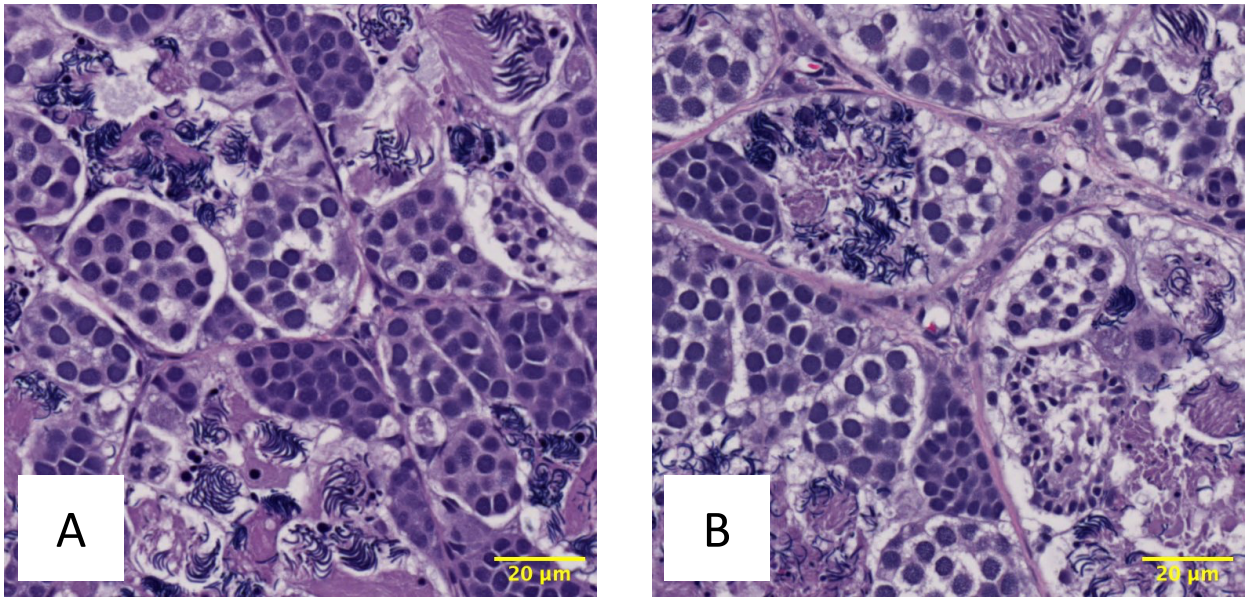

Figure 8. Testis histology from (A) a wildtype male and (B) a stage-matched *dmrt1.S* knockout male. Each image was taken at 10X magnification; yellow scale bars indicate 20 µm.

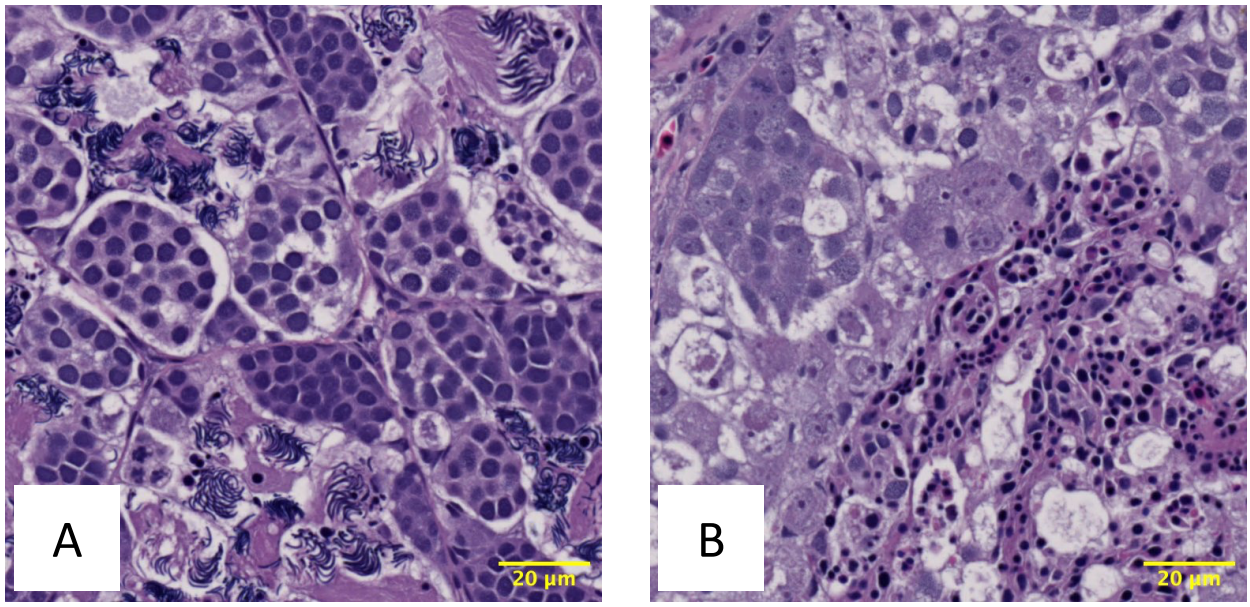

Figure 9. Testis histology of *X. laevis* (A) a wildtype male and (B) a stage-matched a *dmrt1.L* knockout male. Each image was taken at 10X magnification; yellow scale bars indicate 20 µm.

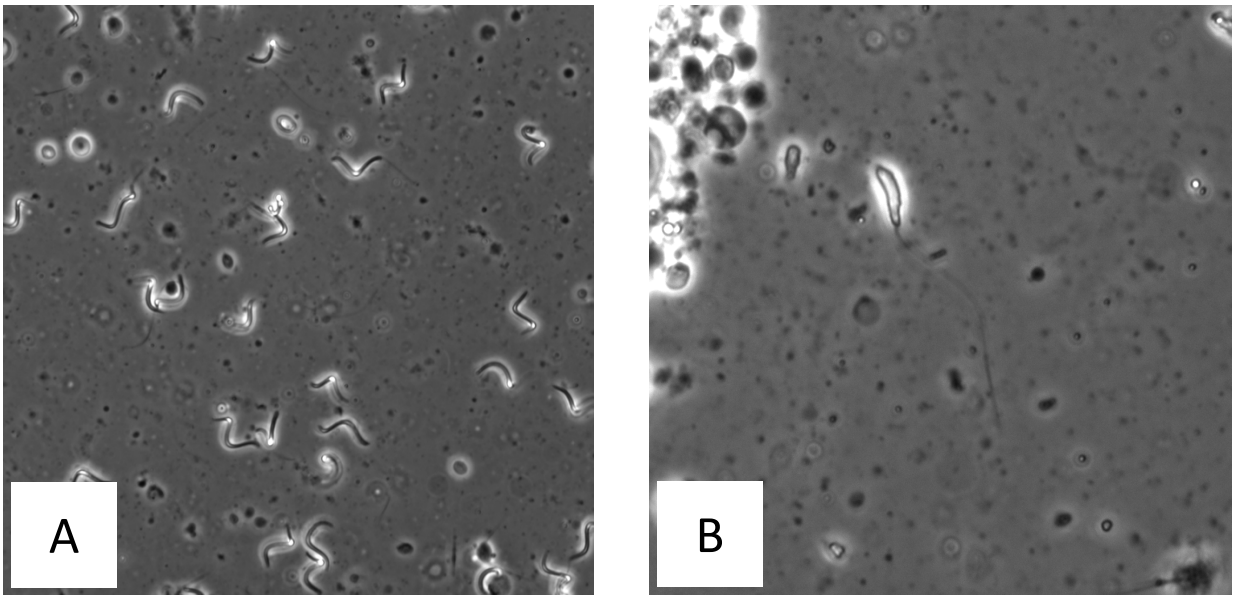

Figure 10. Microscopy of sperm cells taken at 40X with phase contrast for *X. laevis* (A) wildtype and (B) *dmrt1.L* null individuals. Because sperm count was much lower for the null individual, (B) optical zoom was used to highlight structure of an individual sperm cell.

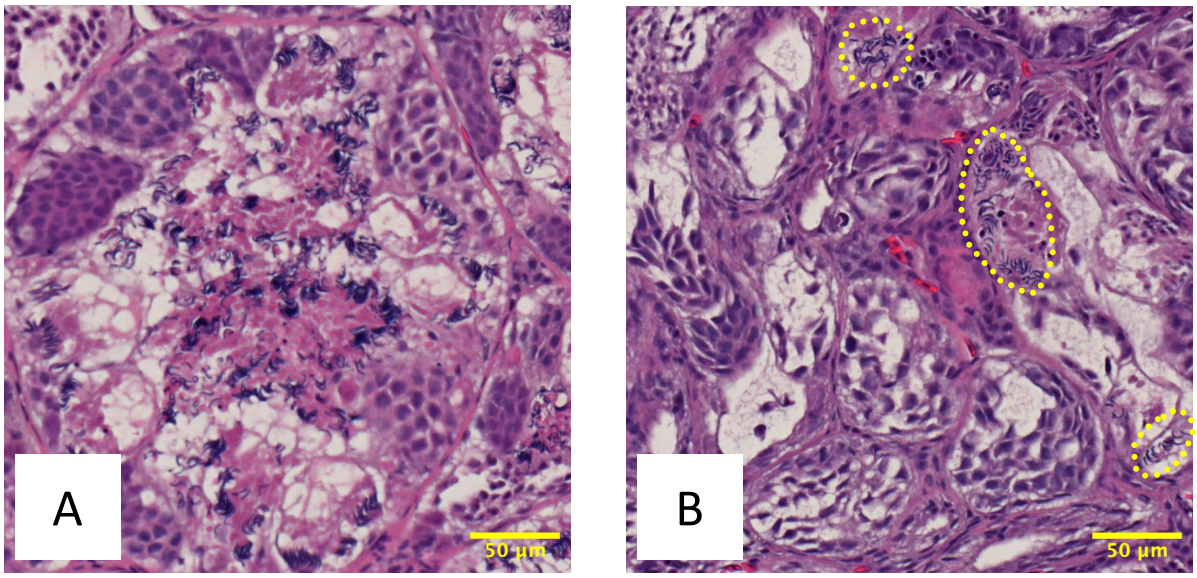

Figure 11. Testis histology from *X. tropicalis* (A) wildtype and (B) *dmrt1* null individuals. Dotted circles indicate small amounts of maturing sperm in (B). The scale bars represent 50 µm under the 10X objective.

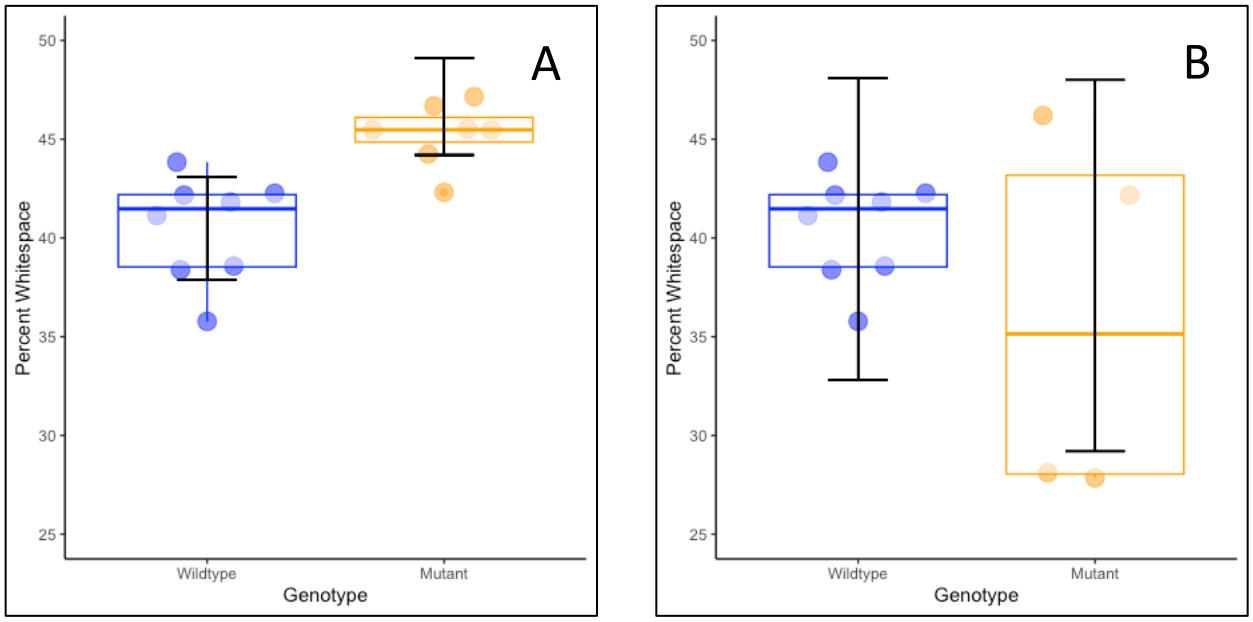

Figure 12. Proportions of whitespace in testis histological cross sections. Comparisons are completed between preparations from (A) wildtype (blue) and *dmrt1.S* knockout (orange) individuals and (B) wildtype (blue) and the *dmrt1.L* knockout (orange) individuals.

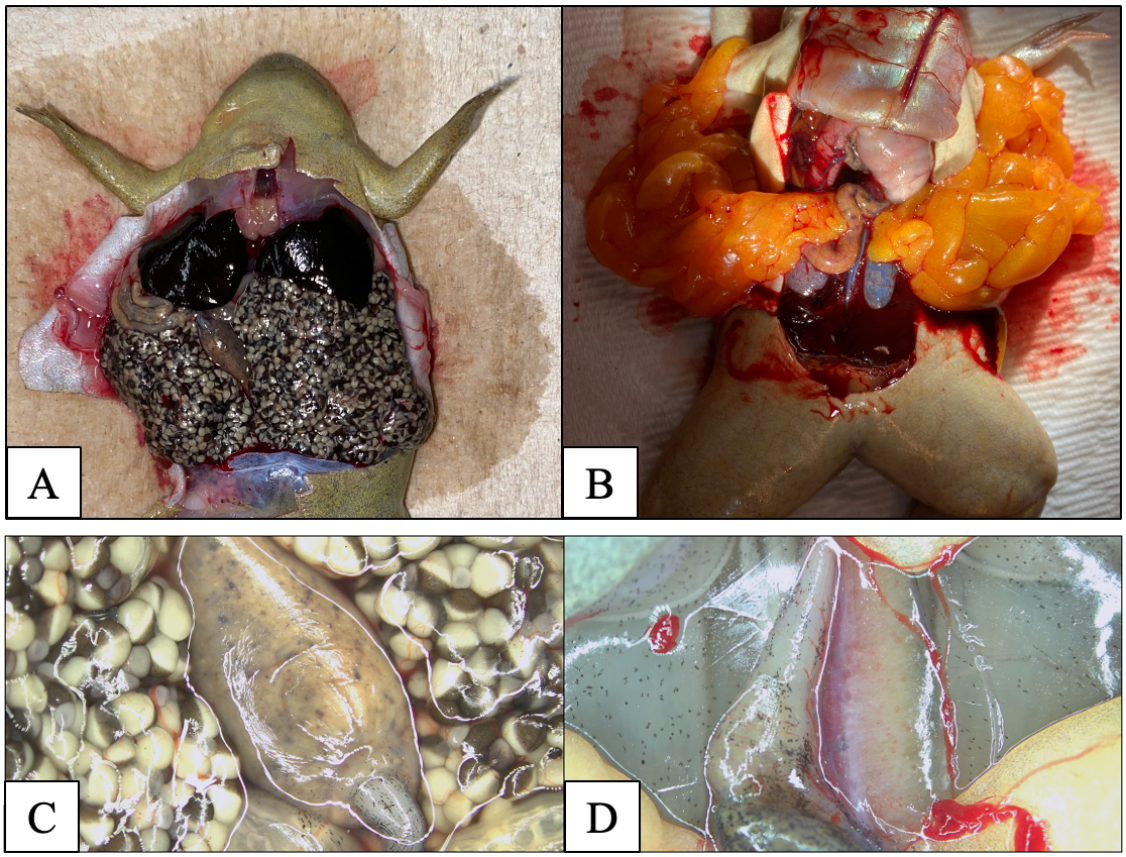

Figure 13. Body cavity of *X. tropicalis* females that are (A&C) wildtype or (B&D) *dmrt1* knockout. In (A&C), black and yellow eggs inside the transparent oviduct are apparent in the lower abdomen below the liver, whereas in (B&D) the body cavity is completely devoid of eggs and oviduct.

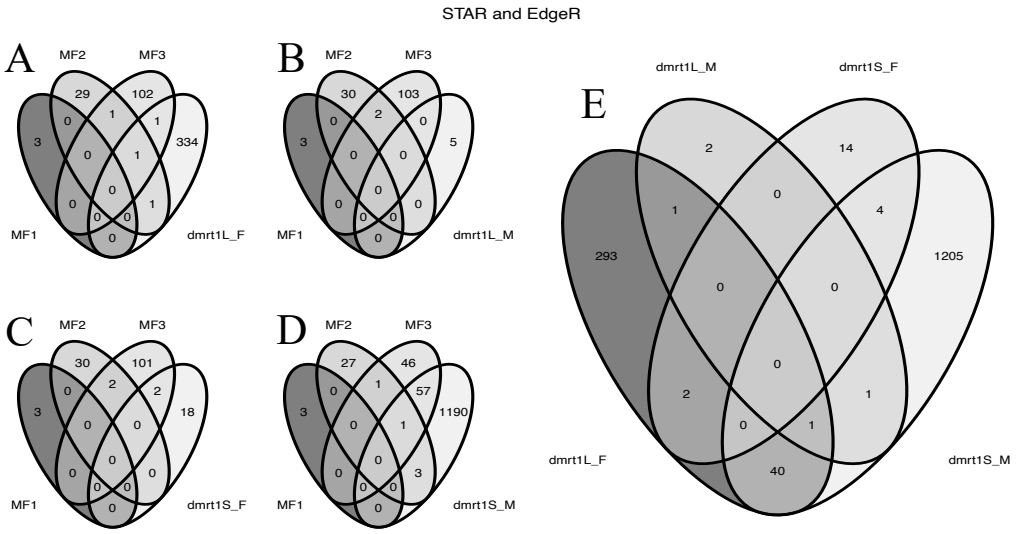

Figure 14. Venn diagrams illustrating the results of the EdgeR analysis using the STAR counts data. Four diagrams on the left illustrate the number of differentially expressed genes each mutant analysis: (A) *dmrt1.L* females (dmrt1L_F), (B) *dmrt1.L* males (dmrt1L_M), (C) *dmrt1.S* females (dmrt1S_F), (D) *dmrt1.S* males (dmrt1S_M) that overlap with the differentially expressed genes from each of three wildtype analyses (MF1, MF2, MF3). The diagram on the right illustrates the number of differentially expressed genes that overlap between the four mutant analyses.

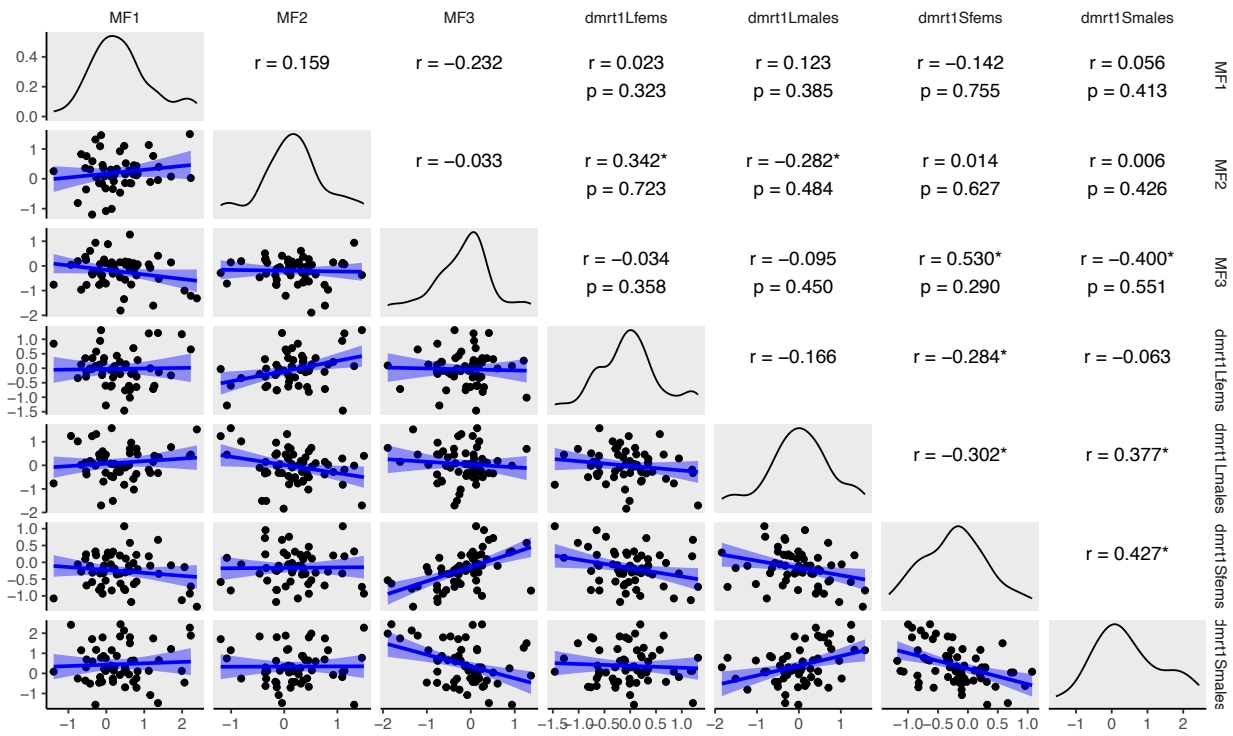

Figure 15. Results of the transcriptome masculinization analysis using EdgeR with STAR count data. Below the diagonal are the pairwise correlations between non-outlier log2 transformed expression ratios of 74 sex related genes for male:female comparisons for the wildtype analyses (x-axis) and mutant:wildtype comparisons for mutant analyses (y axis). Above the diagonal are the Pearson's correlation coefficients with asterisks indicating significant correlations. P values for the permutation tests for the pairwise comparisons between the three wildtype batches (MF1, MF2 and MF3) and the knockout and wildtype analyses (dmrt1Lfems, dmrt1Lmales, dmrt1Sfems and dmrt1Smales) indicate that none of the correlations are more positive or negative than expected by chance.

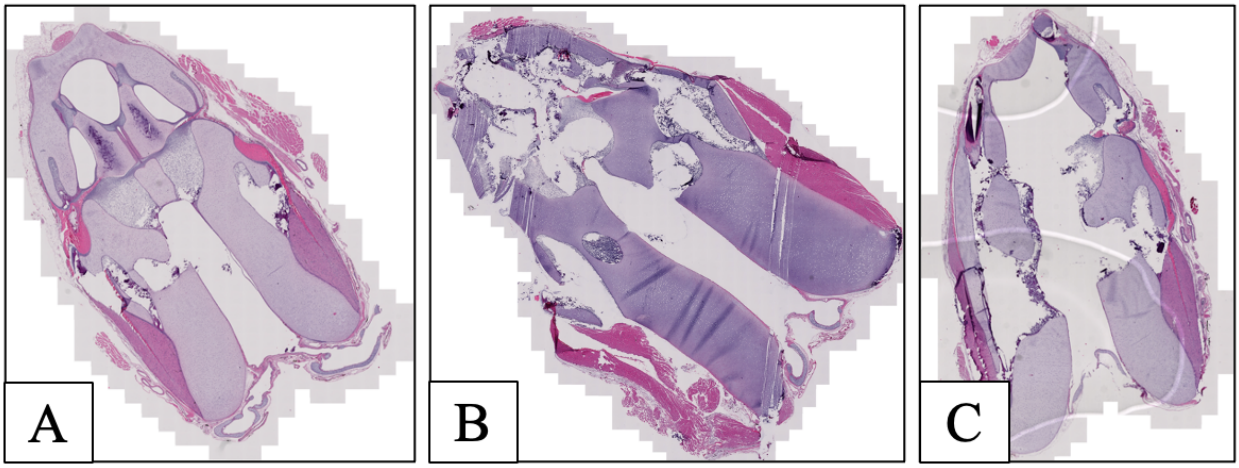

Figure 16. Larynx histology of a wildtype male (A), a *dmrt1.S* null male (B) and a *dmrt1.L* null male (C). Each image was produced by the ZIESS Axioscan 7 slide scanner to take multiple images at 10X magnification which were stitched together to form the comprehensive larynx images.

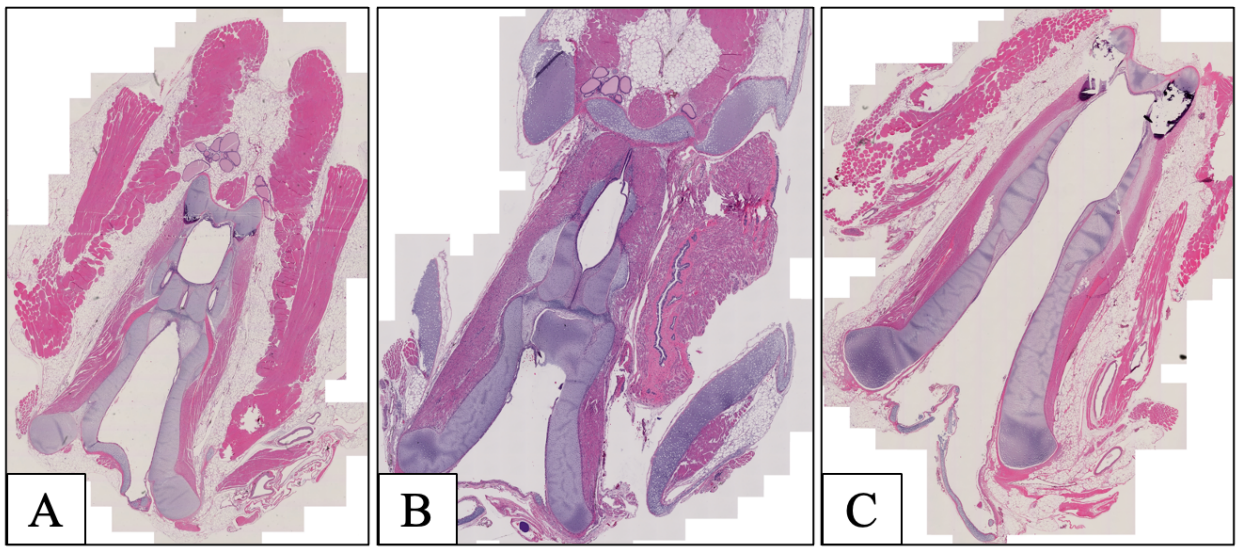

Figure 17. Larynx histology of a wildtype female (A), a *dmrt1.S* null female (B) and a *dmrt1.L* null female (C). Each image was produced by the ZIESS Axioscan 7 slide scanner to take multiple images at 10X magnification which were stitched together to form the comprehensive larynx images.

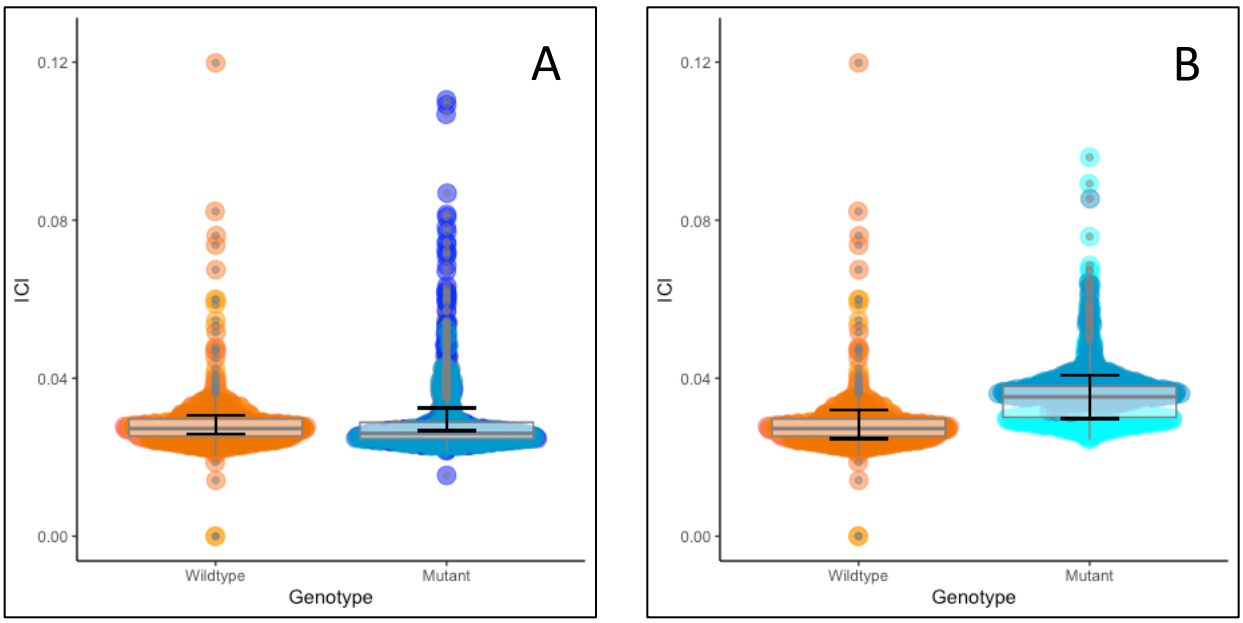

Figure 18. Inter-click-intervals (ICI) coloured by each individual. Comparisons are completed between (A) wildtype (orange) and *dmrt1.S* knockout (blue) individuals and (B) wildtype (orange) and *dmrt1.L* knockout (blue) individuals. The boxplot shows quartiles and the black error bars indicate confidence intervals of the mean ICI for each group.

7 Supplementary Information

Table S1. Summary of histological findings for *dmrt1.S* and *dmrt1.L* null males. The first column shows the pit tag ID belonging to each individual and the second column shows the knockout line each individual belonged to. The third column outlines the number of testes that were present in the individual at the time of dissection. The last column describes whether mature sperm was present in the histology cross sections or if the tissue was lacking sperm.

Individual ID	Gene knockout	Number of Testes	Mature Sperm Present
192F	*Dmrt1.S*	2	Yes
194B	*Dmrt1.S*	2	Yes
197A	*Dmrt1.S*	2	Yes
194A	*Dmrt1.S*	2	Yes
196B	*Dmrt1.S*	2	Yes
1939	*Dmrt1.S*	2	Yes
1880	*Dmrt1.L*	2	No
1929	*Dmrt1.L*	2	No
18A3	*Dmrt1.L*	1	No

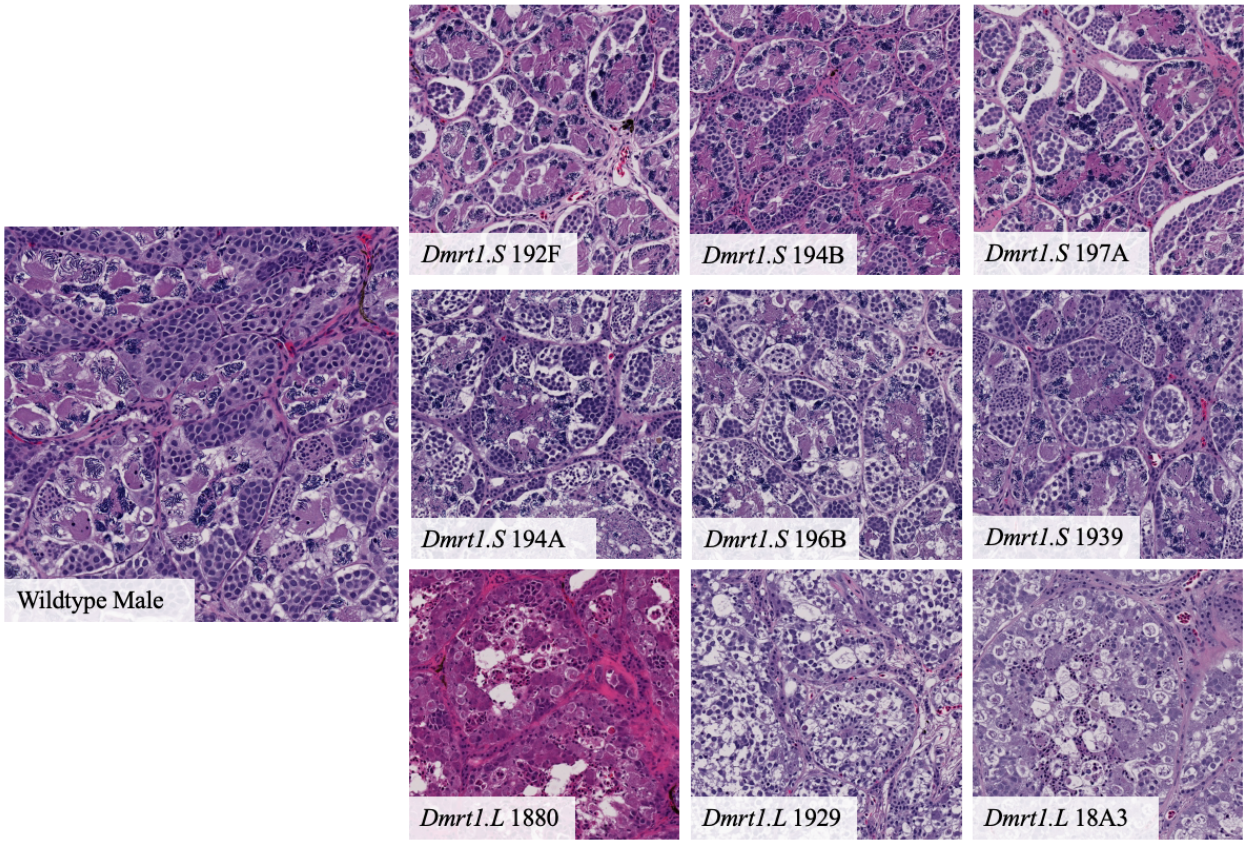

Figure S2. Testis histology from each null male tested compared to a wildtype male. The knockout gene in each individual is indicated in the image label along with the pit tag ID for comparison to Table S1.

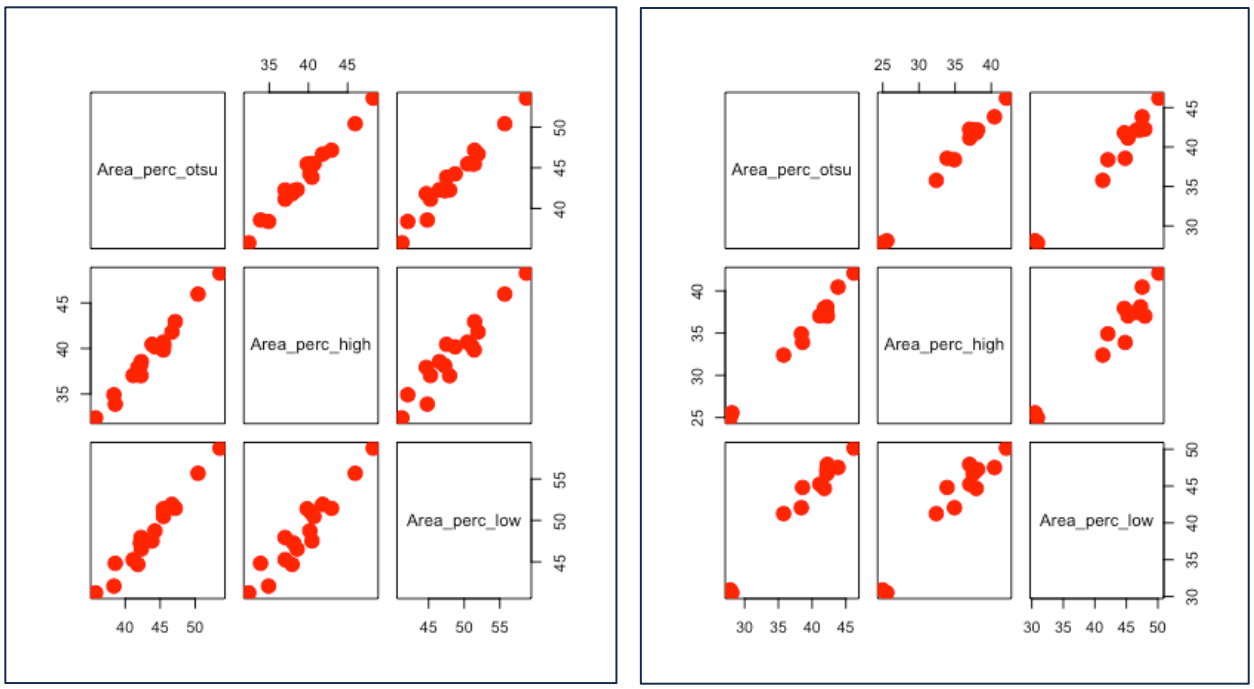

Figure S3. Results of the thresholding checks comparing three different threshold values. (A) Shows the correlation between the three threshold values for each testis image from the *dmrt1.S* analysis. (B) shows the correlation between the different threshold values for the *dmrt1.L* analysis.

Table S4. Significantly differentially expressed transcripts in the mesonephros/gonad of each of three comparisons between wildtype males and females (MF1, MF2, MF3) and each of three comparisons between a knockout line and wildtype siblings (*dmrt1L* females, dmrt1L *males, dmrt1S* females*, dmrt1S* males). Analysis of differential expression were performed using STAR for quantification and two analysis edgeR for analysis of differential expression. The log2 fold change (logFC) and false detection rate P-value is indicated for each significantly differentially expressed gene (FDR). For wildtype comparisons, female expression is the reference and thus the denominator of the log2FC. For mutant comparisons, wildtype expression is the reference and thus the denominator of the log2FC. When identified, the gene acronym of the putative human ortholog is listed (Human).

STAR + EdgeR	GeneID	Gene acronym	logFC	FDR	Human
dmrt1L females					
	XBXL10_1g10280	LOC108709645	1.37553438	0.03715409	–
	XBXL10_1g10352	wsb1.S	1.02490089	0.03334545	WSB1
	XBXL10_1g10365	trmt10c.S	-1.00894598	0.04524353	TRMT10C
	XBXL10_1g10472	LOC108709733	1.97062432	0.01974438	STAG2
	XBXL10_1g10606	rgcc.S	-1.21085569	0.03743264	RGCC
	XBXL10_1g1065	naa16.L	-1.07259823	0.03715409	NAA15
	XBXL10_1g10717	dgka.S	-3.57699335	0.01530346	DGKA
	XBXL10_1g10764	mars1.S	-0.92903779	0.04432002	MARS1
	XBXL10_1g10773	slc26a10.S	1.39753048	0.02012325	SLC26A10
	XBXL10_1g10818	LOC108709885	3.50125435	0.07862648	RAPGEF3
	XBXL10_1g10855	LOC108709904	-2.852749	0.0211413	BMPR2
	XBXL10_1g10981	pdx1.S	-5.36001886	0.07252704	PDX1
	XBXL10_1g11191	serpinh1.S	-1.29479895	0.0557594	SERPINH1
	XBXL10_1g1126	LOC108710167	-1.62244879	0.03157532	ELOVL6
	XBXL10_1g1141	LOC108710290	-5.49481934	0.01561645	ENSG00000287631
	XBXL10_1g11535	LOC121401750	-1.61572686	0.09486475	SNORD3A
	XBXL10_1g12039	vwf.L	-1.44254598	0.04059406	VWF
	XBXL10_1g12063	sqstm1.L	1.13707654	0.08299235	SQSTM1
	XBXL10_1g12357	kiaa1191.L	1.66843786	0.01340317	KIAA1191
	XBXL10_1g12405	LOC108710993	-0.87270697	0.07195131	NHP2
	XBXL10_1g12419	tcp11l2.L	1.49729408	0.00020773	TCP11L2
	XBXL10_1g12677	cav2.L	-1.17691835	0.0321212	CAV2
	XBXL10_1g1274	areg.L	-1.6426697	0.01733631	AREG
	XBXL10_1g12771	hbp1.L	1.61402658	0.00278316	HBP1
	XBXL10_1g12783	pus7.L	-1.10500924	0.01830788	PUS7
	XBXL10_1g12972	LOC108710284	-1.60050606	0.02369815	CRABP1
	XBXL10_1g13213	slc12a1.L	1.12834692	0.09383819	SLC12A1
	XBXL10_1g1324	idua.L	-2.60513646	0.00428155	IDUA
	XBXL10_1g1325	slc26a1.L	-1.83609853	0.02012325	SLC26A2
	XBXL10_1g13378	aldh1a3.L	-2.35815909	0.08807545	ALDH1A3
	XBXL10_1g13550	mat2a.L	-1.30372786	0.02610101	MAT2A
	XBXL10_1g13662	mak16.L	-0.99743833	0.0529964	MAK16
	XBXL10_1g13665	slc18a2.L	-4.27185504	0.05242875	SLC18A1
	XBXL10_1g13703	LOC108711625	1.12455241	0.05359296	–
	XBXL10_1g13756	plpp5.L	-1.0594842	0.09592354	PLPP5
	XBXL10_1g13956	chchd5.L	-1.28660803	0.02440477	–
	XBXL10_1g14108	LOC108711692	2.23641404	0.07663678	–
	XBXL10_1g14123	ppan.L	-1.46369852	0.01036165	PPAN
	XBXL10_1g14255	trmt1.L	-1.4521803	0.03642151	TRMT1
	XBXL10_1g14456	LOC108711757	2.13161753	0.05675096	–
	XBXL10_1g1463	dnaja1.L	-1.15787458	0.00747521	DNAJA1
	XBXL10_1g1464	aptx.L	-1.94258331	5.14E-05	APTX
	XBXL10_1g14988	LOC108712532	-2.83645391	0.00020773	PNPLA2
	XBXL10_1g15045	LOC108712559	1.3829159	0.05009129	TMEM213
	XBXL10_1g15184	lonrf1.S	1.13393566	0.05153857	LONRF3

XBXL10_1g15279	ephx3.S	1.22806601	0.03390803	EPHX4
XBXL10_1g15350	mak16.S	-1.35557827	0.00278316	MAK16
XBXL10_1g15474	fam136a.S	-1.03561347	0.06845068	FAM136A
XBXL10_1g15497	znf703.S	1.2002407	0.06935019	ZNF703
XBXL10_1g15520	kif23.S	1.59697879	0.00883719	KIF23
XBXL10_1g15674	tmc3.S	-5.18945757	0.03696158	TMC3
XBXL10_1g1593	timm10.L	-1.01701105	0.04130092	TIMM10
XBXL10_1g16102	hbp1.S	2.01712365	0.02991123	HBP1
XBXL10_1g16173	LOC108713110	-1.78684183	0.00040325	TFEC
XBXL10_1g1636	plekhj1.L	1.17682103	0.02293806	PLEKHJ1
XBXL10_1g16409	tspan17.S	1.25334077	0.0557594	TSPAN17
XBXL10_1g16443	LOC108712397	3.27252427	0.03642151	HTR4
XBXL10_1g17018	ppan.S	-1.09957721	0.02706136	PPAN
XBXL10_1g1703	LOC121400688	5.07010846	0.03487549	CRYGA
XBXL10_1g17092	raver1.S	1.39243355	0.09944632	RAVER1
XBXL10_1g1740	LOC108695244	2.34662444	0.06668676	–
XBXL10_1g17473	cldn15.1.S	-5.91198663	0.07080675	CLDN15
XBXL10_1g17578	tmem86a.L	1.93002702	0.01974438	TMEM86A
XBXL10_1g17732	cd44.L	1.20091229	0.08526991	–
XBXL10_1g17856	LOC108713799	1.03386488	0.09269563	PPFIBP2
XBXL10_1g18028	polr2l.1.L	-0.86771962	0.06566985	POLR2L
XBXL10_1g1808	polr1e.L	-0.86301388	0.09785107	POLR1E
XBXL10_1g1812	LOC494855	-1.82504473	0.00165337	GRHPR
XBXL10_1g18228	wdr74.L	-1.05103138	0.01064102	WDR74
XBXL10_1g18412	npas4.L	-6.1144557	0.07072374	NPAS4
XBXL10_1g18417	pmt.L	-1.92515401	0.01974438	–
XBXL10_1g18444	zdhhc24.L	-1.04238427	0.02485625	–
XBXL10_1g18597	pdcd2l.L	-0.93946362	0.05588387	PDCD2L
XBXL10_1g18655	aprt.L	-1.06529854	0.03696158	APRT
XBXL10_1g18753	utp4.L	-0.97356749	0.0226726	UTP4
XBXL10_1g18808	klhdc4.L	-1.05619187	0.06402212	KLHDC4
XBXL10_1g18818	mvd.L	-1.79014975	0.00019733	MVD
XBXL10_1g1901	hsd11b1l.L	-1.00940931	0.0529964	DHRS7
XBXL10_1g19141	LOC108714266	-2.60734553	0.04394781	–
XBXL10_1g19202	tspan1.L	1.24711155	0.04968635	TSPAN1
XBXL10_1g1933	LOC108713575	5.12516672	0.03428207	–
XBXL10_1g19451	LOC108714409	-1.33156686	0.02680088	ITPA
XBXL10_1g19458	LOC108714416	-5.75473854	0.0519893	FMO4
XBXL10_1g19719	dbp.L	1.20108229	0.0182674	TEF
XBXL10_1g19766	csf2rb.L	7.29622638	0.02576281	–
XBXL10_1g19785	MGC75753.L	1.16662259	0.04053305	BTG1
XBXL10_1g19842	LOC108714594	1.90861814	0.00516609	SLC38A3
XBXL10_1g19873	acy1.2.L	-1.24592892	0.04497025	ACY1
XBXL10_1g20525	gnl3.L	-0.90861421	0.05177051	GNL3
XBXL10_1g20632	ppp1r14b.S	-1.13366591	0.01265758	PPP1R14B
XBXL10_1g2070	dmrt1.L	-8.57070145	4.88E-09	DMRT1
XBXL10_1g20778	fads1.S	-1.5204348	0.01036165	FADS1
XBXL10_1g20779	fads2.S	-0.85883864	0.05013091	FADS2
XBXL10_1g20797	ins.S	-8.56252374	0.03273451	INS
XBXL10_1g2099	gda.L	-1.56398043	0.00705024	GDA
XBXL10_1g21031	prmt3.S	-0.92870573	0.04576055	PRMT3
XBXL10_1g21060	pik3c2a.S	1.50385321	0.09383819	PIK3C2A
XBXL10_1g2125	psat1.L	-2.30386459	8.68E-05	PSAT1
XBXL10_1g21313	cdh3.S	1.47991188	0.01033697	CDH1
XBXL10_1g21330	LOC108715439	-1.06108013	0.03642151	MPHOSPH6
XBXL10_1g2144	isca1.L	-0.83994482	0.09685989	ISCA1

XBXL10_1g21477	n4bp1.S	1.09815218	0.07252704	N4BP1
XBXL10_1g21548	diras3.S	2.33457101	0.06735624	DIRAS2
XBXL10_1g2157	hsd17b3.L	6.91437381	0.01974438	HSD17B3
XBXL10_1g2160	cdc14b.L	1.36941923	0.04394781	CDC14B
XBXL10_1g22055	tef.S	1.01955181	0.06017849	TEF
XBXL10_1g22105	prkcd.S	1.44423252	0.02293806	PRKCD
XBXL10_1g22113	MGC75753.S	1.3289702	0.02012325	BTG1
XBXL10_1g22170	rrp9.S	-1.16925968	0.04792293	RRP9
XBXL10_1g2222	ngdn.L	-1.28821338	0.00266151	NGDN
XBXL10_1g22233	mrps25.S	-0.98461901	0.03508043	MRPS25
XBXL10_1g22240	chchd4.S	-1.54904732	0.00697965	CHCHD4
XBXL10_1g22256	ruvbl1.S	-1.15827967	0.04087221	RUVBL1
XBXL10_1g2228	LOC108695570	-3.6286929	5.98E-07	CARMIL3
XBXL10_1g22416	LOC108704592	-0.95672511	0.06017849	RPP14
XBXL10_1g2262	LOC121394338	7.63947612	8.96E-05	–
XBXL10_1g22699	coq8a.L	1.29752967	0.05505196	COQ8A
XBXL10_1g22727	trmt61b.L	-1.17761203	0.00923304	TRMT61B
XBXL10_1g22850	pcsk2.L	-7.01898698	4.48E-05	PCSK2
XBXL10_1g22881	LOC108716586	1.39070433	0.05847714	–
XBXL10_1g22948	pygm.L	2.07473628	0.09606051	PYGB
XBXL10_1g23142	rasgrp3.L	1.73257315	0.0557594	RASGRP3
XBXL10_1g23171	c1orf131.L	-1.08092488	0.04780407	C1orf131
XBXL10_1g23218	urb2.L	-1.04401537	0.07252704	URB2
XBXL10_1g2327	abhd4.L	-1.41320694	0.01733631	ABHD4
XBXL10_1g23365	soga3.L	-1.86301704	0.03413628	ENSG00000255330
XBXL10_1g2371	LOC108714907	1.16513896	0.06402212	–
XBXL10_1g2378	LOC121400923	7.04338006	0.01265758	–
XBXL10_1g23781	eif4g1.L	-0.91269115	0.05505196	EIF4G1
XBXL10_1g23907	atp13a5l.2.L	-1.44058882	0.00082583	ATP13A4
XBXL10_1g23913	eif4a2.L	-1.47853594	0.00469183	EIF4A2
XBXL10_1g2399	LOC121394448	6.9014243	0.03313989	–
XBXL10_1g23991	LOC108717013	-1.53636273	0.03157532	CLDN11
XBXL10_1g24021	nmd3.L	-1.02679217	0.04432002	NMD3
XBXL10_1g2433	lpcat4.L	2.6035608	1.48E-08	LPCAT4
XBXL10_1g24512	cyp2e1.L	1.23026892	0.04394781	CYP2C8
XBXL10_1g24557	tdh.L	1.82871964	0.08501819	TDH
XBXL10_1g2479	LOC108715287	-4.09069514	0.01069968	–
XBXL10_1g24817	pcsk2.S	-9.10069674	0.08299235	PCSK2
XBXL10_1g24915	coq8a.S	2.57707589	0.02440477	COQ8A
XBXL10_1g2492	mtfp1.L	-0.9595321	0.02680088	MTFP1
XBXL10_1g2497	castor1.L	1.30836848	0.07676564	CASTOR1
XBXL10_1g25026	socs5.S	1.1451709	0.05371098	SOCS5
XBXL10_1g2504	zmat5.L	-1.78566798	1.41E-09	ZMAT5
XBXL10_1g2514	rhbdd3.L	1.24966231	0.05177051	–
XBXL10_1g2520	ddx54.L	-1.03675009	0.0981115	DDX54
XBXL10_1g25428	LOC108717922	1.88919183	0.07252704	RFX6
XBXL10_1g2546	iscu.L	1.44744621	0.00028297	ISCU
XBXL10_1g2560	gltp.L	1.08736098	0.06668676	GLTP
XBXL10_1g25672	eif4g1.S	-0.97508681	0.06309594	EIF4G1
XBXL10_1g25840	slc2a2.S	-1.74810617	0.03987715	SLC2A2
XBXL10_1g25917	gmps.S	-0.86681621	0.09270546	GMPS
XBXL10_1g2602	prodh.L	1.49244208	0.05505196	PRODH
XBXL10_1g26083	neu4.S	-4.76873891	0.01974438	NEU4
XBXL10_1g2626	srsf9.L	2.05239147	4.88E-09	SRSF9
XBXL10_1g2628	dynll1.L	-1.01114081	0.02021256	DYNLL1
XBXL10_1g2629	coq5.L	0.95858786	0.08847322	COQ5

XBXL10_1g2631	LOC108716019	4.90198836	0.00502795	–
XBXL10_1g2633	cabp1.L	-1.97736211	0.05867243	CABP1
XBXL10_1g2640	c12orf43.L	-1.31589015	0.00428659	C12orf43
XBXL10_1g2644	patz1.L	-2.15865029	9.07E-06	PATZ1
XBXL10_1g2649	LOC108716024	-2.52537944	0.05013091	–
XBXL10_1g2655	gnaz.L	2.25328251	0.02012325	GNAZ
XBXL10_1g2669	klhl22.L	1.47686269	0.08794791	KLHL22
XBXL10_1g26705	LOC121394525	-2.16778218	0.01580076	–
XBXL10_1g2673	ddt.L	-3.58536095	1.90E-17	–
XBXL10_1g26832	crem.L	1.30498132	0.07862648	CREM
XBXL10_1g2684	slc2a11.2.L	-1.84240494	0.00052205	–
XBXL10_1g26933	cyp51a1.L	-1.92652748	0.04338532	CYP51A1
XBXL10_1g2697	LOC121394822	-7.82935722	1.76E-05	–
XBXL10_1g2698	LOC108695663	-3.90432041	0.01733631	–
XBXL10_1g27041	LOC108718861	-1.19649493	0.06638616	–
XBXL10_1g2716	ppm1f.L	1.12611209	0.02684532	PPM1E
XBXL10_1g2736	LOC108716056	5.4451397	0.02653361	COMT
XBXL10_1g2742	trmt2a.L	-1.70535766	0.01737011	TRMT2A
XBXL10_1g27624	LOC734523	-0.87964526	0.07262449	PAK1IP1
XBXL10_1g27640	LOC108718740	2.11991224	0.00019733	ARPC3
XBXL10_1g27645	ranbp9.L	1.08142313	0.05454868	RANBP9
XBXL10_1g2769	stx2.L	1.28730843	0.02576281	STX2
XBXL10_1g27803	lrrc30.L	-1.91747142	0.03334545	LRRC30
XBXL10_1g2782	bri3bp.L	-1.31643916	0.01974438	BRI3BP
XBXL10_1g2783	dhx37.L	-1.27152386	0.02847882	DHX37
XBXL10_1g27887	dsc3.L	-4.53092679	0.02576281	DSCAS
XBXL10_1g27923	LOC108719245	-4.11039564	0.06866673	–
XBXL10_1g28173	polr2k.L	-0.93394035	0.04497025	POLR2K
XBXL10_1g28200	LOC108719356	-1.92949611	0.00013203	MTERF3
XBXL10_1g2861	hvcn1.L	-2.70735242	7.80E-09	HVCN1
XBXL10_1g28856	cyp51a1.S	-2.03318809	0.06143215	CYP51A1
XBXL10_1g2886	tesc.L	-1.000534	0.02813725	TESC
XBXL10_1g2921	hint1.L	0.86785921	0.09685989	HINT1
XBXL10_1g29225	nsun2.S	-1.17546149	0.01974438	NSUN2
XBXL10_1g29234	znf622.S	-0.95453767	0.06845068	ZNF622
XBXL10_1g29495	LOC108719724	-2.99977606	0.06600333	OSBPL1A
XBXL10_1g2953	hsd17b4.L	-1.10946917	0.01733631	HSD17B4
XBXL10_1g29536	LOC108719729	1.64286736	0.02270144	PCMTD1
XBXL10_1g29585	rrs1.S	-1.08956017	0.0881544	RRS1
XBXL10_1g29690	polr2k.S	-0.90898483	0.0405286	POLR2K
XBXL10_1g29700	nipal2.S	-2.20686606	0.06102189	NIPAL2
XBXL10_1g29792	fer1l6.S	-4.76333027	0.07174852	FER1L6
XBXL10_1g2982	wdr36.L	-0.93991096	0.05371098	WDR36
XBXL10_1g29903	bop1.S	-1.22098225	0.03117853	BOP1
XBXL10_1g29947	LOC108695976	-2.61607496	0.00985634	TRPV6
XBXL10_1g30010	dusp5.L	2.13871087	0.06735624	DUSP5
XBXL10_1g30118	emg1.L	-1.18560252	0.01036165	EMG1
XBXL10_1g30180	nop2.L	-1.18232237	0.07473367	NOP2
XBXL10_1g30361	pdcd11.L	-1.56487073	0.01265758	PDCD11
XBXL10_1g30384	LOC121395350	-4.68621932	1.58E-08	SFXN2
XBXL10_1g30420	npm3.L	-1.43710548	0.00117729	–
XBXL10_1g30598	pla2g12b.L	1.57697401	0.0864285	PLA2G12B
XBXL10_1g30619	scd.L	-1.39993828	0.01096837	SCD5
XBXL10_1g32239	ubxn10.L	1.61374661	0.03053562	–
XBXL10_1g32260	mrto4.L	-1.42754787	6.89E-05	MRTO4
XBXL10_1g3227	hmgcs1.L	-2.38185921	0.02293806	HMGCS1

XBXL10_1g32437	emg1.S	-1.03325854	0.04432002	EMG1
XBXL10_1g32496	papss2.S	-1.15307054	0.03487549	PAPSS2
XBXL10_1g32508	LOC121396194	-1.28419551	0.04784897	–
XBXL10_1g32559	eef1akmt2.S	-1.23311567	0.03157532	EEF1AKMT2
XBXL10_1g32729	noc3l.S	-1.13830475	0.05505196	NOC3L
XBXL10_1g32753	slc16a12.S	1.36949005	0.01974438	SLC16A12
XBXL10_1g32858	scd.S	-1.41049883	0.01561645	SCD5
XBXL10_1g33273	sc5d.S	-1.9709713	0.0226726	SC5D
XBXL10_1g33549	per3.S	1.63304092	0.02021256	PER3
XBXL10_1g33705	prmt1.S	-1.07226316	0.01530346	PRMT1
XBXL10_1g33796	LOC108697833	-1.72429393	0.07195131	–
XBXL10_1g33866	LOC108705051	1.6271913	0.01649442	CMKLR1
XBXL10_1g33927	fbl.S	-1.48002784	0.01143093	FBL
XBXL10_1g34373	LOC121396868	-1.30445041	0.00747521	–
XBXL10_1g3456	LOC121396193	-1.62456544	0.01327864	–
XBXL10_1g3484	ca9.L	-5.35484765	0.0529964	MEF2C
XBXL10_1g35261	polr1d.2.L	-1.16598207	0.00428155	POLR1D
XBXL10_1g35265	nsdhl.L	-1.15442302	0.03987715	NSDHL
XBXL10_1g35301	hprt1.L	-0.99500417	0.03715409	HPRT1
XBXL10_1g35618	exosc5.L	-0.85215104	0.08807545	EXOSC5
XBXL10_1g35906	slc25a29.L	2.50205276	0.04056777	SLC25A29
XBXL10_1g35916	LOC108698781	-1.28147466	0.01974438	HSP90AA1
XBXL10_1g35938	trmt61a.L	-0.95445756	0.05454868	TRMT61A
XBXL10_1g36169	coch.L	-5.30412373	0.08307169	COCH
XBXL10_1g36511	LOC108699570	-3.79805577	0.04394781	–
XBXL10_1g36512	LOC108699569	-5.13584619	0.03715409	–
XBXL10_1g36793	LOC121397221	2.13686414	0.03987715	–
XBXL10_1g37270	slc25a29.S	1.81105221	0.01265758	SLC25A29
XBXL10_1g37310	LOC108699795	4.09673801	0.05505196	GPR68
XBXL10_1g3737	sel1l3.S	3.82214869	0.03436247	SEL1L3
XBXL10_1g37400	ahsa1.S	-1.09771397	0.07862648	AHSA1
XBXL10_1g37750	tmem268.S	1.23620123	0.07195131	–
XBXL10_1g37772	ssr4.S	-0.88800232	0.04780407	SSR4
XBXL10_1g37924	LOC121397625	-1.41541402	0.01974438	XIAPP3
XBXL10_1g37997	LOC108700113	-1.89036495	0.00867124	PCDH19
XBXL10_1g38199	gpr4.S	1.69407121	0.07252704	–
XBXL10_1g38321	agbl5.S	2.18918865	0.05443389	AGBL5
XBXL10_1g38413	timm50.S	-0.8723761	0.06221703	TIMM50
XBXL10_1g38552	LOC108705648	-2.32239505	0.02576281	ITLN2
XBXL10_1g38553	LOC121397554	-4.02434738	0.07195131	–
XBXL10_1g38668	LOC108700366	3.90260307	0.07195131	CIART
XBXL10_1g38960	LOC108700761	2.79483563	0.02813725	KRT222
XBXL10_1g38964	igfbp4.L	-1.37537594	0.0211413	IGFBP4
XBXL10_1g3907	ppid.S	-0.89912013	0.09944632	PPID
XBXL10_1g39423	pcmtd2.L	1.25179588	0.01974438	PCMTD2
XBXL10_1g39677	LOC108701784	6.82984176	0.01558763	ABCA9
XBXL10_1g3968	ucp1.S	2.27056873	0.0881544	UCP3
XBXL10_1g39756	LOC108701789	1.06250771	0.02706136	BECN1
XBXL10_1g39760	utp18.L	-1.31239528	0.00211549	UTP18
XBXL10_1g40029	LOC108701807	-5.22808377	0.02152355	–
XBXL10_1g40357	utp6.L	-0.9623437	0.07077487	UTP6
XBXL10_1g40387	sctr.L	-6.39651533	0.03642151	SCTR
XBXL10_1g40400	LOC108701824	-5.69701295	0.03047316	PARP14
XBXL10_1g40430	slc49a4.L	1.61216177	0.08807545	SLC49A4
XBXL10_1g40486	XB5760632.L	-1.24403803	0.03487549	–
XBXL10_1g40670	fastkd1.L	-1.34435971	0.06380675	FASTKD1

XBXL10_1g40804	trpm8.L	-6.47450001	0.03696158	TRPM8
XBXL10_1g40885	wdr12.L	-1.52900005	7.60E-06	WDR12
XBXL10_1g41040	eef2kmt.L	-1.07189191	0.03642151	EEF2KMT
XBXL10_1g41148	zfand2a.L	-1.4149429	0.07077487	ZFAND2A
XBXL10_1g41178	nptx2.L	-6.2878112	0.0321212	NPTX2
XBXL10_1g41261	ears2.L	-0.84435027	0.09511788	EARS2
XBXL10_1g41430	pemt.L	-1.12071278	0.01997733	PEMT
XBXL10_1g41603	bicdl2.L	1.78075831	0.01830788	–
XBXL10_1g41847	LOC108703857	-4.63168217	0.0881544	URGCP
XBXL10_1g42010	LOC108703776	5.28886834	0.01974438	ZNF180
XBXL10_1g42243	fbxl20.S	1.22010987	0.07080675	FBXL20
XBXL10_1g42430	dcaf7.S	2.04856878	0.05997663	DCAF7
XBXL10_1g42455	hnf4a.S	1.4771953	0.07252704	HNF4A
XBXL10_1g42843	nbr1.S	1.38332814	0.06402212	NBR1
XBXL10_1g42942	fam83d.S	1.89824114	0.0662378	FAM83D
XBXL10_1g4325	dnaja1.S	-1.23464802	0.00066059	DNAJA1
XBXL10_1g43256	ddx18.S	-0.98496616	0.07252704	DDX18
XBXL10_1g43265	tmem37.S	-1.22121408	0.03053562	TMEM37
XBXL10_1g43371	prkag3.S	-1.47755797	0.09347337	PRKAG3
XBXL10_1g43448	upp2.S	3.11100744	0.00020773	UPP2
XBXL10_1g43494	sp5.S	6.5853198	0.02492259	SP3
XBXL10_1g43573	lss.S	-1.78098214	0.00020009	LSS
XBXL10_1g43660	wdr12.S	-1.68356294	0.00106792	WDR12
XBXL10_1g43664	nop58.S	-1.10253986	0.03313989	NOP58
XBXL10_1g43710	wdr75.S	-1.33066687	0.03696158	WDR75
XBXL10_1g438	nat8.3.L	-3.39344572	0.06735624	NAT8
XBXL10_1g439	nat8.2.L	-1.46306511	0.05505196	–
XBXL10_1g43903	aimp2.S	-1.28683105	0.01561645	AIMP2
XBXL10_1g4400	polr2e.S	-1.01286613	0.03596326	POLR2E
XBXL10_1g44074	LOC121399076	-1.60319071	0.06921766	–
XBXL10_1g44083	XB5962511.S	3.17933145	0.07578132	GALR2
XBXL10_1g458	cyp26b1.L	1.96479638	0.00089519	CYP26B1
XBXL10_1g4900	psat1.S	-1.00429668	0.08987337	PSAT1
XBXL10_1g5270	mmp11.S	3.20402693	0.03487549	MMP11
XBXL10_1g5358	ddx55.S	-0.98968324	0.07916623	DDX55
XBXL10_1g5427	nos1.S	-4.74433338	0.0355608	NOS1
XBXL10_1g5465	LOC108707195	4.91705094	0.08807545	C5orf63
XBXL10_1g5594	utp15.S	-0.86402501	0.08807545	UTP15
XBXL10_1g568	smyd1.L	-2.42402863	0.07268852	SMYD1
XBXL10_1g569	LOC108696295	-1.39345914	0.00545103	FABP1
XBXL10_1g5761	hmgcs1.S	-2.25593206	0.06668676	HMGCS1
XBXL10_1g5935	LOC121399557	-4.77506367	0.03715409	TRIM65
XBXL10_1g6529	tsr1.L	-1.32763985	0.03157532	TSR1
XBXL10_1g6672	abhd15.L	-1.57450632	0.0226726	ABHD15
XBXL10_1g6901	ctps1.L	-1.36750219	0.02039876	CTPS1
XBXL10_1g7050	znhit3.L	-0.98063966	0.0865029	–
XBXL10_1g7250	LOC108708226	-1.23129486	0.08847322	–
XBXL10_1g7431	LOC108707516	-1.06867974	0.09627439	–
XBXL10_1g7640	wsb1.L	1.15638918	0.01580076	WSB1
XBXL10_1g7831	LOC108708464	-1.30837297	0.06017849	SLC10A2
XBXL10_1g7850	zic5.L	6.21139118	0.04497025	ZIC5
XBXL10_1g8122	mars1.L	-1.11204319	0.01733631	MARS1
XBXL10_1g8166	mettl1.L	-1.32402832	0.01295498	METTL1
XBXL10_1g8218	rapgef3.L	4.98650087	0.01974438	RAPGEF3
XBXL10_1g8707	slco2b1.L	1.50230531	0.03157532	SLCO2B1
XBXL10_1g8729	xdm-w	-1.90461153	0.03487549	DMRT1

	XBXL10_1g8981	LOC108708847	-4.97506331	0.04087221	RTN4RL1
	XBXL10_1g899	LOC108698820	-2.0494665	0.00018815	TENM3
	XBXL10_1g9018	trarg1.S	-4.22167716	0.01552213	TRARG1
	XBXL10_1g9109	usp16.S	-2.01129689	0.05847714	USP16
	XBXL10_1g9289	rrp1b.S	-1.10658466	0.02293806	RRP1B
	XBXL10_1g9312	wdr4.S	-1.09050315	0.01265758	WDR4
	XBXL10_1g9549	ngf.S	-1.28158646	0.08878044	NGF
	XBXL10_1g9729	bysl.S	-1.40098011	0.00014505	BYSL
	XBXL10_1g9888	LOC108709510	-1.68431277	0.00040325	PLCXD2
	XBXL10_1g9892	LOC108709511	-5.10771649	0.00010032	–
	XBXL10_1g9902	LOC108709514	1.26383722	0.0557594	–
	XBXL10_1g9966	rcc1.S	-1.54377361	0.03413628	RCC1
dmrt1L males					
	XBXL10_1g10081	LOC108708928	5.17601357	0.00011736	TRIM5
	XBXL10_1g12137	dnd1.L	2.25964299	0.00512753	DND1
	XBXL10_1g2697	LOC121394822	-3.66517532	0.0530821	–
	XBXL10_1g2861	hvcn1.L	-1.69256899	0.00512753	HVCN1
	XBXL10_1g4144	herc6.S	2.0836401	0.09139719	HERC3
dmrt1S females					
	XBXL10_1g15119	ano2.S	-4.7626911	0.00743935	ANO2
	XBXL10_1g15231	cd74.S	1.22172219	0.09080953	–
	XBXL10_1g2253	LOC108714884	1.55106009	0.00743935	IGHV3OR16-13
	XBXL10_1g2283	LOC121394372	2.65153017	0.08840626	–
	XBXL10_1g2691	XB5865341.S	2.3659337	0.09080953	–
	XBXL10_1g29991	LOC121395800	-5.03568469	0.00608725	–
	XBXL10_1g31480	LOC108696640	-5.46151501	0.01623575	–
	XBXL10_1g31674	cd79a.L	1.74054637	0.07023516	CD79A
	XBXL10_1g3450	LOC108719144	1.83317802	0.07023516	–
	XBXL10_1g35418	XB5827395.L	1.26771308	0.09080953	HLA-DRB1
	XBXL10_1g35916	LOC108698781	-2.0944146	0.00743935	HSP90AA1
	XBXL10_1g36783	LOC121397218	3.05043434	0.09080953	–
	XBXL10_1g39458	tnfrsf6b.L	-3.33528727	0.09080953	RYR1
	XBXL10_1g41148	zfand2a.L	-3.10222166	0.09080953	ZFAND2A
	XBXL10_1g42135	LOC121398165	1.22688694	0.09080953	–
	XBXL10_1g4787	ttc39b.S	-5.1925464	0.01955776	TTC39B
	XBXL10_1g4804	LOC108706955	-2.35503241	0.00685273	–
	XBXL10_1g4846	LOC108706960	4.68043218	0.00743935	–
	XBXL10_1g551	LOC108697575	2.16799718	0.00743935	IGKV3-15
	XBXL10_1g6378	pir.L	-1.73167247	0.01013162	PIR
dmrt1S males					
*** mtDNA	XBmRNA83514		0.86103316	0.05270507	–
*** mtDNA	XBmRNA83526		0.9709033	0.08703685	–
	XBXL10_1g10010	XB5907626.S	1.46795855	0.01888028	–
	XBXL10_1g10042	psmb2.S	-0.76961264	0.06771662	PSMB2
	XBXL10_1g10048	znf706l.S	-0.92498018	0.0400308	ZNF706
	XBXL10_1g10052	dlgap3.S	5.93253364	0.01532462	DLGAP3
	XBXL10_1g10077	cited4.S	-1.75022951	0.00159012	CITED2
	XBXL10_1g10104	LOC108709579	-1.01355443	0.02582152	TOR2A
	XBXL10_1g1016	smad1.L	0.65474809	0.07843314	SMAD1
	XBXL10_1g10220	nle1.S	-1.18922174	0.01345414	NLE1
	XBXL10_1g10230	mmp28.S	-1.10558571	0.01258341	MMP28
	XBXL10_1g10236	srrm3.S	3.21755465	0.08353974	SRRM3
	XBXL10_1g10323	ube2g1.S	-0.89082211	0.00997873	UBE2G1

XBXL10_1g10470	jade3.S	-0.86781031	0.08760058	JADE3
XBXL10_1g10477	atp4b.S	3.14633321	0.08199359	ATP4B
XBXL10_1g10493	sox1.S	4.97129627	0.01377495	SOX1
XBXL10_1g10505	LOC108708968	5.54180345	0.08530951	LIG4
XBXL10_1g10546	LOC108709757	-1.46734943	0.05899301	ABCC4
XBXL10_1g10565	ednrb.S	1.2264816	0.07843314	EDNRB
XBXL10_1g10568	LOC108709769	1.59988522	0.02437716	SCEL
XBXL10_1g10574	uchl3.S	-0.84837464	0.04618132	UCHL3
XBXL10_1g10584	mzt1.S	-0.95963973	0.04151686	–
XBXL10_1g10593	pcdh17.S	2.18377052	0.03384704	PCDH17
XBXL10_1g10643	lpar6.S	-0.98946297	0.03452135	LPAR6
XBXL10_1g10683	dnajc22.S	-1.12154319	0.01895304	DNAJC22
XBXL10_1g10703	myl6.S	-0.97882557	0.00626312	MYL6
XBXL10_1g10783	cyp27b1.S	5.64213626	0.03228289	CYP27B1
XBXL10_1g10799	galnt6.2.S	3.75221856	0.05519435	GALNT6
XBXL10_1g10800	tankl.S	-1.38666272	0.03784531	–
XBXL10_1g10804	LOC496010	-0.75941422	0.08337501	METTL7A
XBXL10_1g10822	LOC108709888	-1.94679419	0.00018295	–
XBXL10_1g10869	krt8.1.S	1.22438797	0.00410253	KRT8
XBXL10_1g10880	krt7.S	1.84988043	0.00021169	KRT8
XBXL10_1g10932	frem2.S	0.9008795	0.08428086	FREM2
XBXL10_1g10938	alg5.S	-0.73694333	0.07714323	ALG5
XBXL10_1g11025	mmp13.S	-1.06471952	0.07346202	MMP3
XBXL10_1g11112	LOC108710022	2.95931602	0.08214895	GRM5
XBXL10_1g1117	LOC108710147	1.57084102	0.0747306	COL25A1
XBXL10_1g11191	serpinh1.S	1.09414453	0.0939586	SERPINH1
XBXL10_1g11225	ucp2.S	-1.14702015	0.00151178	UCP2
XBXL10_1g11242	slco2b1.S	2.95173003	0.00410253	SLCO2B1
XBXL10_1g1126	LOC108710167	-0.97043967	0.08987188	ELOVL6
XBXL10_1g1127	egf.L	2.62470454	0.05588336	EGF
XBXL10_1g11301	LOC108710093	1.10803843	0.08428086	–
XBXL10_1g11302	trim39l.1.S	1.3575819	0.08337501	ENSG00000267801
XBXL10_1g11373	LOC108710708	-2.20901055	0.00364826	INTS13
XBXL10_1g11376	cyb5r3.L	1.80465092	0.00126033	CYB5R3
XBXL10_1g11390	LOC121401119	4.1458194	0.05721626	MED21
XBXL10_1g11405	mcat.L	-0.70819555	0.06806062	MCAT
XBXL10_1g11497	XB5891636.L	3.47081687	0.04262417	–
XBXL10_1g1150	LOC108710474	3.84264952	0.04454243	NDST3
XBXL10_1g1154	prss12.L	1.67688302	0.00904935	PRSS12
XBXL10_1g11542	lrp6.L	1.61257616	0.00632874	LRP6
XBXL10_1g11544	borcs5.L	-0.86626204	0.06101998	BORCS5
XBXL10_1g11583	LOC121401005	-1.22534691	0.08492216	PPM1L
XBXL10_1g11888	itk.L	5.5648299	0.02353093	ITK
XBXL10_1g11911	skp1.L	-0.73379221	0.07121508	ENSG00000272772
XBXL10_1g11920	mterf2.L	-1.03413413	0.01345414	–
XBXL10_1g12039	vwf.L	-1.01382611	0.03069778	VWF
XBXL10_1g12091	sec24a.L	0.77791941	0.03452135	SEC24A
XBXL10_1g12098	pitx1.L	2.47575575	0.04780062	PITX1
XBXL10_1g12108	LOC108710847	-2.33596589	0.07701028	–
XBXL10_1g12256	gnpda1.L	-0.98057747	0.00522436	GNPDA1
XBXL10_1g12277	kif3a.L	0.80301086	0.06632227	KIF3A
XBXL10_1g12291	grxcr2.L	4.18075037	0.02582152	GRXCR2
XBXL10_1g12336	rpl26.L	-0.76423283	0.06282312	RPL26L1
XBXL10_1g12353	hrh2.L	-0.89315051	0.0966915	HRH2
XBXL10_1g12391	sncb.L	2.14169195	0.04119756	SNCB
XBXL10_1g1242	LOC108719625	5.06424605	0.01862502	CELA3A

XBXL10_1g1245	jchain.L	-1.47481621	0.0558175	JCHAIN
XBXL10_1g12489	acss3.L	1.67279286	0.06389998	ACSS3
XBXL10_1g12497	rassf9.L	-1.04622504	0.05180544	RASSF9
XBXL10_1g12515	btg1.L	-1.08927717	0.01345414	BTG1
XBXL10_1g12517	plekhg7.L	4.40810708	0.07885872	PLEKHG7
XBXL10_1g12616	csrp2.L	1.02015744	0.00569957	CSRP2
XBXL10_1g12631	slc38a4.L	2.24815653	0.03522754	SLC38A4
XBXL10_1g12664	znf277.L	-0.80214901	0.05121616	ZNF277
XBXL10_1g12670	gpr85.L	-1.37010838	0.06806062	GPR85
XBXL10_1g1274	areg.L	-1.28055114	0.0984431	AREG
XBXL10_1g12814	sema3d.L	1.64947603	0.00752177	SEMA3D
XBXL10_1g1283	rassf6.L	-1.17365471	0.00410253	RASSF6
XBXL10_1g12868	LOC108711235	0.86631003	0.0747306	PODXL
XBXL10_1g12879	LOC121401523	-1.14223957	0.0101263	SMKR1
XBXL10_1g12927	odf3.L	-1.14429271	0.00262842	–
XBXL10_1g12952	etfa.L	-1.08862258	0.00997873	ETFA
XBXL10_1g12963	LOC108711279	-5.54465673	0.08760058	–
XBXL10_1g12965	LOC108711280	-2.02463155	0.02436328	MALT1
XBXL10_1g12972	LOC108710284	1.56213681	0.00690289	CRABP1
XBXL10_1g12991	vps13c.L	0.73534743	0.08326527	VPS13C
XBXL10_1g13017	LOC108711307	1.09701057	0.00450861	LINGO1
XBXL10_1g13023	anxa2.L	0.84812369	0.05081386	ANXA2
XBXL10_1g13033	ulk3.L	-0.91073778	0.04356124	ULK3
XBXL10_1g13037	cyp1a1.L	1.93138693	0.0791753	CYP1A1
XBXL10_1g13050	snx22.L	-1.36107303	0.01117796	–
XBXL10_1g13066	LOC108711334	1.67665224	0.0242025	–
XBXL10_1g13074	ctsl.L	1.07950722	0.02607802	CTSK
XBXL10_1g13078	mrpl18.L	-0.80384678	0.05565102	MRPL18
XBXL10_1g1314	cnot6l.L	0.77671288	0.04000662	CNOT6L
XBXL10_1g13149	thsd4.L	1.352294	0.09452853	THSD4
XBXL10_1g13155	myo1e.1.L	1.28853917	0.07201468	MYO1E
XBXL10_1g13164	aqp9.L	1.63309409	0.01540511	AQP9
XBXL10_1g13165	aldh1a2.L	0.75510821	0.04598697	ALDH1A2
XBXL10_1g13189	onecut1.L	6.17407279	0.01019125	ONECUT1
XBXL10_1g13195	LOC108711385	-1.40482562	0.0101263	GNB5
XBXL10_1g13214	dut.L	-0.92786774	0.05008283	DUT
XBXL10_1g13234	sppl2a.L	0.9280539	0.09037014	SPPL2A
XBXL10_1g13237	selenow2.L	-0.77623598	0.06000436	–
XBXL10_1g1324	idua.L	-1.78311458	0.00669464	IDUA
XBXL10_1g1325	slc26a1.L	-1.38489534	0.0647764	SLC26A2
XBXL10_1g13253	bnc1.L	1.11950692	0.07258421	BNC1
XBXL10_1g13348	mrps11.L	-0.83760835	0.06454458	–
XBXL10_1g13351	LOC108711464	2.05855084	0.05565763	NTRK3
XBXL10_1g13437	pias1.L	1.78448486	0.0931156	PIAS1
XBXL10_1g13493	c2orf42.L	1.09612327	0.02757151	C2orf42
XBXL10_1g13517	pcna.L	-0.99685385	0.07502061	PCNA
XBXL10_1g13523	LOC108711553	1.44727169	0.03404715	LRRTM4
XBXL10_1g13564	nt5dc4.L	1.40984176	0.07128052	NT5C2
XBXL10_1g13684	dmtn.L	1.73904749	0.02837147	DMTN
XBXL10_1g13740	LOC108711632	4.83344593	0.08142161	ZNF84
XBXL10_1g13816	pet100.L	-0.71978455	0.06567134	ENSG00000283390
XBXL10_1g13854	LOC121401622	2.61014979	0.08492216	–
XBXL10_1g13866	lrrc8e.L	1.13472193	0.05192146	LRRC8C
XBXL10_1g14168	LOC108710164	-0.94212247	0.09385533	–
XBXL10_1g14205	elof1.S	-0.74725739	0.08636708	ELOF1
XBXL10_1g14232	tmem205.L	-0.74338665	0.07128052	TMEM205

XBXL10_1g14239	mast1.L	4.7908782	0.01975394	MAST1
XBXL10_1g14251	dhps.L	-0.79290839	0.06517724	DHPS
XBXL10_1g14253	wdr83os.L	-0.88845796	0.0435752	WDR83OS
XBXL10_1g14289	c3.L	1.6733435	0.000345	C3
XBXL10_1g14295	LOC108711733	1.06444991	0.01440793	C3
XBXL10_1g14635	LOC108711770	1.24327286	0.07128052	TIPARP
XBXL10_1g14638	naa38.L	-0.87031521	0.02353093	NAA38
XBXL10_1g1464	aptx.L	-0.92373954	0.05317372	APTX
XBXL10_1g14647	LOC108711777	-0.79516283	0.04526352	EIF4E2
XBXL10_1g14650	rangrf.L	-0.8321202	0.03522754	–
XBXL10_1g14706	LOC108711786	2.30293933	0.01536739	–
XBXL10_1g14718	cldn15.1.L	2.51371462	0.07497598	CLDN15
XBXL10_1g1475	bmp3.L	0.68350163	0.08530951	BMP3
XBXL10_1g14937	slco1b3.S	3.25321195	0.0991322	SLCO1C1
XBXL10_1g14962	ppfibp1.S	0.83952794	0.06035329	PPFIBP1
XBXL10_1g14996	LOC121402088	-1.41602861	0.01816117	–
XBXL10_1g15005	dennd2a.S	2.5798826	0.04403508	DENND2A
XBXL10_1g15018	mrps33.S	-0.78376104	0.04294929	MRPS33P2
XBXL10_1g15021	LOC108706056	-0.7844358	0.04976642	STMP1
XBXL10_1g15052	LOC108712252	1.79586086	0.00321868	PARP12
XBXL10_1g15064	usp18.S	2.50389646	0.05853693	–
XBXL10_1g15075	dcp1b.S	1.05660566	0.02353093	DCP1B
XBXL10_1g15115	LOC443642	0.78776403	0.08337501	CALD1
XBXL10_1g15142	ergic2.S	-0.7373529	0.06907758	ERGIC2
XBXL10_1g15145	LOC108712601	3.00992557	0.06806062	–
XBXL10_1g15149	rhno1.S	-0.71218907	0.08942236	–
XBXL10_1g15185	LOC108712611	1.98941714	0.08760058	–
XBXL10_1g15186	LOC108712612	2.69376457	3.84E-05	–
XBXL10_1g15193	ube2b.S	-0.81816337	0.0647764	UBE2B
XBXL10_1g15313	ank1.S	1.28614184	0.06522422	ANK1
XBXL10_1g15332	sftpc.S	3.3414397	0.04454243	SFTPC
XBXL10_1g15347	LOC108712707	5.7229917	0.03801284	SLC18A1
XBXL10_1g15353	LOC108712710	1.08187803	0.08636708	ADRB1
XBXL10_1g15383	tcim.S	-0.81977818	0.08663149	TCIM
XBXL10_1g15395	gck.S	4.32317989	0.07346202	GCK
XBXL10_1g15424	vamp5.S	-1.8365155	0.00024858	–
XBXL10_1g1545	reep6.L	-1.14054785	0.01004921	REEP5
XBXL10_1g15458	pcna.S	-1.13120343	0.02375806	PCNA
XBXL10_1g15466	LOC108712294	3.7222822	0.03384704	–
XBXL10_1g15474	fam136a.S	-1.06116538	0.01558425	FAM136A
XBXL10_1g1549	rps15.L	-0.82843305	0.05192146	RPS15
XBXL10_1g1551	gamt.L	-0.82342849	0.07808471	GAMT
XBXL10_1g15535	aagab.S	-1.40625906	0.00055796	AAGAB
XBXL10_1g15558	igdcc4.S	1.61985796	0.0594442	IGDCC4
XBXL10_1g15611	mrps11.S	-0.90310904	0.04962861	MRPS11
XBXL10_1g15616	mfge8.S	1.56250687	9.70E-06	EDIL3
XBXL10_1g15685	bnc1.S	1.50565957	0.0747306	BNC1
XBXL10_1g15698	selenow2.S	-1.0717652	0.02582152	–
XBXL10_1g1571	gpx4.L	-0.66538346	0.09637239	GPX4
XBXL10_1g15739	LOC108712923	6.76351378	0.00109704	ONECUT1
XBXL10_1g15743	rsl24d1.S	-0.93209057	0.02368351	RSL24D1
XBXL10_1g15760	LOC108712939	1.91535519	0.03859697	AQP9
XBXL10_1g1592	LOC108712617	-1.28032199	0.00839396	PGPEP1
XBXL10_1g15922	neo1.S	0.79539789	0.04555164	NEO1
XBXL10_1g15969	mapk8ip2.S	3.46395989	0.09578457	MAPK8IP2
XBXL10_1g16015	LOC121402177	-0.75543379	0.08057675	SMKR1

XBXL10_1g1605	LOC108712686	-0.8956647	0.01709223	MARCHF2
XBXL10_1g16058	fam107b.S	-0.67845952	0.09717071	FAM107B
XBXL10_1g16159	ing3.S	-0.73872502	0.07044345	ING3
XBXL10_1g16173	LOC108713110	-1.11051423	0.08337501	TFEC
XBXL10_1g16210	slc38a4.S	3.95591109	0.07701028	SLC38A4
XBXL10_1g16243	myrfl.S	5.80867658	0.0318387	MYRFL
XBXL10_1g16273	llphp3.S	-0.828455	0.02875538	–
XBXL10_1g16304	btg1.S	-0.99684748	0.00622698	BTG1
XBXL10_1g16381	LOC108713216	-1.69904136	0.05582389	–
XBXL10_1g16388	gfra3.S	3.66038914	0.02367819	–
XBXL10_1g16519	gnpda1.S	-0.83018231	0.03522754	GNPDA1
XBXL10_1g1654	enc1.2.L	-1.27056258	0.01345414	ENC1
XBXL10_1g16569	LOC108712504	6.18276417	0.01086847	PCDHGC5
XBXL10_1g17163	LOC108703481	2.32192169	0.04403508	ELAVL3
XBXL10_1g17197	wdr83os.S	-0.86408801	0.03979949	WDR83OS
XBXL10_1g17204	clpp.S	-0.76050798	0.08971677	CLPP
XBXL10_1g17451	naa38.S	-0.75933168	0.05068248	NAA38
XBXL10_1g1749	prss57.L	-1.09516246	0.06538164	OVCH1
XBXL10_1g17490	LOC108703553	6.59449848	0.00487979	–
XBXL10_1g17511	pcolce.S	1.1851718	0.03683869	PCOLCE
XBXL10_1g17545	LOC108703443	-4.20250487	0.05951694	–
XBXL10_1g1755	isyna1.L	-0.85006428	0.06447567	ISYNA1
XBXL10_1g17562	LOC108703581	-0.77937407	0.09452853	–
XBXL10_1g17569	tp53.S	1.16118638	0.09578457	TP53
XBXL10_1g1759	fkbp8.L	-0.63972849	0.0918168	FKBP8
XBXL10_1g17597	LOC108713706	1.89916908	0.05436935	–
XBXL10_1g1765	klhl26.L	-0.83639464	0.06943384	KLHL26
XBXL10_1g17661	nell1.L	6.25680618	0.00500051	NELL1
XBXL10_1g17700	lrrc4c.L	1.98823644	0.0879752	LRRC4C
XBXL10_1g17718	cd82.L	0.86964553	0.02875538	CD82
XBXL10_1g1775	tdrd7.L	1.08975754	0.07808471	TDRD7
XBXL10_1g17752	f2.L	2.42194774	0.0400308	F2
XBXL10_1g17796	large2.L	0.80950837	0.09605255	LARGE1
XBXL10_1g17877	pax6.L	6.26312115	0.0057219	PAX6
XBXL10_1g17902	ifitm3.L	0.73720778	0.05192146	–
XBXL10_1g1791	LOC108713377	3.29763473	0.08636708	–
XBXL10_1g17913	cd81.L	0.64435797	0.06522422	CD81
XBXL10_1g17942	myrf.L	1.14869456	0.03522754	MYRF
XBXL10_1g17955	XB990428.L	-1.43316115	0.00569957	IFITM3P7
XBXL10_1g17981	LOC108704982	3.00043084	0.00013541	MUC5AC
XBXL10_1g18018	LOC108713473	2.1132151	0.02183481	MUC5AC
XBXL10_1g18023	muc6.L	4.35647887	0.02485711	MUC6
XBXL10_1g18028	polr2l.1.L	-0.82732167	0.06771662	POLR2L
XBXL10_1g18191	LOC108713901	-1.11264479	0.00632847	–
XBXL10_1g18199	kcnk4.L	-2.76757418	0.02212481	KCNK2
XBXL10_1g18204	ppp1r14b.L	-0.87883104	0.04033088	PPP1R14B
XBXL10_1g18222	zfta.L	0.97847765	0.06101998	ZFTA
XBXL10_1g18256	gal.1.L	4.81725356	0.04698731	GAL
XBXL10_1g1826	clta.L	-0.91449009	0.02607802	CLTA
XBXL10_1g18316	LOC108705472	-1.3140552	0.01532462	CTSF
XBXL10_1g1845	LOC108713403	2.3525299	0.08896572	B3GNT3
XBXL10_1g18487	nutf2.L	-0.75526707	0.0480112	NUTF2
XBXL10_1g18550	osgin1.L	1.25480011	0.02140165	OSGIN1
XBXL10_1g18555	LOC108714002	4.63228213	0.07940259	–
XBXL10_1g18588	mt4.L	0.90673595	0.01564178	MT1F
XBXL10_1g18596	tradd.L	-0.84289862	0.09012309	–

XBXL10_1g18651	ctu2	-0.9045033	0.0833011	CTU2
XBXL10_1g18655	aprt.L	-0.79880125	0.07910198	APRT
XBXL10_1g18690	urah.L	-0.85554073	0.07279326	URAHP
XBXL10_1g18762	hnf4b.L	5.52912355	0.00170859	HNF4G
XBXL10_1g18766	cotl1.L	-0.82361634	0.03151245	COTL1
XBXL10_1g1879	dda1	-0.69081881	0.07128052	DDA1
XBXL10_1g18809	slc7a5.L	0.87153249	0.07044345	SLC7A5
XBXL10_1g18813	LOC108714099	1.20538913	0.01804243	ZFPM1
XBXL10_1g18828	LOC108714107	1.88320044	0.07112016	CES5A
XBXL10_1g18834	ss18l2.L	-0.76304561	0.09594197	SS18L2
XBXL10_1g18875	mcoln2.L	-2.43032326	0.0950919	MCOLN2
XBXL10_1g18929	calb2.L	4.79689731	0.04971753	CALB2
XBXL10_1g1894	tmem221.L	-0.87844807	0.09359215	–
XBXL10_1g19030	erich3.L	2.11214008	0.08853299	ERICH3
XBXL10_1g19065	ak4.L	-1.15497578	0.09452853	AK4
XBXL10_1g19084	tm2d1.L	-0.93905183	0.00842874	TM2D1
XBXL10_1g1909	gna11.L	0.94446313	0.07301305	GNA11
XBXL10_1g19090	XB5864909.L	-1.24910108	0.00278343	RNF170
XBXL10_1g19102	LOC108714247	4.70431542	0.0102929	–
XBXL10_1g1913	igfbpl1.L	4.88147714	0.00291812	IGFBPL1
XBXL10_1g19130	dph2.L	-1.08429077	0.06806062	DPH2
XBXL10_1g19138	prdx1.L	-1.02736948	0.01365224	PRDX1
XBXL10_1g19198	pik3r3.L	0.75802623	0.08726806	PIK3R3
XBXL10_1g19207	uqcrh.L	-0.76220177	0.08632834	UQCRH
XBXL10_1g19316	pappa2.L	1.44392095	0.04613674	PAPPA2
XBXL10_1g19332	tor3a.L	1.05597875	0.00836998	TOR3A
XBXL10_1g19344	rgs16.L	5.59691713	0.01532076	RGS16
XBXL10_1g19345	glul-like.1.L	-1.25959955	0.0106772	GLUL
XBXL10_1g19356	qsox1.L	1.71622916	0.05878243	QSOX1
XBXL10_1g19367	frrs1.L	1.13671221	0.01213285	FRRS1
XBXL10_1g19375	hccs.L	-0.99282012	0.04119756	HCCS
XBXL10_1g19382	LOC108714376	4.24697944	0.01518856	PLPPR4
XBXL10_1g19399	dipk1a.L	-0.7277316	0.07294992	DIPK1A
XBXL10_1g19439	clca1.1.L	3.71773008	0.04613674	CLCA3P
XBXL10_1g19441	ankrd45.L	-0.99545806	0.05204342	–
XBXL10_1g19486	extl2.L	-0.84978348	0.02607802	EXTL2
XBXL10_1g19488	s1pr1.L	-0.83213369	0.07338373	S1PR1
XBXL10_1g19504	lhx9.L	2.10704546	3.71E-06	LHX9
XBXL10_1g1953	txn.L	-0.83520795	0.07044345	–
XBXL10_1g19531	LOC121403083	3.31797449	0.02353093	–
XBXL10_1g19533	cfh.L	1.10158685	0.01936467	–
XBXL10_1g19547	desi1.L	-0.76925218	0.09333763	DESI1
XBXL10_1g19563	rasd2.L	-1.0075416	0.06522422	RASD2
XBXL10_1g19578	fmc1.L	-0.73229824	0.08337501	FMC1
XBXL10_1g19580	rpsa.L	-0.75121563	0.0671417	RPSA
XBXL10_1g1960	ddx58.L	1.69670024	0.03522754	DDX58
XBXL10_1g19602	xpnpep3.L	-0.99303115	0.07044345	XPNPEP3
XBXL10_1g19604	rbx1.L	-0.69167748	0.08937969	RBX1
XBXL10_1g19609	gprc5a.L	3.43288806	0.03452135	GPRC5D
XBXL10_1g19657	mgst3.L	-1.07530549	0.00780032	MGST3
XBXL10_1g19691	ddx17.L	1.03224927	0.02960385	DDX17
XBXL10_1g19733	tmem184b.L	1.05909575	0.06389998	TMEM184B
XBXL10_1g19748	lgals1.2.L	5.87115772	0.01532076	–
XBXL10_1g19749	lgals1.3.L	5.94095551	1.24E-05	–
XBXL10_1g19758	rac2.L	-0.97165888	0.05937571	RAC2
XBXL10_1g1976	rps6.L	-0.84108052	0.04555164	RPS6

XBXL10_1g19766	csf2rb.L	2.83355931	0.06035329	–
XBXL10_1g19778	LOC108714571	1.54185091	6.19E-05	–
XBXL10_1g19849	tusc2.L	-0.75771678	0.0872031	TUSC2
XBXL10_1g19871	abhd14b.L	-0.97100461	0.01881439	–
XBXL10_1g19873	acy1.2.L	-1.24516091	0.05957098	ACY1
XBXL10_1g19889	arhgdib.L	-0.86517644	0.08078023	ARHGDIB
XBXL10_1g1990	LOC121393901	5.75309123	0.01709223	TAL2
XBXL10_1g19906	tnnc1.L	2.01886071	0.04345838	TNNC1
XBXL10_1g19956	lsm3.L	-0.74861133	0.08760058	LSM3
XBXL10_1g20055	LOC108714705	-0.8086687	0.0467767	ARPC4
XBXL10_1g20092	slc25a26.L	-1.06960623	0.01696219	SLC25A26
XBXL10_1g20165	LOC108704036	4.06229084	0.08767825	SLC6A1
XBXL10_1g20558	LOC121393148	-1.27041979	0.0622009	–
XBXL10_1g20632	ppp1r14b.S	-0.84612294	0.04613674	PPP1R14B
XBXL10_1g20675	slc25a45.S	-0.97493634	0.09478417	SLC25A45
XBXL10_1g20691	LOC108715167	6.07629987	0.02733126	–
XBXL10_1g20713	fau.S	-0.80978813	0.05372224	FAU
XBXL10_1g20734	LOC121393158	3.09930277	0.07112016	MUC2
XBXL10_1g20735	XB5761341.S	2.89818607	0.0777023	MUC2
XBXL10_1g20737	LOC121393422	3.01333576	0.02607802	MIR4435-2HG
XBXL10_1g20743	LOC108715185	3.44898228	3.73E-05	RBM12
XBXL10_1g20744	LOC108714924	4.65534818	3.71E-06	MUC5AC
XBXL10_1g20750	LOC121393160	2.56565606	0.02973011	–
XBXL10_1g20779	fads2.S	-0.96642867	0.02368351	FADS2
XBXL10_1g20784	sdhaf2.S	-0.82025036	0.0382218	SDHAF2
XBXL10_1g20792	pkp3.S	1.11446513	0.07714323	PKP3
XBXL10_1g20809	LOC108715206	-0.70410389	0.0758163	MOB2
XBXL10_1g2082	tmem252.L	-2.47157635	0.00203908	–
XBXL10_1g20830	pax6.S	4.72429911	0.02968976	PAX6
XBXL10_1g20908	fadd.S	-1.20481787	0.000783	–
XBXL10_1g20967	LOC108715264	1.30985816	0.05565102	ALX4
XBXL10_1g21052	LOC108715307	0.93263028	0.0747306	PDE3B
XBXL10_1g21108	ntf2	-0.76331656	0.07154765	NUTF2
XBXL10_1g21150	MGC147117.S	-0.83907127	0.06655029	–
XBXL10_1g21193	cmc2.S	-0.89896703	0.01124109	CMC2
XBXL10_1g21292	LOC121393244	-1.81722949	0.06314787	ZFHX3
XBXL10_1g21317	hnf4b.S	2.94996521	0.02614628	HNF4G
XBXL10_1g2132	c15orf40.L	-0.95870228	0.09132338	C15orf40
XBXL10_1g21358	LOC121393266	4.88194921	0.01709223	–
XBXL10_1g21426	tshz3.S	1.32891436	0.00619736	TSHZ3
XBXL10_1g2150	fbp1.L	-1.08997368	0.04390154	FBP1
XBXL10_1g21533	erich3.S	1.77477519	0.04143366	ERICH3
XBXL10_1g21540	cth.S	-1.55425574	0.00150546	CTH
XBXL10_1g21557	insl5.S	-5.99653778	0.03404715	–
XBXL10_1g21558	dynlt5.S	-0.74998346	0.08760058	DYNLT5
XBXL10_1g21563	leprot.S	-0.91337684	0.01281773	LEPROT
XBXL10_1g21588	LOC108715540	2.54656961	0.05193868	–
XBXL10_1g21664	pik3r3.S	0.83125223	0.09632297	PIK3R3
XBXL10_1g21673	nsun4.S	-0.73357186	0.06765825	NSUN4
XBXL10_1g21686	tal1.S	1.4273059	0.04686387	TAL1
XBXL10_1g21732	fam151a.S	-0.90452947	0.01862502	FAM151A
XBXL10_1g21773	npl.S	-1.19049416	0.06690872	NPL
XBXL10_1g2178	cks2.L	-1.01444727	0.02353093	CKS2
XBXL10_1g21798	hccs.S	-1.11562696	0.02211568	HCCS
XBXL10_1g21860	rgs4.S	-1.29649125	0.07246971	RGS4
XBXL10_1g21863	pbx1.S	0.71654642	0.0968139	PBX1

XBXL10_1g21879	XB5731323.S	-1.00749881	0.00462209	–
XBXL10_1g21882	LOC121393333	-1.25159173	0.02353093	–
XBXL10_1g21892	lhx9.S	1.6207831	0.02353093	LHX9
XBXL10_1g21916	snu13.S	-0.80118459	0.06672494	SNU13
XBXL10_1g21948	hmox1.S	-0.94506625	0.0938312	HMOX1
XBXL10_1g21962	rbx1.S	-0.84485513	0.05241337	RBX1
XBXL10_1g21979	mettl11b.S	-2.39750157	0.02780869	NTMT2
XBXL10_1g21997	uck2.S	-0.9120713	0.06035329	UCK2
XBXL10_1g2202	LOC108714859	-1.27911141	0.02382843	–
XBXL10_1g2203	LOC108714860	-1.32926423	0.04454243	RNF31
XBXL10_1g22070	kcnj4.S	4.8028939	0.01281773	KCNJ4
XBXL10_1g22088	LOC108715797	-1.09751281	0.04555164	RAC2
XBXL10_1g22094	tst.S	-1.41944989	0.00843601	–
XBXL10_1g22097	LOC121393351	-1.70216203	0.01881439	–
XBXL10_1g22126	gpx1.S	-0.81065153	0.02694379	GPX1
XBXL10_1g22158	mapkapk3.S	-0.86856628	0.02111617	MAPKAPK3
XBXL10_1g22189	itih4.S	1.30012996	0.07808471	ITIH3
XBXL10_1g22207	lrrn1.S	6.65274189	0.00094914	LRRN1
XBXL10_1g22240	chchd4.S	-1.18660159	0.09800388	CHCHD4
XBXL10_1g22362	thoc7.S	-0.73312523	0.06771662	THOC7
XBXL10_1g22396	LOC121393393	-0.95963789	0.06518557	ABHD6
XBXL10_1g22415	rpp14.S	-0.83086184	0.0747306	–
XBXL10_1g22443	XB5944457.S	7.17993509	0.00034495	SLC6A1
XBXL10_1g22459	LOC108704415	-0.82018964	0.0980397	TAMM41
XBXL10_1g2248	slc7a7.L	-1.01959368	0.05192146	SLC7A7
XBXL10_1g22533	LOC108716082	3.53126307	0.01888028	NRXN1
XBXL10_1g22570	prepl.L	1.0418512	0.05976228	PREPL
XBXL10_1g22571	slc3a1.L	-1.29686718	0.06018973	SLC3A1
XBXL10_1g22579	zfp36l2.L	0.94523644	0.03465092	ZFP36L2
XBXL10_1g22605	slc30a1.L	0.81501287	0.03095157	SLC30A1
XBXL10_1g22680	dnah14.L	-1.48344251	0.05565763	DNAH14
XBXL10_1g22751	glo1.L	-0.78435195	0.04613674	GLO1
XBXL10_1g22810	capn11.L	0.6938941	0.07121508	CAPN1
XBXL10_1g2283	LOC121394372	-2.97986663	0.02675727	–
XBXL10_1g22833	LOC108716104	-1.81239132	0.00410253	–
XBXL10_1g22855	LOC108716579	-1.43400051	0.05367805	–
XBXL10_1g22867	meis2.L	0.86285351	0.02902379	MEIS1
XBXL10_1g23035	pkr2.L	1.11404152	0.01497417	–
XBXL10_1g23052	LOC108716659	2.79745244	0.0001198	–
XBXL10_1g23166	sult6b1.1.L	-0.77194792	0.05582389	SULT6B1
XBXL10_1g23214	pigh.L	-1.05856702	0.0022379	PIGH
XBXL10_1g23247	LOC108716727	-1.49282414	0.07128052	–
XBXL10_1g23268	LOC108716742	-5.94289519	0.09332809	–
XBXL10_1g23273	nid1.L	0.94431393	0.05317372	NID1
XBXL10_1g23384	enpp1.L	1.29204043	0.0461029	ENPP1
XBXL10_1g23395	LOC108705439	1.68235622	0.00653294	VNN1
XBXL10_1g23398	rps12.L	-0.97411278	0.03522754	ENSG00000227615
XBXL10_1g23415	gja1.L	-1.20607272	0.09452853	GJA1
XBXL10_1g23428	LOC121393704	-8.48474964	0.0286203	–
XBXL10_1g23448	rwdd1.L	-0.75738569	0.07910198	RWDD1
XBXL10_1g23478	slc16a10.L	0.74780943	0.0647764	SLC16A10
XBXL10_1g23479	LOC121393712	-3.49416836	0.02607802	–
XBXL10_1g23499	nr2e1.L	4.51924864	0.04748231	NR2E1
XBXL10_1g23533	pou3f2.L	5.72803854	0.00081981	POU3F2
XBXL10_1g2371	LOC108714907	-1.2861259	0.04712571	–
XBXL10_1g23801	dvl3.L	0.88415514	0.07637479	DVL3

XBXL10_1g23833	nmur1.L	4.02053048	0.02353093	NMUR1
XBXL10_1g2386	LOC108696994	-3.30591421	0.04080668	IGHV1-46
XBXL10_1g23867	LOC108716955	3.02662897	0.00473243	JAG1
XBXL10_1g23883	LOC121393551	3.52524578	0.02968976	–
XBXL10_1g23886	sst.1.L	3.23949938	0.07065938	SST
XBXL10_1g2391	sall2.L	3.91920243	0.02500581	SALL2
XBXL10_1g23927	meltf.L	-1.11350603	0.0747306	MELTF
XBXL10_1g23937	tmem44.L	-1.02777343	0.01564178	–
XBXL10_1g23942	LOC121393936	2.58976906	0.00109252	–
XBXL10_1g23945	atp13a4.L	5.10143825	0.01055451	ATP13A4
XBXL10_1g23988	eif5a.L	-0.88422425	0.02582152	EIF5A2
XBXL10_1g24015	bche.L	-0.98580198	0.09326401	BCHE
XBXL10_1g24021	nmd3.L	-0.90910198	0.03649266	NMD3
XBXL10_1g24051	slc66a1l.L	-0.78960012	0.05582389	SLC66A1L
XBXL10_1g24090	LOC108717061	4.68980009	0.04555164	–
XBXL10_1g24102	LOC121393810	-1.78140976	0.06642754	–
XBXL10_1g24120	LOC108717074	-1.81237471	0.06960911	PLSCR1
XBXL10_1g24123	zic4.L	4.30798292	0.05288473	ZIC4
XBXL10_1g24131	LOC121393816	2.01108213	0.04604274	CPB1
XBXL10_1g24132	gyg1.L	-0.88764454	0.09452853	GYG1
XBXL10_1g24158	awat1.L	-0.93862397	0.09421888	MOGAT1
XBXL10_1g24186	lamtor3-like.L	-0.97008315	0.01576938	LAMTOR3
XBXL10_1g24289	rab6b.L	4.13848895	0.03562279	RAB6B
XBXL10_1g24302	LOC108717148	-1.09348252	0.00410253	PDCD6IP
XBXL10_1g24353	eipr1.L	-0.68891534	0.09216232	EIPR1
XBXL10_1g24369	cmpk2.L	2.22759167	0.02865858	CMPK2
XBXL10_1g24399	LOC121393840	1.89609122	0.09452853	–
XBXL10_1g24467	itsn2.L	0.92564794	0.07017961	ITSN2
XBXL10_1g24484	LOC108717215	3.8719867	0.03836658	ADGRF5
XBXL10_1g24526	XB5848842.L	-4.14483469	0.00328753	CYP2C8
XBXL10_1g24554	gata4.L	1.79903271	0.09910409	GATA4
XBXL10_1g24573	pnoc.L	-1.1436603	0.01488697	–
XBXL10_1g24584	pomc.L	8.43021527	0.0139193	POMC
XBXL10_1g24730	gtf3c2.L	1.19955541	0.05338122	GTF3C2
XBXL10_1g24761	LOC108717285	1.65154983	0.06035329	–
XBXL10_1g24877	ccdc167.S	-0.90078859	0.03375619	CCDC167
XBXL10_1g2490	gal3st1.L	-1.04540275	0.01345414	GAL3ST1
XBXL10_1g2491	LOC108715337	-1.1508176	0.05317372	–
XBXL10_1g24913	ciao2b.S	-0.91767067	0.0286203	CIAO2B
XBXL10_1g24935	LOC121394156	-1.01020959	0.07595737	–
XBXL10_1g24938	wdr26.S	0.7213992	0.08542561	WDR26
XBXL10_1g24939	cnih4.S	-0.85011448	0.05594094	CNIH4
XBXL10_1g2497	castor1.L	-1.92202219	0.05192146	CASTOR1
XBXL10_1g24990	slc30a1.S	0.71343069	0.07940259	SLC30A1
XBXL10_1g24995	ubr2.S	0.83191132	0.07843314	UBR2
XBXL10_1g25008	zfp36l2.S	0.80859378	0.04431759	ZFP36L2
XBXL10_1g2511	rasl10a.L	-1.44989889	0.0286203	RASL10B
XBXL10_1g25182	LOC108717807	2.48559957	0.03409323	–
XBXL10_1g25249	shprh.S	1.28308131	0.06314787	SHPRH
XBXL10_1g25250	sult6b1.5.S	-0.88374507	0.04608941	–
XBXL10_1g2528	tbx5.L	5.22465042	0.05957098	TBX5
XBXL10_1g25296	capn9.S	1.75710367	0.0287799	CAPN9
XBXL10_1g25320	trim50.S	6.23826811	0.00500051	TRIM50
XBXL10_1g25345	map7.S	1.940608	0.08096525	MAP7
XBXL10_1g25366	LOC108717894	-1.70711503	0.01346613	–
XBXL10_1g25367	LOC108705638	-1.78487726	0.00109252	NTPCR

XBXL10_1g25368	LOC121394210	-1.88177099	6.93E-05	NTPCR
XBXL10_1g2541	dao.L	-1.42749231	0.02704975	DAO
XBXL10_1g2546	iscu.L	-1.91378098	0.00997818	ISCU
XBXL10_1g25471	rps12.S	-0.69782751	0.09681378	RPS12
XBXL10_1g2551	kctd10.L	-1.21342803	0.0622009	KCTD10
XBXL10_1g25522	grik2.S	4.32413818	0.02437716	GRIK2
XBXL10_1g25559	rars2.S	-0.79851755	0.07940259	RARS2
XBXL10_1g25604	cox7a2.S	-0.73242902	0.06806062	COX7A2
XBXL10_1g25677	LOC108718031	-0.93783503	0.01497066	–
XBXL10_1g25711	LOC121394111	-4.29680127	0.09734396	CDK4
XBXL10_1g25725	cldn1.S	-0.83674583	0.07522722	CLDN1
XBXL10_1g25731	sst.1.S	3.38954495	0.03151989	SST
XBXL10_1g25771	fetub.S	3.05343384	0.08169941	–
XBXL10_1g25775	meltf.S	-0.9448386	0.04604274	MELTF
XBXL10_1g25840	slc2a2.S	-1.74563555	0.04330698	SLC2A2
XBXL10_1g25853	LOC108705376	-1.03291867	0.06522422	–
XBXL10_1g25866	pdcd10.S	-1.00702003	0.0106772	PDCD10
XBXL10_1g25939	selenot.S	-1.06992394	0.00182499	SELENOT
XBXL10_1g25969	zic1.S	5.64644519	0.04533922	ZIC1
XBXL10_1g25987	epha4.S	1.05085813	0.0777023	EPHA4
XBXL10_1g26053	LOC108717591	-1.33696996	0.07270259	–
XBXL10_1g26068	tm4sf20.S	-1.54515525	0.02971541	TDRD9
XBXL10_1g26082	ubxn7.S	-1.57411855	0.05347478	UBXN7
XBXL10_1g26117	cldn18.S	4.15141377	0.08494548	CLDN18
XBXL10_1g26143	LOC108718228	3.04535067	0.07338373	MYT1L
XBXL10_1g26195	mycn.S	0.84551763	0.08353974	MYCN
XBXL10_1g26250	LOC108717500	4.82967677	0.01226323	ADGRF5
XBXL10_1g26263	crisp1.3.S	2.94649452	0.00410253	CRISP3
XBXL10_1g26296	stk35.S	-1.70512884	0.00576513	PDIK1L
XBXL10_1g26299	LOC108718301	2.00726537	0.01558425	–
XBXL10_1g26306	pomc.S	3.92790657	0.03008655	POMC
XBXL10_1g26348	otof.S	2.63301887	0.01399884	OTOF
XBXL10_1g26372	tmem214.S	0.68755266	0.07128052	TMEM214
XBXL10_1g2640	c12orf43.L	-0.93404048	0.03375619	C12orf43
XBXL10_1g2653	slc5a1.2.L	-1.17843405	0.04604274	SLC5A1
XBXL10_1g26676	LOC108718674	-0.71423156	0.044008	NDUFB10
XBXL10_1g26703	LOC108718460	-1.06046574	0.06771662	–
XBXL10_1g2673	ddt.L	-1.05204772	0.00450861	–
XBXL10_1g26736	vipr1.L	1.19869729	0.05121616	VIPR1
XBXL10_1g2674	LOC108716035	1.41777277	0.05392457	GSTT2B
XBXL10_1g2682	slc2a11l3.l	-1.27983705	0.0139193	–
XBXL10_1g2684	slc2a11.2.L	-1.03569059	0.03522754	–
XBXL10_1g2685	slc2a11.L	-2.06714158	0.00151178	SLC2A11
XBXL10_1g26861	gad2.L	4.10013091	0.02416194	GAD2
XBXL10_1g26899	trdmt1.L	-0.94484623	0.01696299	TRDMT1
XBXL10_1g26903	pter.L	-0.74105473	0.04533922	PTER
XBXL10_1g26908	LOC108718821	-1.13694307	0.01840625	–
XBXL10_1g2691	XB5865341.S	-3.28532295	0.00213962	–
XBXL10_1g26927	pttg1ip2.L	-0.70753169	0.0918168	PTTG1IP
XBXL10_1g26938	LOC108718478	3.65190444	0.03785278	FAIM2
XBXL10_1g26993	LOC108718856	-1.0008224	0.02708059	–
XBXL10_1g27026	tmem196.L	5.62530319	0.02968976	TMEM196
XBXL10_1g2706	slc25a1.L	-1.09563221	0.00839396	SLC25A1
XBXL10_1g27143	rpl15.L	-1.01551052	0.00755071	RPL15
XBXL10_1g27259	acad11.L	-3.0579907	0.03404715	ACAD11
XBXL10_1g27270	pgla.L	7.01834651	0.00115968	–

XBXL10_1g27272	levi.L	5.65141562	0.00586891	–
XBXL10_1g27274	magainins.L	2.52200665	0.02560373	–
XBXL10_1g27275	xt6l.L	5.64796738	0.00107404	–
XBXL10_1g27290	LOC108718975	-0.93314974	0.0758163	EXOSC7
XBXL10_1g27317	slc6a19.L	-0.79638561	0.04882674	SLC6A19
XBXL10_1g2732	gnb1l.L	-1.10615774	0.03452135	GNB1L
XBXL10_1g27332	spata48.L	-1.57895364	0.08428481	–
XBXL10_1g27346	ppp1r17.L	-1.41480037	0.0101263	–
XBXL10_1g27440	pigm.L	-0.81296459	0.07365774	PIGM
XBXL10_1g27443	znfx1.2.L	2.47211565	0.00223549	ZNFX1
XBXL10_1g27446	cmbl.L	-0.72770709	0.05961917	CMBL
XBXL10_1g27453	LOC108718510	-3.01029449	0.04080668	CTNND2
XBXL10_1g27479	bag1.L	-4.9738448	0.00221399	BAG1
XBXL10_1g27482	LOC121394666	-7.06967975	0.00424585	–
XBXL10_1g27530	LOC121394681	-7.37162342	0.00072909	–
XBXL10_1g27531	LOC121394682	-7.88373348	3.15E-05	–
XBXL10_1g27541	rnf152.L	-1.54365538	0.00355293	RNF152
XBXL10_1g27557	serpinb6.L	-0.9114277	0.02199226	SERPINB8
XBXL10_1g27566	foxq1.L	2.86247134	0.00424585	FOXQ1
XBXL10_1g27584	eci2.L	-0.76316002	0.07128052	ECI2
XBXL10_1g27643	sirt5.L	-0.7164095	0.0747306	SIRT5
XBXL10_1g27708	LOC108719158	-4.15362797	0.0872031	CTXN3
XBXL10_1g27734	cndp1.L	-1.7700597	0.02754557	CNDP1
XBXL10_1g27737	cyb5a.L	-0.83883986	0.07919594	CYB5A
XBXL10_1g27740	timm21.L	-0.84614685	0.05273014	TIMM21
XBXL10_1g27741	LOC121394476	4.78579297	0.00262842	NETO1
XBXL10_1g27742	neto1.L	3.98224897	0.00321868	NETO1
XBXL10_1g27743	cbln2.L	1.37610465	0.00109252	CBLN2
XBXL10_1g2778	LOC108716396	-3.21835533	0.04735613	TMEM132B
XBXL10_1g27781	LOC108719192	-0.86234223	0.06378494	ELOC
XBXL10_1g27790	twsg1.L	0.92297599	0.06907671	TWSG1
XBXL10_1g2782	bri3bp.L	-0.78310792	0.08861621	BRI3BP
XBXL10_1g27861	hrh4.c9.L	5.75355623	0.02353093	–
XBXL10_1g27887	dsc3.L	3.16715712	0.03877133	DSCAS
XBXL10_1g27893	opn7a.L	6.64753882	0.00424585	–
XBXL10_1g27982	ttpa.L	2.33964521	0.04414611	TTPA
XBXL10_1g28052	rdh10.L	0.83183018	0.01058859	RDH10
XBXL10_1g28096	tpd52.L	-0.66631985	0.07910198	TPD52
XBXL10_1g28103	mrpl53.L	-1.08397405	0.0106772	–
XBXL10_1g28169	cibar1.L	-0.76815926	0.08636708	CIBAR1
XBXL10_1g2817	LOC121395056	4.13346508	0.06806062	–
XBXL10_1g28170	esrp1.L	0.81210271	0.08937969	ESRP1
XBXL10_1g28274	derl1.L	-0.77899198	0.08760058	DERL1
XBXL10_1g28354	LOC121394768	3.33098495	0.03535983	–
XBXL10_1g28389	pycr3.L	-0.87135736	0.04751939	PYCR3
XBXL10_1g28392	XB22062350.L	-0.78289014	0.0581877	–
XBXL10_1g28445	fam83h.L	1.32599267	0.09632297	FAM83H
XBXL10_1g28455	LOC108718625	1.02599995	0.07374689	–
XBXL10_1g2846	rnf34.L	-0.86239018	0.07077716	RNF34
XBXL10_1g28511	LOC100158309	5.95804305	0.00151178	TYR
XBXL10_1g28521	LOC108695552	2.9466886	0.08341981	TRIM11
XBXL10_1g2855	arpc3.L	-1.05419902	0.01399884	ARPC3
XBXL10_1g2861	hvcn1.L	-1.46783549	1.20E-05	HVCN1
XBXL10_1g28653	scap.S	0.98683324	0.07128052	SCAP
XBXL10_1g28655	ndufb10.S	-1.05713488	0.00755071	NDUFB10
XBXL10_1g28667	nradd.S	1.07492092	0.02367819	NGFR

XBXL10_1g28677	wnt3a.S	5.68481593	0.01377495	WNT3
XBXL10_1g28680	guk1.S	-1.07060948	0.05808413	GUK1
XBXL10_1g28684	cyp8b1.1.S	1.05139743	0.06632227	CYP8B1
XBXL10_1g28691	LOC108719808	1.20959094	0.03894292	VIPR1
XBXL10_1g28704	myd88.S	-0.84548606	0.08000078	MYD88
XBXL10_1g28709	LOC108719814	5.90084176	0.05739897	FCN2
XBXL10_1g2874	LOC108716941	1.18821023	0.09594197	TRAFD1
XBXL10_1g28749	klf6.S	-0.80694406	0.07514508	KLF6
XBXL10_1g28849	sri.S	-0.80186456	0.06071726	SRI
XBXL10_1g28875	calcr.S	3.49700854	0.0522144	CALCR
XBXL10_1g28909	dgkb.S	3.73735514	0.07246971	DGKB
XBXL10_1g28913	sostdc1.S	-2.28672317	0.02353093	SOSTDC1
XBXL10_1g28955	nfe2l3.S	0.80527985	0.08515631	NFE2L3P1
XBXL10_1g29007	rpl15.S	-0.79857601	0.06806062	RPL15
XBXL10_1g29026	cmtm7.S	-1.0810703	0.05617914	CMTM7
XBXL10_1g29049	mettl6.S	-0.91023873	0.03047566	METTL6
XBXL10_1g29081	LOC121395042	5.55662571	0.0343112	–
XBXL10_1g2910	dusp18.L	-0.70195823	0.08096525	DUSP21
XBXL10_1g29166	ino80c.S	-0.79875888	0.07572375	INO80C
XBXL10_1g29259	rnf152.S	-1.66160616	3.15E-05	RNF152
XBXL10_1g29287	psmg4.S	-1.1454636	0.00424585	–
XBXL10_1g29335	elovl2.S	-5.1836682	0.00013541	ELOVL2
XBXL10_1g29395	kcng2.S	1.61095095	0.05317372	KCNG1
XBXL10_1g29414	cyb5a.S	-0.99307513	0.0286203	CYB5A
XBXL10_1g29418	cbln2.S	1.2855346	0.07941219	CBLN2
XBXL10_1g29431	mc5r.S	-1.83567217	0.01759828	MC5R
XBXL10_1g2945	snx2.L	-0.70488256	0.0777023	SNX2
XBXL10_1g29504	cdh2.S	0.97844082	0.04735613	CDH2
XBXL10_1g2953	hsd17b4.L	-1.02796769	0.04555164	HSD17B4
XBXL10_1g29557	rps20.S	-0.75939228	0.0542316	RPS20
XBXL10_1g29559	plag1.S	2.88922343	0.02353093	PLAG1
XBXL10_1g29560	penk.S	-1.18136556	0.01709223	PENK
XBXL10_1g2958	sema6a.L	1.21593209	0.00021169	SEMA6A
XBXL10_1g29616	LOC108695345	-0.76503982	0.05878243	RPL7
XBXL10_1g29647	pmp2.S	-1.32523637	0.00669464	PMP2
XBXL10_1g29683	gem.S	-1.23067177	0.0263004	GEM
XBXL10_1g29710	mterf3.S	-1.55577147	0.00081484	MTERF3
XBXL10_1g29720	LOC108719749	-1.34722992	0.0176051	–
XBXL10_1g29878	psca.S	2.60470759	0.00610393	–
XBXL10_1g29890	LOC108719772	-0.95668912	0.04565082	LRRC14
XBXL10_1g29930	fam83h.S	4.58428271	0.02582152	FAM83H
XBXL10_1g29991	LOC121395800	-4.03411103	0.0872031	–
XBXL10_1g30005	bbip1.L	-1.02856991	0.00583953	BBIP1
XBXL10_1g30076	prdx3.L	-0.69890083	0.07197379	PRDX3
XBXL10_1g30178	gapdh.L	-1.37960914	0.02436328	GAPDH
XBXL10_1g30194	LOC108695739	-5.85985212	0.0747306	ASAH2
XBXL10_1g30200	cisd1.L	-0.86697804	0.02368351	CISD1
XBXL10_1g30211	rhobtb1.L	1.14869645	0.04604274	RHOBTB1
XBXL10_1g30226	LOC121395810	3.67836812	5.45E-06	–
XBXL10_1g30336	ventx2.2.L	3.43702618	0.02441789	VENTX
XBXL10_1g30347	LOC108696140	-1.15286356	0.0758163	GSTO1
XBXL10_1g30348	sfr1.L	-1.03831065	0.00364826	–
XBXL10_1g30349	col17a1.L	2.7039676	0.04454243	COL17A1
XBXL10_1g30362	atp5mk.L	-0.75371454	0.09867992	ATP5MK
XBXL10_1g30374	cnnm2.L	0.95351401	0.02367819	CNNM2
XBXL10_1g30396	mfsd13a.L	1.18504361	0.08337501	MFSD13A

XBXL10_1g30403	mrpl43.L	-1.14085094	0.00483557	MRPL43
XBXL10_1g30477	LOC121395725	-2.24316834	0.04613674	–
XBXL10_1g3048	LOC108717625	-1.31445059	0.0101263	–
XBXL10_1g30495	ifit1b.L	2.48584647	0.0791753	–
XBXL10_1g30497	LOC108705597	3.40596488	0.00021169	IFIT1
XBXL10_1g30498	LOC108705596	3.09331108	3.84E-05	–
XBXL10_1g30500	LOC108695773	3.64253875	0.02417019	IFIT1
XBXL10_1g30501	LOC108696188	4.57861539	0.00576513	–
XBXL10_1g30519	LOC108696199	1.97111595	0.00450861	ABCB1
XBXL10_1g30521	cox5b.2.L	-0.79984599	0.05079408	–
XBXL10_1g30528	bloc1s2.L	-0.74431377	0.07202038	BLOC1S2
XBXL10_1g30579	LOC121395392	3.83107091	0.09281974	–
XBXL10_1g30622	ndufb8.L	-0.89983448	0.03174659	NDUFB8
XBXL10_1g30629	nfkb2.L	-0.76921036	0.07945628	NFKB2
XBXL10_1g30636	synpo2l.L	-2.14754746	0.05582389	SYNPO2L
XBXL10_1g30654	psap.L	0.97718197	0.01076067	PSAP
XBXL10_1g30714	LOC121395414	3.32771661	0.0542316	–
XBXL10_1g30720	prxl2a.L	-0.7676476	0.04009657	PRXL2A
XBXL10_1g3082	LOC108717780	-1.15997159	0.01748995	BTF3
XBXL10_1g30820	LOC108696310	-1.57489407	0.00410253	–
XBXL10_1g30897	pex14.L	-0.89631399	0.0208755	PEX14
XBXL10_1g30902	srm.L	-0.74867301	0.09605255	SRM
XBXL10_1g30929	atp12a.L	2.47119007	4.67E-05	ATP12A
XBXL10_1g30972	tmem45b.L	0.81421974	0.07333488	TMEM45B
XBXL10_1g30991	LOC108695823	-1.10376582	0.03437396	–
XBXL10_1g31071	cxcr5.L	-2.68481073	0.06241445	CXCR1
XBXL10_1g31093	fxyd2.L	-1.29567635	0.04080668	–
XBXL10_1g31148	LOC108696493	1.43987889	0.04410518	–
XBXL10_1g31196	LOC108696519	-0.76361621	0.0794409	–
XBXL10_1g31242	slc35e2b.L	-0.78133208	0.04780062	SLC35E2B
XBXL10_1g31261	mxra8.L	1.72856567	0.04976642	MXRA8
XBXL10_1g31304	c1orf50.L	-0.93668296	0.0538375	C1orf50
XBXL10_1g31506	lig1.L	0.79269007	0.0758163	LIG1
XBXL10_1g31536	LOC108696667	2.05457726	0.00107404	SACS
XBXL10_1g31544	ndufa3.L	-0.7266118	0.08663149	NDUFA3P1
XBXL10_1g31671	LOC108696694	3.51523834	0.03047566	–
XBXL10_1g31674	cd79a.L	-2.05615556	0.05801316	CD79A
XBXL10_1g31694	LOC108696707	-1.07594754	0.0872031	–
XBXL10_1g31700	LOC121395610	7.10549434	0.00017624	–
XBXL10_1g31731	ceacam19lz.L	-0.88973289	0.05726535	–
XBXL10_1g31734	bcam.L	0.94781279	0.0286203	–
XBXL10_1g31738	apoc1.L	1.95246565	0.0400063	–
XBXL10_1g31742	LOC108695898	5.78443828	0.03409323	PRSS3P1
XBXL10_1g31745	LOC108697037	-1.15077981	0.00213962	–
XBXL10_1g31760	emc10.L	-0.92487578	0.04627619	EMC10
XBXL10_1g31778	prmt1.L	-1.00713181	0.04139116	PRMT1
XBXL10_1g31784	fut2.L	5.13090759	0.00602974	FUT2
XBXL10_1g31826	otogl2.L	2.76307412	3.15E-05	ENSG00000253107
XBXL10_1g31893	rps9.L	-0.87679147	0.02975692	RPS9
XBXL10_1g32042	LOC108696821	-1.49010246	0.09910409	–
XBXL10_1g3210	ndufs4.L	-0.96968107	0.03372956	NDUFS4
XBXL10_1g32111	XB5760648.L	0.78193367	0.06522422	–
XBXL10_1g32128	LOC108696931	3.62110615	0.02535037	–
XBXL10_1g32129	LOC108695967	4.8055705	0.00016783	–
XBXL10_1g3213	mocs2.L	-0.7452476	0.06825365	MOCS2
XBXL10_1g32147	LOC108696926	-1.69051743	0.03047566	–

XBXL10_1g32166	fxyd1.L	0.80817372	0.09065524	FXYD1
XBXL10_1g32195	LOC108696889	1.70526654	0.01012531	FCGBP
XBXL10_1g32198	LOC108696888	3.08124714	0.01960092	–
XBXL10_1g32199	tyrobp.L	-1.20234257	0.05961917	–
XBXL10_1g32223	LOC121395792	-2.04101788	0.01732925	–
XBXL10_1g32225	LOC108696872	3.45199982	0.03047566	ATP4A
XBXL10_1g32242	nbl1.L	1.05590944	0.03437396	NBL1
XBXL10_1g32260	mrto4.L	-0.89852271	0.04815781	MRTO4
XBXL10_1g32286	clcnkb.L	0.90416955	0.0813177	CLCNKA
XBXL10_1g3230	selenop1.L	-1.05163517	0.02535037	SELENOP
XBXL10_1g32323	znf362.L	1.11390975	0.07488007	ZNF362
XBXL10_1g32358	pdcd4.S	1.09884382	0.02251956	PDCD4
XBXL10_1g3238	c6.2.L	6.74249218	0.00321868	C6
XBXL10_1g32414	LOC108697326	0.90823178	0.04555164	CASP2
XBXL10_1g3246	c9.L	1.22961408	0.03815076	C9
XBXL10_1g32515	LOC108697176	1.16552511	0.0762097	ANK3
XBXL10_1g32531	LOC121396199	3.64427601	1.90E-05	–
XBXL10_1g32572	LOC108697180	3.64587046	0.07077716	TCERG1L
XBXL10_1g32587	bccip.S	-0.74723598	0.0931156	BCCIP
XBXL10_1g32615	stn1.S	-0.80592093	0.05617914	STN1
XBXL10_1g3262	slc1a3.L	3.41064322	0.05853693	SLC1A3
XBXL10_1g32624	atp5mk.S	-0.85071845	0.04767981	ATP5MK
XBXL10_1g32627	nt5c2.S	0.82691901	0.07158899	NT5C2
XBXL10_1g32681	pgam1.S	-0.71692127	0.08057675	PGAM1
XBXL10_1g32707	LOC108697440	-0.96485188	0.05961917	–
XBXL10_1g3271	agxt2.L	-0.89242822	0.05739897	AGXT2
XBXL10_1g32759	LOC108697460	2.30009244	0.00109252	SGTA
XBXL10_1g32833	LOC108697209	2.78204607	0.07373838	–
XBXL10_1g32868	LOC108697492	-0.65501392	0.09867992	–
XBXL10_1g32969	LOC108703391	1.68300874	0.00997873	MAT1A
XBXL10_1g32977	LOC121396009	4.1595259	0.08905686	–
XBXL10_1g33009	tmem254l.S	-0.89598316	0.07944875	–
XBXL10_1g3309	onecut2.L	3.73258161	0.02441789	ONECUT2
XBXL10_1g33095	fbxo2.S	-1.23309515	0.06000595	FBXO2
XBXL10_1g33116	atp12a.S	1.72745932	0.02716087	ATP12A
XBXL10_1g33123	LOC108697224	-1.36412338	0.08755006	OPCML
XBXL10_1g33152	tmem45b.S	2.240592	0.01011845	TMEM45B
XBXL10_1g3325	tspan36.L	0.92943047	0.03965622	–
XBXL10_1g33337	fxyd2.S	-0.94892659	0.04357092	–
XBXL10_1g3343	c18orf32.L	-0.72191069	0.07588414	C18orf32
XBXL10_1g33435	mxra8.S	1.74237137	0.00483245	MXRA8
XBXL10_1g33493	aadacl4.S	-1.09242862	0.02367819	–
XBXL10_1g33584	LOC108697723	0.91510215	0.07863528	NPM1P21
XBXL10_1g33604	mpv17l.S	-0.92097583	0.09421345	–
XBXL10_1g33607	LOC108697739	3.33045029	0.00051737	SACS
XBXL10_1g33639	atg12.S	-0.73488387	0.04735613	ATG12
XBXL10_1g33641	cd79a.S	-2.00074671	0.03111471	CD79A
XBXL10_1g33647	znf574.S	0.70720439	0.09800388	ZNF574
XBXL10_1g33653	erf.S	0.86288466	0.09244538	ERF
XBXL10_1g33655	pafah1b3.S	-0.7001675	0.0538375	PAFAH1B3
XBXL10_1g33679	prss1.2.S	6.52608303	0.01044594	PRSS1
XBXL10_1g33683	xcxcra	-1.26029314	0.03370204	–
XBXL10_1g33714	slc6a16.S	1.1416897	0.04020289	SLC6A15
XBXL10_1g33737	LOC108697796	5.78344197	0.01088018	–
XBXL10_1g3380	aqp7.L	-7.2935428	0.01497066	AQP3
XBXL10_1g33820	LOC108705380	4.596594	0.0440164	–

XBXL10_1g33821	LOC121396168	4.76834046	0.03522754	–
XBXL10_1g33822	LOC100126637	4.47682418	0.03649266	–
XBXL10_1g33823	gbp6.L	1.00326442	0.05367805	GBP2
XBXL10_1g33862	btg5.1.S	5.64089897	0.02603105	TOB2
XBXL10_1g33885	LOC108705485	1.99695736	0.08345145	–
XBXL10_1g33905	LOC108697060	4.23844924	0.09502394	–
XBXL10_1g33938	LOC108705702	3.82050203	0.07808471	–
XBXL10_1g3394	vwa5a.2.L	0.98091781	0.02968976	VWA5A
XBXL10_1g33965	XB5897453.S	2.2128173	0.06567134	–
XBXL10_1g33967	tyrobp.S	-0.94064873	0.08302643	–
XBXL10_1g34002	micos10.S	-0.95540851	0.02353093	MICOS10
XBXL10_1g34086	rpl10.L	-1.09276929	0.01518856	RPL10
XBXL10_1g34133	ssna1.L	-0.65831532	0.08224361	SSNA1
XBXL10_1g34201	LOC121396852	2.72619193	0.0139193	–
XBXL10_1g34211	mrpl41.L	-0.88497645	0.05500854	MRPL41
XBXL10_1g34218	LOC108706083	-0.87277366	0.07112016	–
XBXL10_1g34289	tmem250.L	-0.98521757	0.04403508	TMEM250
XBXL10_1g34332	c5.2.L	1.70820637	0.01207803	C5
XBXL10_1g34336	slc2a8.L	1.79117149	0.07862673	SLC2A8
XBXL10_1g34373	LOC121396868	-0.81660896	0.08862882	–
XBXL10_1g34385	spaca9.L	-1.0198181	0.08095912	SPACA9
XBXL10_1g34391	setx.L	0.99270186	0.09421345	SETX
XBXL10_1g34410	prdm12.L	6.03803913	0.01277539	PRDM12
XBXL10_1g34458	LOC108704482	-0.93421567	0.03524784	PHYHD1
XBXL10_1g34459	lrrc8a.L	0.86841401	0.06393273	LRRC8A
XBXL10_1g34460	kyat1.L	-0.94035283	0.03522754	KYAT1
XBXL10_1g3449	LOC121396185	-3.3303154	0.01345414	–
XBXL10_1g34493	sephs3.L	-0.72204635	0.04678105	SEPHS2
XBXL10_1g34540	LOC108706216	-1.56045032	0.00058402	ATRIP
XBXL10_1g34615	crb2.L	1.33123484	0.05618748	CRB2
XBXL10_1g34625	nr5a1.L	1.79166914	0.00424585	NR5A2
XBXL10_1g34629	wdr38.L	-1.23127484	0.0777023	WDR38
XBXL10_1g34689	LOC108698244	2.13814766	0.0791753	MYH4
XBXL10_1g34719	renbp.L	-1.02437335	0.04882674	RENBP
XBXL10_1g34756	LOC108698272	-0.93430932	0.04735613	–
XBXL10_1g34769	klf8.L	1.01046565	0.01399884	KLF12
XBXL10_1g34787	tsc22d3.L	-1.04849282	0.00752177	TSC22D3
XBXL10_1g34967	XB5730431.L	-1.52997602	0.01346694	–
XBXL10_1g3498	pcgf1.S	-0.92592048	0.04454243	PCGF1
XBXL10_1g34994	LOC108698345	2.31405674	0.01004921	ACOD1
XBXL10_1g34996	phyhdlc.1.L	4.64184074	0.00151178	–
XBXL10_1g35012	phyhdla.1.L	6.47435572	0.00445832	–
XBXL10_1g35047	LOC108698897	3.76537132	0.05739897	FIP1L1
XBXL10_1g35056	rlim.L	0.74529083	0.03452135	RLIM
XBXL10_1g35087	col4a5.L	1.02334003	0.03690455	COL4A5
XBXL10_1g35114	LOC108698411	1.00312377	0.03522754	PCDH19
XBXL10_1g35207	sash3.L	-0.94264872	0.07077716	SASH3
XBXL10_1g35213	klhl4.L	1.58584529	0.01490376	KLHL4
XBXL10_1g35297	gpc3.L	1.17518057	0.0217952	GPC3
XBXL10_1g35309	mmgt1.L	-0.93647351	0.02245085	MMGT1
XBXL10_1g35387	rack1.L	-0.92142352	0.02607802	RACK1
XBXL10_1g35409	LOC108698547	-0.82845052	0.06632227	RGL2
XBXL10_1g35437	agpat1.L	-0.72319125	0.07915921	AGPAT1
XBXL10_1g35439	c4a.L	1.5790552	0.00410253	C4A
XBXL10_1g35565	dpf1.L	3.10936257	0.08726806	DPF1
XBXL10_1g35618	exosc5.L	-0.99140402	0.0872031	EXOSC5

XBXL10_1g35631	LOC108698636	3.41342571	0.03815137	CAPN12
XBXL10_1g35637	psmd8.L	-0.84157887	0.04971753	PSMD8
XBXL10_1g35661	mrps12.L	-0.99272851	0.03166744	MRPS12
XBXL10_1g35692	entpd5.L	-1.07340099	0.06538164	ENTPD5
XBXL10_1g35702	fcf1.L	-0.79267601	0.0594442	FCF1
XBXL10_1g35712	batf.L	-1.52092437	0.08987188	BATF
XBXL10_1g35769	LOC108698710	-0.76831486	0.06001248	CALM1
XBXL10_1g35802	serpina3m.L	4.4386152	0.06127354	SERPINB12
XBXL10_1g35805	serpina3k.L	3.65967879	0.00402198	SERPINA7
XBXL10_1g35811	clmn.L	1.74526768	0.09421888	CLMN
XBXL10_1g35814	glrx5.L	-0.79108524	0.04823864	GLRX5
XBXL10_1g35817	bdkrb2.L	1.14824259	0.01576938	BDKRB2
XBXL10_1g35892	gng2.L	-0.98484431	0.09065524	GNG2
XBXL10_1g35897	trim9.L	-1.4436667	0.08428086	TRIM9
XBXL10_1g35910	begain.L	5.48626716	0.04139048	BEGAIN
XBXL10_1g35925	rcor1.L	1.10824267	0.05241337	RCOR1
XBXL10_1g35970	btbd6.L	-0.93334336	0.07062568	BTBD6
XBXL10_1g35978	LOC108698814	3.23913137	0.07521587	–
XBXL10_1g36020	actr10.L	-0.66868637	0.09451798	ACTR10
XBXL10_1g36023	slc35f4.L	-1.45419672	0.07232962	SLC35F4
XBXL10_1g36071	LOC121397138	-5.98613023	0.06165451	–
XBXL10_1g36094	sptb.L	1.51752372	0.07342915	SPTB
XBXL10_1g36114	foxa1.L	2.29610046	0.00215298	FOXA1
XBXL10_1g36122	fam177a1.L	-0.85642801	0.04322825	FAM177A1
XBXL10_1g36133	erh.L	-0.95923589	0.02627729	ERH
XBXL10_1g36153	dph6.L	1.01287167	0.0747306	DPH6
XBXL10_1g36154	znf770.L	-1.28850775	0.08002452	ZNF770
XBXL10_1g36174	dtd2.L	-0.85487318	0.06468747	DTD2
XBXL10_1g36215	gchfr.L	-0.86850873	0.04604274	GCHFR
XBXL10_1g3630	maea.S	-0.81291243	0.05582389	MAEA
XBXL10_1g36321	LOC121397396	-3.00568998	0.07649552	U2
XBXL10_1g36360	thbs1.L	1.29671469	0.03384704	THBS1
XBXL10_1g36392	LOC121397178	3.12769564	0.06806062	–
XBXL10_1g3655	add1.S	0.73617406	0.08078023	ADD1
XBXL10_1g36581	LOC108699362	0.64642727	0.09100763	NR2F1
XBXL10_1g36660	LOC121397341	3.52523528	0.03801284	–
XBXL10_1g36661	LOC108699114	4.03910267	6.40E-05	–
XBXL10_1g36670	mrpl24.L	-0.78895026	0.04526352	MRPL24
XBXL10_1g36697	LOC108699394	6.59602862	0.00107404	MIR9-1
XBXL10_1g36708	ca14.L	0.95413035	0.05490254	CA14
XBXL10_1g3671	cpz.S	1.88879909	0.00973676	CPZ
XBXL10_1g36710	LOC108699399	1.40837194	0.07306981	KIRREL1
XBXL10_1g36759	LOC108699405	-1.23843124	0.06771662	–
XBXL10_1g36892	LOC108699447	2.31094544	0.02271749	–
XBXL10_1g36899	LOC108699158	-0.76301275	0.04604274	EIF3F
XBXL10_1g3691	msx1.S	0.90859957	0.04431759	MSX1
XBXL10_1g36935	LOC108699617	-0.84262535	0.04330698	UFC1
XBXL10_1g37065	LOC108699492	4.08758662	0.05192146	KCNJ9
XBXL10_1g37106	g2e3.S	-1.30291441	0.06771662	G2E3
XBXL10_1g3712	fgfbp1.S	2.40241234	0.05758573	OR8G1
XBXL10_1g37140	foxa1.S	2.76325735	8.45E-05	FOXA1
XBXL10_1g3717	qdpr.S	-1.42333855	0.00997873	QDPR
XBXL10_1g37171	ptgr2.S	-0.66476795	0.09452853	PTGR2
XBXL10_1g37181	jmjd7.S	-1.05184095	0.02375806	JMJD7
XBXL10_1g37233	LOC108699763	2.74448703	0.00164498	–
XBXL10_1g37234	LOC121397762	3.10297884	0.01532462	–

XBXL10_1g3724	LOC108706551	-1.28399782	0.08760058	KCNIP4
XBXL10_1g3742	pcdh7.S	1.58555722	0.02438838	PCDH7
XBXL10_1g37486	ptgds.S	1.83907612	0.00522436	PTGDS
XBXL10_1g37498	mrpl41.S	-1.00477827	0.03522754	MRPL41
XBXL10_1g37507	entpd2.S	0.92160143	0.08096525	ENTPD2
XBXL10_1g37553	LOC108699910	-1.04820444	0.02697134	–
XBXL10_1g37574	LOC108699917	4.33428309	0.09632297	TRAF1
XBXL10_1g37673	phyhd1.S	-0.88348706	0.03127345	PHYHD1
XBXL10_1g37730	ccnq.S	-0.87455345	0.03286254	CCNQ
XBXL10_1g37801	olfml2a.S	0.98706706	0.06035329	OLFML2A
XBXL10_1g37848	XB5932841.S	-1.63667399	0.03971114	–
XBXL10_1g37868	tsc22d3.S	-0.88388357	0.02353093	TSC22D3
XBXL10_1g3790	LOC121399278	4.37964915	0.04080668	–
XBXL10_1g37924	LOC121397625	-1.35107642	0.07945628	XIAPP3
XBXL10_1g37929	LOC121397580	-2.07348106	0.05240236	–
XBXL10_1g37948	LOC108700083	5.48451043	0.03452135	AMER1
XBXL10_1g38054	LOC108700139	-1.05473905	0.02875538	SOWAHC
XBXL10_1g38085	XB5776174.S	-1.52114157	0.00168586	–
XBXL10_1g38173	vgll1.S	2.62675034	0.04735613	VGLL1
XBXL10_1g38221	tbcb.S	-0.83858308	0.04143366	TBCB
XBXL10_1g38223	polr2i.S	-0.97454981	0.03522754	POLR2I
XBXL10_1g38253	pfdn6.S	-0.98945144	0.02159199	PFDN6
XBXL10_1g38294	csnk2b.S	-0.75563025	0.05853693	CSNK2B
XBXL10_1g38378	ehd2.S	0.85663592	0.06032128	EHD2
XBXL10_1g38390	clip3.S	0.960906	0.02240955	CLIP3
XBXL10_1g38393	arf6.S	-0.73395396	0.08096525	ARF6
XBXL10_1g38404	lrfn1.1.S	4.38683281	0.03452135	LRFN5
XBXL10_1g38418	pqbp1.S	-0.84212865	0.03202045	PQBP1
XBXL10_1g38422	LOC447781	0.82243547	0.0833011	COMT
XBXL10_1g38429	LOC108700302	2.19105661	0.03877133	MYH1
XBXL10_1g3849	casp3.2.S	1.38545048	0.00142478	CASP3
XBXL10_1g3855	rwdd4.S	-1.06585381	0.03803739	RWDD4
XBXL10_1g38550	LOC108700682	6.75081682	0.00109252	–
XBXL10_1g38561	LOC121397641	5.70479175	0.06018017	BCHE
XBXL10_1g38660	LOC121397571	6.02530194	0.00576513	MIR9-1
XBXL10_1g38678	LOC121397574	4.29085205	0.07714323	–
XBXL10_1g3868	gpm6a.S	3.95364854	0.03377234	GPM6A
XBXL10_1g38688	tnfaip8l2.S	-0.89489707	0.03448132	TNFAIP8L3
XBXL10_1g38701	pex19.S	-0.8048905	0.03859697	PEX19
XBXL10_1g3875	sap30.S	-1.03338484	0.08986039	SAP30
XBXL10_1g38784	adar.S	0.87298796	0.03824678	ADAR
XBXL10_1g3887	LOC108704313	1.95259991	0.04604274	DDX60
XBXL10_1g38892	tbc1d20.1.L	-0.82392036	0.07910198	TBC1D20
XBXL10_1g38898	mlx.L	-0.83939339	0.04712571	MLX
XBXL10_1g3892	cpe.S	0.77560655	0.0931156	CPE
XBXL10_1g38937	krt19.L	0.93718981	0.03837197	KRT19
XBXL10_1g38964	igfbp4.L	-1.20364155	0.06632227	IGFBP4
XBXL10_1g38995	LOC108700778	1.65793385	0.00355293	PPP1R1B
XBXL10_1g39009	LOC108700789	2.03980148	0.07393393	PLXDC1
XBXL10_1g39015	LOC108700787	-0.84016194	0.06378494	RPL23
XBXL10_1g39144	LOC108700827	1.03201091	0.05726535	FZD2
XBXL10_1g39152	slc4a1.L	1.41047153	0.06381613	SLC4A1
XBXL10_1g39223	MGC82392	0.85787561	0.05799786	DCAF7
XBXL10_1g39348	LOC108700918	1.6800337	0.00145234	–
XBXL10_1g39376	phactr3.L	4.7122253	0.02159199	PHACTR3
XBXL10_1g39377	edn3.L	1.80908976	0.0001198	EDN3

XBXL10_1g39399	LOC108702031	1.19459463	0.05039604	OGFR
XBXL10_1g39426	LOC108702045	6.93163845	0.02485711	FUT10
XBXL10_1g39437	LOC121398202	-6.21471449	0.03630416	TCEA2
XBXL10_1g39455	LOC108700949	-1.80961296	0.01327069	–
XBXL10_1g39671	dusp3.L	-1.49472842	0.00107404	DUSP3
XBXL10_1g3968	ucp1.S	-3.36744718	0.00821348	UCP3
XBXL10_1g39779	enpp7.L	3.89759294	0.06538164	ENPP7
XBXL10_1g39793	ccdc56.L	-0.75756494	0.04555164	–
XBXL10_1g39807	g6pc1.1.L	-3.25377858	0.05180544	G6PC1
XBXL10_1g39809	g6pc1.3.L	-2.7902458	0.00927761	G6PC1
XBXL10_1g3982	LOC108706683	-0.75322758	0.06771662	–
XBXL10_1g39829	slc12a5.L	4.95582538	0.02788868	SLC12A5
XBXL10_1g39860	znfx1.L	3.08487152	0.00035791	ZNFX1
XBXL10_1g39891	tti1.L	0.92068962	0.0747306	TTI1
XBXL10_1g39897	manbal.L	-0.79381324	0.02865858	MANBAL
XBXL10_1g39905	tgif2.L	3.15142247	0.07944875	TGIF2
XBXL10_1g39918	LOC108705538	5.84578044	0.0101263	SLC32A1
XBXL10_1g39919	arhgap40.L	4.07948896	0.04897155	ARHGAP40
XBXL10_1g4	mrps26.L	-0.72848779	0.09503618	–
XBXL10_1g40020	ndrg3.L	0.69048471	0.04971753	NDRG3
XBXL10_1g40094	LOC108701125	1.79095778	0.01211775	EVPL
XBXL10_1g40110	LOC121398233	-4.00393807	0.00448327	–
XBXL10_1g40120	LOC108701136	4.80403994	0.0139193	ST6GALNAC2
XBXL10_1g4024	ostc.S	-1.02127914	0.01499783	OSTC
XBXL10_1g40299	LOC108701818	6.51733774	0.00143302	MYH4
XBXL10_1g40320	prkca.L	0.89211292	0.0449599	PRKCA
XBXL10_1g40337	polg2.L	-0.93321529	0.02697134	POLG2
XBXL10_1g40340	LOC108701212	-1.16529489	0.0758163	–
XBXL10_1g40344	XB5880825.L	1.23745026	0.03631925	SAMD9
XBXL10_1g40353	tefm.L	-0.87097853	0.03174659	–
XBXL10_1g40363	trim25.L	0.92640198	0.05961917	TRIM25
XBXL10_1g40382	steap3.L	1.34101747	0.00381154	STEAP3
XBXL10_1g40394	dtx3l.L	1.47730329	0.00175592	DTX3L
XBXL10_1g4041	cfi.S	1.45912466	0.05961917	CFI
XBXL10_1g40416	LOC108701252	4.56991105	0.06538164	–
XBXL10_1g40479	LOC108701269	-0.84991573	0.03008655	–
XBXL10_1g40487	LOC108701272	2.01577877	0.01358652	TMEM198
XBXL10_1g40516	tuba1cl.2.L	-1.49133891	0.00034606	TUBA1B
XBXL10_1g40522	LOC121397893	-1.05714253	0.0212755	TUBA1B
XBXL10_1g40524	tuba1cl.3.L	-0.97492404	0.04698731	TUBA1B
XBXL10_1g40542	XB984297.L	1.58125728	0.02968976	CYP27A1
XBXL10_1g40703	cdca7.L	0.64653641	0.07910198	CDCA7
XBXL10_1g40770	LOC108701405	-1.38036815	0.07270259	SLC19A1
XBXL10_1g40776	ybey.L	-0.75046032	0.05582389	YBEY
XBXL10_1g40798	ackr3.L	0.81436151	0.05565102	ACKR3
XBXL10_1g40815	LOC108701422	2.93071884	0.00538948	ABCA12
XBXL10_1g40843	sumo3.L	-0.80466633	0.04143366	SUMO3
XBXL10_1g40844	LOC108705838	-0.88630982	0.0209518	SUMO3
XBXL10_1g40848	dbr1.L	-0.83557645	0.05726535	DBR1
XBXL10_1g40863	LOC121398237	-1.4458407	0.04604274	–
XBXL10_1g40875	maip1.L	-0.78706436	0.08096525	MAIP1
XBXL10_1g40878	LOC108701447	1.45020594	0.07808471	AOX1
XBXL10_1g40907	eef1b2.L	-0.81422729	0.03452135	EEF1B2
XBXL10_1g40957	slc40a1.L	-1.1686732	0.05582389	SLC40A1
XBXL10_1g40958	asnsd1.L	-0.97939219	0.01862502	ASNSD1
XBXL10_1g41004	arpc1b.L	-0.72680979	0.06273607	ARPC1B

XBXL10_1g41006	natd1.L	-0.85476428	0.02257186	NATD1
XBXL10_1g41029	LOC108701509	1.42253721	0.07128052	HBZ
XBXL10_1g4107	dapp1.S	-1.31884774	0.03384704	DAPP1
XBXL10_1g41090	ndufb7.L	-0.93042898	0.01399884	NDUFB7
XBXL10_1g4114	metap1.S	-0.86570861	0.07090464	METAP1
XBXL10_1g41169	get4.L	-2.07886163	0.00055672	GET4
XBXL10_1g41234	pdilt.L	4.00373433	0.08942236	P4HB
XBXL10_1g4125	XB5957215.S	1.47339204	0.04081044	OPN4
XBXL10_1g41279	MGC145260.L	1.18988131	0.07112016	–
XBXL10_1g41352	slc5a11.L	-1.14689661	0.06632227	SLC5A11
XBXL10_1g41370	grap.L	-1.34751188	0.03836658	GRAP
XBXL10_1g41384	LOC108701662	0.82509364	0.03452135	SSTR3
XBXL10_1g41390	rps2.L	-0.78900307	0.05582389	RPS2
XBXL10_1g41405	thdl20.L	2.97936303	0.0193842	–
XBXL10_1g41412	LOC108701676	4.4784844	0.09532941	–
XBXL10_1g41430	pemt.L	-1.01108827	0.07712034	PEMT
XBXL10_1g41436	atpaf2.L	-1.14459043	0.00904935	ATPAF2
XBXL10_1g4144	herc6.S	1.76578224	0.00107404	HERC3
XBXL10_1g41482	slc5a2.L	-1.03185958	0.08199359	SLC5A2
XBXL10_1g41503	LOC108701721	1.78295626	8.05E-05	–
XBXL10_1g41671	LOC108701960	2.02815459	0.05582389	KIF13A
XBXL10_1g41706	MGC79752.L	-0.71722516	0.05961917	–
XBXL10_1g41721	LOC121398003	6.06862886	0.00653294	–
XBXL10_1g41761	xenoxin1.L	4.55364119	0.04326199	–
XBXL10_1g4177	cxcl11.S	-1.52943336	0.06684541	–
XBXL10_1g41811	mfap4.1.L	-1.07440057	0.02353093	MFAP4
XBXL10_1g41819	LOC108703896	3.56669092	0.01440793	URGCP
XBXL10_1g4182	scarb2.S	0.87776254	0.0747306	SCARB2
XBXL10_1g41837	LOC108703861	5.96143792	0.0101263	URGCP
XBXL10_1g41866	XB994846.L	2.52290411	0.03202045	–
XBXL10_1g4190	ccng2.S	-1.3942498	0.05347478	CCNG2
XBXL10_1g41980	LOC121398054	-1.86032806	0.09948331	–
XBXL10_1g42079	LOC108703917	3.12546307	0.04555164	–
XBXL10_1g42140	LOC108704730	-0.88597952	0.09738963	CDKL4
XBXL10_1g42141	nmral1.L	-1.39744031	0.00487047	NMRAL2P
XBXL10_1g42142	LOC121397868	-1.13803196	0.07044345	NMRAL2P
XBXL10_1g42146	fbxl16.L	3.64692358	0.03631925	FBXL16
XBXL10_1g42167	cavin1.S	0.92176549	0.07154659	CAVIN1
XBXL10_1g4217	LOC108704562	5.84628466	0.01004921	EPHA5
XBXL10_1g422	glod5.L	-0.70266761	0.0777023	GLOD5
XBXL10_1g42365	phb.S	-0.94613694	0.05192146	PHB1
XBXL10_1g42384	slc4a1.S	1.39639969	0.04454243	SLC4A1
XBXL10_1g42396	pyy.S	5.54104162	0.01981548	–
XBXL10_1g42416	mapt.S	1.27543733	0.02211568	MAPT
XBXL10_1g42502	pard6b.S	1.3890233	0.05193868	PARD6B
XBXL10_1g42539	gata5.S	1.17977977	0.02990064	GATA5
XBXL10_1g42672	LOC108702671	-1.41411434	0.00424585	–
XBXL10_1g42697	LOC108702687	2.33704071	0.06632227	NUP160
XBXL10_1g42708	bcl2l1.S	-0.69280092	0.08862882	BCL2L1
XBXL10_1g42820	enpp7.S	3.53170955	0.0730426	ENPP7
XBXL10_1g42821	LOC121398749	5.23927265	0.00709241	–
XBXL10_1g42836	g6pc1.1.S	-2.80909165	0.00872664	G6PC1
XBXL10_1g42838	g6pc1.3.S	-1.87703252	0.00401207	G6PC1
XBXL10_1g4289	LOC108706796	-1.28683097	0.07551207	MFSD12
XBXL10_1g42890	tgm5.S	3.54691835	0.00568223	TGM5
XBXL10_1g42972	ahcy.S	-1.02127564	0.05079408	AHCY

XBXL10_1g430	pced1a.L	1.60745012	0.02189588	PCED1A
XBXL10_1g43022	LOC108702797	-1.4180726	0.05192146	RAB37
XBXL10_1g43099	LOC108702825	-1.08164258	0.00445832	–
XBXL10_1g43106	LOC108702827	6.00739934	0.00724409	ST6GALNAC2
XBXL10_1g43109	mettl23.S	-0.79183672	0.09734396	METTL23
XBXL10_1g43130	uts2r.S	-3.64093233	0.00619736	UTS2R
XBXL10_1g43167	tekt3.S	-1.16569071	0.0467767	TEKT3
XBXL10_1g43252	lypd1.S	-1.36471126	0.09675694	LYPD1
XBXL10_1g43265	tmem37.S	-0.7068231	0.06632227	TMEM37
XBXL10_1g43273	dtx3l.S	2.18047318	0.00669464	–
XBXL10_1g43287	LOC121399241	-1.47587581	0.01816117	–
XBXL10_1g43289	gli2.S	2.84047317	0.01198548	GLI2
XBXL10_1g43297	slc15a2.S	-0.92081761	0.06655029	SLC15A2
XBXL10_1g43298	eaf2.S	-0.97825881	0.01862502	EAF2
XBXL10_1g43329	krt18.3.S	-1.0430069	0.07084384	KRT18
XBXL10_1g43353	atg9a.S	1.3610759	0.0747306	ATG9A
XBXL10_1g43371	prkag3.S	-1.19156476	0.06378494	PRKAG3
XBXL10_1g43381	wnt6.S	5.59463469	0.01668397	WNT6
XBXL10_1g43429	arl5a.S	-0.7720162	0.04604274	ARL5A
XBXL10_1g43444	galnt5.S	1.25943839	0.04735613	GALNT5
XBXL10_1g43495	gad1.1.S	4.2573636	0.05114091	GAD1
XBXL10_1g4357	rorb.2.S	3.97127992	0.0581877	RORB
XBXL10_1g43596	arl4c.S	0.86600338	0.03631925	ARL4C
XBXL10_1g43598	ugt1a6.S	1.69353213	0.02505439	UGT1A6
XBXL10_1g43618	rab5d.S	-0.80421372	0.06806062	RAB5B
XBXL10_1g43622	map2.S	3.32619651	5.45E-06	MAP2
XBXL10_1g43627	LOC108702286	-0.77065505	0.0777023	UBE2G2
XBXL10_1g43630	dbr1.S	-0.79657913	0.03785278	DBR1
XBXL10_1g43638	cd28.S	-1.65138354	0.0542316	–
XBXL10_1g43649	LOC108702410	-2.65320655	0.02353093	–
XBXL10_1g43658	maip1.S	-0.65039252	0.09400929	MAIP1
XBXL10_1g4367	ap1m1.S	-0.80336959	0.0581877	AP1M1
XBXL10_1g437	nat8.5.L	-1.48716571	0.00869516	–
XBXL10_1g43721	stat1.S	1.13904946	0.02068405	STAT1
XBXL10_1g43727	mob4.S	-0.90858661	0.02642041	MOB4
XBXL10_1g43741	arpc1b.S	-0.70867957	0.07227085	ARPC1B
XBXL10_1g43742	arpc1a.S	-0.95204244	0.00709241	ARPC1A
XBXL10_1g43743	natd1.S	-0.85900774	0.02061134	NATD1
XBXL10_1g43763	LOC108702421	2.0279487	0.02159199	HBQ1
XBXL10_1g4385	rps15.S	-0.6917875	0.09832158	RPS15
XBXL10_1g43867	c7orf50.S	-0.8472106	0.06538164	C7orf50
XBXL10_1g43923	LOC108702428	5.13733388	0.05228498	MCHR1
XBXL10_1g43935	scnn1g.S	1.83783006	0.00364228	SCNN1G
XBXL10_1g43996	lcmt1.S	-0.8688091	0.09452853	LCMT1
XBXL10_1g4400	polr2e.S	-0.98327702	0.03927902	POLR2E
XBXL10_1g44031	LOC108703225	-0.82063411	0.02582152	RPS2
XBXL10_1g44040	thdl20.S	3.36038896	0.02436328	–
XBXL10_1g44041	LOC108703229	4.34228467	0.0747306	–
XBXL10_1g44079	ppl.S	1.50155586	0.00632847	PPL
XBXL10_1g44155	LOC108702444	3.09457795	0.07817392	–
XBXL10_1g4431	angptl4.S	1.13087808	0.03522754	ANGPTL4
XBXL10_1g44341	trim7.L	2.48795733	0.07189688	TRIM5
XBXL10_1g44379	LOC108704190	-0.79531974	0.06378494	PITPNA
XBXL10_1g44409	LOC121398931	3.55376186	0.06000436	–
XBXL10_1g44432	hmox2.S	-0.80661013	0.06907671	HMOX2
XBXL10_1g44433	nmral1.S	-1.28001129	0.05419291	NMRAL2P

*** mtDNA	XBXL10_1g44448	COX2	0.70284454	0.0876235	–
	XBXL10_1g4454	LOC108704680	3.18698938	0.06282312	ZFX
	XBXL10_1g447	lyrm2.L	-0.87737868	0.02134031	–
	XBXL10_1g4559	comp.S	6.73480356	0.00740348	THBS4
	XBXL10_1g4573	sdsl.S	-0.91267282	0.06282312	SDSL
	XBXL10_1g4629	LOC108703688	4.6185274	0.02603105	–
	XBXL10_1g4677	borcs8.S	-1.23776269	0.00070372	BORCS8-MEF2B
	XBXL10_1g4678	nr2c2ap.S	-0.809373	0.06522422	–
	XBXL10_1g4725	smim7.S	-0.73153593	0.08937969	SMIM7
	XBXL10_1g4752	rps6.S	-0.88406123	0.02582152	RPS6
	XBXL10_1g4822	ak3.S	-0.96966849	0.02607802	AK3
	XBXL10_1g4861	tmem252.S	-2.22071722	0.00116822	–
	XBXL10_1g4866	fam189a2.S	-1.05829082	0.04555164	FAM189A2
	XBXL10_1g4883	aldh1a1.S	1.44129884	0.00568223	ALDH1A1
	XBXL10_1g4890	ostf1.S	-1.00019214	0.06378494	OSTF1
	XBXL10_1g4935	prxl2c.S	-0.80863345	0.06538164	PRXL2C
	XBXL10_1g4953	syk.S	-1.31136811	0.01536739	SYK
	XBXL10_1g5031	sall2.S	6.15165881	0.00445832	SALL2
	XBXL10_1g5112	sec14l3.S	2.35341535	0.09212897	SEC14L2
	XBXL10_1g5123	zmat5.S	-0.76747081	0.06852393	ZMAT5
	XBXL10_1g5206	dgcr6.S	-0.95700884	0.01004921	DGCR6
	XBXL10_1g5225	LOC121399481	4.35965024	0.0705302	–
	XBXL10_1g5235	sppl3.S	0.75727922	0.0777023	SPPL3
	XBXL10_1g5260	ggt5.S	0.97628386	0.07979075	GGT5
	XBXL10_1g5347	ubc.S	-1.13556018	0.06035329	UBC
	XBXL10_1g5413	LOC108707171	1.65958068	0.01888028	–
	XBXL10_1g5446	osbp2.S	6.09186585	0.00086197	OSBP2
	XBXL10_1g5484	tnfaip8.S	-1.04758578	0.03008655	TNFAIP8
	XBXL10_1g5506	reep5.S	-0.871075	0.0286203	REEP5
	XBXL10_1g5536	LOC108707228	0.95873743	0.04454243	CAST
	XBXL10_1g5539	glrx.S	-0.69177274	0.05582389	–
	XBXL10_1g5583	LOC108707252	-0.70276085	0.09332809	–
	XBXL10_1g5593	btf3.S	-0.98061209	0.05240236	BTF3
	XBXL10_1g5683	smim15.S	-1.05397429	0.03522754	SMIM15
	XBXL10_1g5742	esm1.S	-1.27587511	0.03758007	ESM1
	XBXL10_1g5848	baat.S	-1.117519	0.04139048	BAAT
	XBXL10_1g6055	hao2.L	2.08168495	0.08853299	HAO2
	XBXL10_1g6073	ndufb4.L	-0.92565432	0.02505439	NDUFB4P2
	XBXL10_1g6081	sidt1.L	4.42637938	0.0350593	SIDT1
	XBXL10_1g6099	LOC108707818	1.44155101	0.03384704	–
	XBXL10_1g6135	LOC108707830	-1.10172401	0.0286203	–
	XBXL10_1g6194	tmprss2.2.L	3.84909575	0.06538164	TMPRSS2
	XBXL10_1g6195	tmprss2.3.L	5.008568	0.02211568	TMPRSS2
	XBXL10_1g6196	tmprss2.4.L	4.75514718	0.00552155	TMPRSS2
	XBXL10_1g6204	tmprss2.12.L	4.45627719	0.03859697	TMPRSS2
	XBXL10_1g6206	tmprss2.14.L	4.71207977	0.03375619	TMPRSS2
	XBXL10_1g6208	mx1.L	2.13172195	0.00328753	MX1
	XBXL10_1g6248	LOC108707869	5.24857317	0.03384704	CLIC6
	XBXL10_1g6310	atp5pf.L	-0.70548898	0.08423317	ATP5PF
	XBXL10_1g6337	cadm2.L	3.23552234	0.01840625	CADM2
	XBXL10_1g6344	rbm11.L	-0.77110365	0.03877133	RBM11
	XBXL10_1g6374	asb9.L	-1.17175261	0.0594442	ASB9
	XBXL10_1g640	hgfac.L	1.41395553	0.05490254	HGFAC
	XBXL10_1g6419	abr.L	0.96656915	0.01938401	ABR
	XBXL10_1g6422	LOC108707940	-1.23330096	0.0943991	–
	XBXL10_1g6497	flot2.L	0.73062828	0.0747306	FLOT2

XBXL10_1g6516	sdf2.L	-0.80335218	0.09452853	SDF2
XBXL10_1g6568	arx.L	1.992916	0.03309254	ARX
XBXL10_1g6599	eln1.L	-1.35351554	0.03531044	ELN
XBXL10_1g6607	hpd-like.2.L	1.79179981	0.01440064	HPD
XBXL10_1g6631	sat1.L	-0.72062581	0.05582389	SAT1
XBXL10_1g6636	LOC108708008	1.00516413	0.04618132	MAP3K15
XBXL10_1g6797	ngf.L	-1.13008912	0.02437716	NGF
XBXL10_1g6814	csde1.L	0.6623674	0.07910198	CSDE1
XBXL10_1g6851	pnrc2.L	0.78069564	0.09812155	PNRC2
XBXL10_1g6905	asap3.L	1.60343177	0.00586891	ASAP3
XBXL10_1g6913	msra.2.L	-1.03360761	0.08530951	MSRA
XBXL10_1g6916	med18.L	-0.78065504	0.08862882	MED18
XBXL10_1g6922	tmem222.L	-0.82794951	0.0671417	TMEM222
XBXL10_1g6944	LOC108708105	-0.86773534	0.02535037	–
XBXL10_1g6945	LOC108708106	2.62099974	0.0350593	–
XBXL10_1g6946	thdl17.L	2.85122616	0.01081257	–
XBXL10_1g696	LOC108698040	-1.26036315	0.03452135	–
XBXL10_1g6964	LOC108708110	3.05920691	0.02954754	–
XBXL10_1g6966	LOC108708112	3.61161002	0.00230658	–
XBXL10_1g6967	pafah2.L	-0.94396334	0.07808471	PAFAH2
XBXL10_1g7005	dynll2.L	-0.78051631	0.02975692	DYNLL2
XBXL10_1g706	tapt1.L	1.12956973	0.02697134	TAPT1
XBXL10_1g709	qdpr.L	-1.11718538	0.02353093	QDPR
XBXL10_1g7091	LOC108708144	-0.84757652	0.03662879	MAPK13
XBXL10_1g7224	psmb2.L	-1.17422778	0.00405714	PSMB2
XBXL10_1g7260	cited4.L	-1.26364726	0.00927752	CITED2
XBXL10_1g7284	zc3h12a.L	-0.97485224	0.05277372	ZC3H12B
XBXL10_1g7350	LOC108708261	2.18924449	0.07945628	GJB5
XBXL10_1g736	slc34a2.L	4.69791125	0.01124109	SLC34A2
XBXL10_1g7406	ptrh2.L	-0.88581471	0.09012309	PTRH2
XBXL10_1g7428	aldh3a2.L	0.95182297	0.09062821	ALDH3A2
XBXL10_1g7453	rad51d.L	-0.90738259	0.04707099	RAD51D
XBXL10_1g7463	LOC108708308	7.82070037	9.70E-06	–
XBXL10_1g7468	LOC108708312	1.1419677	0.02627729	CYP4F22
XBXL10_1g7478	rph3al.L	-0.84625828	0.05270507	RPH3AL
XBXL10_1g7560	psph.L	-1.06415291	0.08492216	PSPH
XBXL10_1g7599	eif4h.L	0.94438958	0.01518856	EIF4H
XBXL10_1g7634	c1qbp.L	-0.97736142	0.08903648	C1QBP
XBXL10_1g7642	omg.L	1.80988693	0.0747306	–
XBXL10_1g7667	tmsb4x.L	-1.00058828	0.01804243	TMSB4X
XBXL10_1g7684	gk.L	0.73947126	0.0777023	GK
XBXL10_1g7787	rgn.L	-1.04108482	0.02907387	RGN
XBXL10_1g7818	rab20.L	-1.43164801	0.02902379	RAB20
XBXL10_1g7831	LOC108708464	-1.78063699	0.02505439	SLC10A2
XBXL10_1g7834	tex30.L	-1.73067871	0.04456715	TEX30
XBXL10_1g7847	ggact.L	-1.51888542	0.02556016	GGACT
XBXL10_1g7877	dct.L	1.0676955	0.06771662	DCT
XBXL10_1g7898	scel.L	2.3235011	0.00050383	SCEL
XBXL10_1g7908	uchl3.L	-0.7846698	0.07044345	UCHL3
XBXL10_1g7909	commd6.L	-1.49688655	0.00343874	COMMD6
XBXL10_1g7930	cnmd.L	1.77485271	0.02211568	CNMD
XBXL10_1g7944	LOC108708519	1.74279564	0.00269673	–
XBXL10_1g7963	cpb2.L	1.8467477	0.07166642	CPB2
XBXL10_1g7984	atg101.L	-1.30658496	0.00151178	ATG101
XBXL10_1g7986	nckap5l.L	0.94264917	0.07283111	NCKAP5L
XBXL10_1g799	slc10a4.L	3.23715801	0.00501766	SLC10A4

XBXL10_1g8049	rnf41.L	-0.79570677	0.07910198	RNF41
XBXL10_1g8056	LOC108708564	-1.00904606	0.02597448	RPL41P1
XBXL10_1g8068	sarnp.L	-0.67753921	0.09062114	SARNP
XBXL10_1g8075	stat2.L	1.32803678	0.0872031	STAT2
XBXL10_1g8082	rbms2.L	0.81903576	0.07232977	RBMS2
XBXL10_1g8092	naca.L	-0.76937819	0.06381613	NACA
XBXL10_1g8094	rdh7.2.L	1.58444845	0.0471929	RDH16
XBXL10_1g8114	LOC108708585	-1.87965224	0.00113279	–
XBXL10_1g8118	inhbc.1.L	5.8999702	0.0274397	INHBC
XBXL10_1g8165	cyp27b1.L	3.04544279	0.04555164	CYP27B1
XBXL10_1g8188	tankl.L	-1.56065186	0.0273016	–
XBXL10_1g8195	mettl7a.2.L	-0.76277817	0.06666249	METTL7A
XBXL10_1g8208	arl11l.1.L	2.90198672	0.08326003	ARF5
XBXL10_1g8255	tarbp2.L	-0.98038859	0.04627619	TARBP2
XBXL10_1g8256	XB5957062.L	1.81988746	0.09734396	PLEKHA8
XBXL10_1g8295	krt7.L	0.94251601	0.01709223	KRT8
XBXL10_1g8321	arl11.L	-1.3646461	0.02387483	ARL11
XBXL10_1g8339	vps36.L	-0.70234827	0.09451798	VPS36
XBXL10_1g8343	slc25a15.2.L	-0.98674754	0.02875538	SLC25A15
XBXL10_1g8344	LOC108707754	-2.14484661	0.01172663	SLC25A15
XBXL10_1g8386	alox5ap.L	-1.41602397	0.03309254	ALOX5AP
XBXL10_1g8391	hmgb1.L	-0.85256432	0.06778413	HMGB1
XBXL10_1g8454	mmp3.L	1.12252133	0.04454243	MMP13
XBXL10_1g8489	fdx1.L	-0.65967263	0.09717071	FDX1
XBXL10_1g850	slc7a2.1.L	2.07290913	0.05347478	SLC7A2
XBXL10_1g8649	taf10.L	-0.79994258	0.08303774	TAF10
XBXL10_1g8801	klhl35.L	3.76709335	0.08078023	KLHL35
XBXL10_1g8821	tmem126a.L	-0.76819665	0.07394173	–
XBXL10_1g8853	rsph1.L	-0.80367863	0.05853693	RSPH1
XBXL10_1g8968	p2ry8.S	-1.2287945	0.02971541	SSTR2
XBXL10_1g897	wwc2.L	0.86888964	0.07077716	WWC2
XBXL10_1g9021	LOC108709182	-0.81488473	0.05582389	TIMM22
XBXL10_1g9026	ubb.S	-0.82623429	0.09612504	UBC
XBXL10_1g9093	ncam2.S	2.06438028	0.02582152	NCAM2
XBXL10_1g9149	LOC108709237	2.59448578	0.00355293	CLIC6
XBXL10_1g9164	kcnj15.S	-1.18193405	0.01134227	KCNJ15
XBXL10_1g9176	bace2.S	1.02652427	0.00109704	BACE2
XBXL10_1g920	aadat.L	-1.11971702	0.01709223	AADAT
XBXL10_1g9206	LOC108709263	-0.97337706	0.05582389	–
XBXL10_1g9241	mix23.S	-1.04576476	0.01709223	MIX23
XBXL10_1g9257	ndufb4.S	-0.73075325	0.06655029	NDUFB4P2
XBXL10_1g9261	LOC108705578	1.45204885	0.00842874	TENT5C
XBXL10_1g931	anxa10.L	2.95751362	0.06273607	ANXA10
XBXL10_1g9312	wdr4.S	-0.92601511	0.02937104	WDR4
XBXL10_1g9415	bclaf3.S	0.88706369	0.09012309	–
XBXL10_1g942	npy5r.L	4.56917485	0.09899346	NPY5R
XBXL10_1g9520	XB5951253.S	2.63430552	0.0172662	MOV10
XBXL10_1g9564	ampd1.S	-1.61652551	0.0440164	AMPD1
XBXL10_1g9719	btg2.S	-1.48994494	0.03236341	BTG1
XBXL10_1g9723	chia.S	-1.20796491	0.01938401	CHIA
XBXL10_1g9740	foxp4.S	0.94911588	0.05121616	FOXP4
XBXL10_1g9765	strip1.S	0.75847879	0.06208399	STRIP1
XBXL10_1g9769	lamtor5.S	-0.84609932	0.03404715	LAMTOR5
XBXL10_1g9781	rnpep.S	1.31658128	0.09421888	RNPEP
XBXL10_1g9785	nuak2.S	-1.17144864	0.0274397	NUAK2
XBXL10_1g9803	slc26a9.S	5.20007998	0.0030732	SLC26A9

	XBXL10_1g9866	rabif.S	-0.85848338	0.04403508	RABIF
	XBXL10_1g9893	thdl18.S	2.68133641	0.00047591	–
	XBXL10_1g9894	LOC121400559	5.94049723	1.48E-07	–
	XBXL10_1g9904	LOC108708919	8.47802456	6.61E-08	–
	XBXL10_1g9907	LOC108709109	3.16507894	0.00085954	–
	XBXL10_1g993	fhip1a.L	3.42206728	0.00752177	FHIP1A
MF1					
	XBXL10_1g3050	LOC108697111	-7.520	0.01586	–
	XBXL10_1g43040	cdr2l.S	-8.439	0.01586	CDR2L
	XBXL10_1g3473	LOC108696007	9.507	0.01586	ZSCAN2
MF2					
	XBXL10_1g8729	xdm-w	-8.262	0.00000	DMRT1
	XBXL10_1g31107	apoa5.L	-7.306	0.00237	–
	XBXL10_1g28440	LOC100127252	-6.013	0.00279	CYP2W1
	XBXL10_1g28511	LOC100158309	-9.238	0.00356	TYR
	XBXL10_1g30091	LOC108696033	-7.778	0.01438	PZP
	XBXL10_1g44212	LOC121399024	-3.423	0.01508	MFAP4
	XBXL10_1g3968	ucp1.S	2.446	0.02063	UCP3
	XBXL10_1g30717	LOC121395415	-2.881	0.02120	–
	XBXL10_1g8948	hpx.L	-5.190	0.02120	–
	XBXL10_1g22487	LOC108705534	3.917	0.02319	–
	XBXL10_1g28385	LOC496175	-2.788	0.02319	–
	XBXL10_1g33085	masp2.S	-5.538	0.02324	MASP2
	XBXL10_1g32966	LOC101027275	-4.777	0.02358	–
	XBXL10_1g25989	sgpp2.S	-5.657	0.02396	SGPP2
	XBXL10_1g26938	LOC108718478	-7.245	0.02592	FAIM2
	XBXL10_1g11202	LOC108710052	-9.160	0.02592	THRSP
	XBXL10_1g6540	serpinf2.L	-4.020	0.02592	–
	XBXL10_1g23366	c6orf58.L	-8.710	0.03360	–
	XBXL10_1g15042	akr1d1.S	-2.328	0.03360	AKR1D1
	XBXL10_1g37344	serpina1.S	-2.948	0.03772	SERPINA1
	XBXL10_1g7963	cpb2.L	-3.142	0.04754	CPB2
	XBXL10_1g31213	ca6.L	-5.471	0.04898	CA6
	XBXL10_1g24521	cyp2b6.L	-7.558	0.05069	CYP2C8
	XBXL10_1g7804	proz.L	-2.459	0.05430	F10
	XBXL10_1g32518	tmem26.S	2.430	0.05774	TMEM26
	XBXL10_1g17575	phlda2.L	4.625	0.05774	PHLDA2
	XBXL10_1g40319	apoh.L	-1.644	0.05774	–
	XBXL10_1g17518	clec10a.S	-6.968	0.05862	–
	XBXL10_1g5635	thbs4.S	7.879	0.06728	THBS4
	XBXL10_1g8098	LOC108708580	-6.947	0.08165	SDR9C7
	XBXL10_1g17574	slc22a18.L	3.632	0.08563	SLC22A18
	XBXL10_1g44213	LOC121399151	-4.075	0.08563	MFAP4
MF3					
	XBXL10_1g11376	cyb5r3.L	-1.977	0.00002	CYB5R3
	XBXL10_1g23052	LOC108716659	-2.543	0.00011	–
	XBXL10_1g9723	chia.S	2.116	0.00025	CHIA
	XBXL10_1g8729	xdm-w	-8.849	0.00064	–
	XBXL10_1g24761	LOC108717285	-2.175	0.00245	–
	XBXL10_1g33743	LOC100036823	-1.735	0.00249	FTH1
	XBXL10_1g30226	LOC121395810	-2.784	0.00250	–
	XBXL10_1g30929	atp12a.L	-2.530	0.00258	ATP12A
	XBXL10_1g20744	LOC108714924	-4.108	0.00424	MUC5AC
	XBXL10_1g41866	XB994846.L	-3.620	0.00424	–
	XBXL10_1g31784	fut2.L	-5.368	0.00456	FUT2

XBXL10_1g6099	LOC108707818	-1.976	0.00617	–
XBXL10_1g20743	LOC108715185	-3.341	0.00868	RBM12
XBXL10_1g32531	LOC121396199	-3.124	0.01065	–
XBXL10_1g43622	map2.S	-2.521	0.01090	MAP2
XBXL10_1g6966	LOC108708112	-2.953	0.01168	–
XBXL10_1g38949	krt12.5.L	-1.888	0.01168	KRT24
XBXL10_1g32129	LOC108695967	-4.070	0.01168	–
XBXL10_1g9904	LOC108708919	-7.033	0.01245	–
XBXL10_1g41031	hba2.L	-1.748	0.01326	HBZ
XBXL10_1g1797	LOC108713383	1.744	0.01326	–
XBXL10_1g11415	LOC108710720	-4.221	0.01326	–
XBXL10_1g5949	LOC121398736	5.310	0.01326	–
XBXL10_1g8825	prcp.L	-1.154	0.01326	PRCP
XBXL10_1g1913	igfbpl1.L	-4.865	0.01326	IGFBPL1
XBXL10_1g21588	LOC108715540	-2.866	0.01401	–
XBXL10_1g19367	frrs1.L	-1.282	0.01401	FRRS1
XBXL10_1g11373	LOC108710708	2.078	0.01667	INTS13
XBXL10_1g44393	LOC108704227	-1.909	0.01969	–
XBXL10_1g23886	sst.1.L	-4.032	0.01969	SST
XBXL10_1g36987	s100a1.L	-2.138	0.02078	S100A1
XBXL10_1g22181	mgp.S	-2.645	0.02078	–
XBXL10_1g15424	vamp5.S	1.665	0.02902	–
XBXL10_1g7463	LOC108708308	-6.406	0.02902	–
XBXL10_1g11333	rerg.L	3.251	0.02902	RERG
XBXL10_1g36661	LOC108699114	-2.879	0.02934	–
XBXL10_1g33737	LOC108697796	-6.480	0.03002	–
XBXL10_1g23945	atp13a4.L	-5.015	0.03002	ATP13A4
XBXL10_1g25731	sst.1.S	-5.131	0.03009	SST
XBXL10_1g38451	LOC121397797	-2.069	0.03196	–
XBXL10_1g13564	nt5dc4.L	-1.917	0.03196	NT5C2
XBXL10_1g42672	LOC108702671	1.228	0.03220	–
XBXL10_1g37233	LOC108699763	-2.240	0.03360	–
XBXL10_1g43750	hbd.S	-1.560	0.03502	–
XBXL10_1g16960	clec4e.S	1.345	0.03558	PPFIA2
XBXL10_1g6659	ptchd1.L	-5.427	0.03678	PTCHD1
XBXL10_1g24584	pomc.L	-5.694	0.03722	POMC
XBXL10_1g20691	LOC108715167	-5.678	0.03722	–
XBXL10_1g34160	LOC108698118	-0.914	0.03722	–
XBXL10_1g17981	LOC108704982	-3.080	0.03722	MUC5AC
XBXL10_1g41029	LOC108701509	-1.548	0.03762	HBZ
XBXL10_1g43022	LOC108702797	1.299	0.03885	RAB37
XBXL10_1g28511	LOC100158309	-3.443	0.04088	–
XBXL10_1g21184	LOC108715076	-5.871	0.04088	CHST5
XBXL10_1g9676	mkrn3.S	1.476	0.04305	MKRN6P
XBXL10_1g41035	hbg1.L	-1.789	0.04305	–
XBXL10_1g43763	LOC108702421	-1.672	0.04378	HBQ1
XBXL10_1g38688	tnfaip8l2.S	1.090	0.04743	TNFAIP8L3
XBXL10_1g22833	LOC108716104	1.808	0.04784	–
XBXL10_1g41015	hbe1.L	-1.593	0.04837	HBG2
XBXL10_1g14235	epor.L	-1.435	0.05289	EPOR
XBXL10_1g2823	LOC108697103	3.142	0.05408	–
XBXL10_1g41503	LOC108701721	-1.449	0.05408	–
XBXL10_1g32223	LOC121395792	2.080	0.05683	–
XBXL10_1g42081	LOC108703916	0.885	0.05683	TRIM65
XBXL10_1g44438	fbxl16.S	4.839	0.05683	FBXL16
XBXL10_1g28691	LOC108719808	-1.371	0.05789	VIPR1

XBXL10_1g8295	krt7.L	-0.929	0.05789	KRT8
XBXL10_1g38809	s100a11.S	-1.535	0.06090	–
XBXL10_1g9894	LOC121400559	-4.476	0.06090	–
XBXL10_1g13740	LOC108711632	-4.831	0.06090	ZNF84
XBXL10_1g27370	trg.L	1.299	0.06090	–
XBXL10_1g32007	btg5.2.L	-1.381	0.06118	–
XBXL10_1g33116	atp12a.S	-1.897	0.06282	ATP12A
XBXL10_1g18725	LOC121403015	1.094	0.06465	MC3R
XBXL10_1g19102	LOC108714247	-3.888	0.06465	–
XBXL10_1g39458	tnfrsf6b.L	-3.292	0.06587	RYR1
XBXL10_1g7453	rad51d.L	0.845	0.06742	RAD51D
XBXL10_1g2283	LOC121394372	2.704	0.06742	–
XBXL10_1g12298	gpr151.L	-3.711	0.06742	GPR151
XBXL10_1g21864	lmx1a.S	-4.634	0.06742	LMX1A
XBXL10_1g15186	LOC108712612	-2.083	0.06742	–
XBXL10_1g2056	rfx3.L	-2.977	0.06926	RFX3
XBXL10_1g7623	zpld1.L	-5.457	0.07128	ZPLD1
XBXL10_1g13334	LOC108711460	-3.850	0.07152	MIR9-3
XBXL10_1g28578	LOC121395207	0.943	0.07494	–
XBXL10_1g13799	plekha2.L	1.394	0.07494	PLEKHA2
XBXL10_1g25853	LOC108705376	1.064	0.07739	–
XBXL10_1g3038	hapln1.L	-4.687	0.07739	HAPLN1
XBXL10_1g25182	LOC108717807	-2.243	0.07790	–
XBXL10_1g32759	LOC108697460	-1.468	0.07984	SGTA
XBXL10_1g14344	gal3st4.2.L	-3.561	0.08172	GAL3ST1
XBXL10_1g5031	sall2.S	-5.566	0.08304	SALL2
XBXL10_1g29857	chrac1.S	0.983	0.08605	CHRAC1
XBXL10_1g26263	crisp1.3.S	-2.788	0.08605	CRISP3
XBXL10_1g40289	LOC108701187	-3.657	0.08605	–
XBXL10_1g22073	nog4.S	-3.681	0.08819	–
XBXL10_1g28709	LOC108719814	-5.978	0.08884	FCN2
XBXL10_1g9333	LOC108709314	4.577	0.08884	–
XBXL10_1g24489	mep1a.L	-5.128	0.09036	MEP1A
XBXL10_1g21540	cth.S	1.186	0.09036	CTH
XBXL10_1g42068	LOC108703829	-1.447	0.09036	SULT1C2
XBXL10_1g20797	ins.S	-3.934	0.09036	INS
XBXL10_1g41370	grap.L	1.293	0.09179	GRAP
XBXL10_1g26152	LOC121394366	1.980	0.09261	SNORA73

Table S5. Gene ontology analysis of differentially expression genes in the developing gonads for three knockout lines (*dmrt1L* females, *dmrt1L* males, *dmrt1S* females, *dmrt1S* males) compared to wildtype sisters, and for wildtype males compared to wildtype females (MF1, MF2, MF3). Results are listed for three gene ontology categories (biological process, molecular function, cellular component); subcategories with significant enrichment follow their parent category and are indicated with ">"s, which reflect the degree of nestedness. For each gene and analyis, the number of differentially expressed genes is indicated (# DE) and NS indicates no significant enrichment. Analyses were performed for one quantification method (STAR) and one method for analysis of differential expression (edgeR) and the false detection rate P-value is indicated for each significantly enriched annotation (FDR). Because a putative human ortholog was not identified for some transcripts (Table S1), the number of genes used in the gene ontology analysis was generally lower than the number of differentially expressed genes.

Analysis and gene	# DE	GO Biological process	FDR	GO molecular function	FDR	GO cellular component	FDR
STAR + EdgeR							
dmrt1L females	337						
		mRNA methylation	0.048	mRNA (adenine-N1-)-methyltransferase activity	0.011	tRNA methyltransferase complex	0.000
		>mRNA modification	0.038	>mRNA methyltransferase activity	0.011	>methyltransferase complex	0.033
		>>RNA modification	0.000	>>RNA methyltransferase activity	0.000	>>intracellular anatomical structure	0.000
		>>>>macromolecule metabolic process	0.016	>>>catalytic activity, acting on RNA	0.000	>>>cellular anatomical entity	0.000
		>>>>>organic substance metabolic process	0.000	>>>>catalytic activity, acting on a nucleic acid	0.000	>>transferase complex	0.005
		>>>>>>metabolic process	0.000	>>>>>catalytic activity	0.000	Pwp2p-containing subcomplex of 90S preribosome	0.015
		>>>RNA metabolic process	0.000	>>>methyltransferase activity	0.000	>nucleolus	0.000
		>>>>nucleic acid metabolic process	0.000	>>>>transferase activity, transferring one-carbon groups	0.000	>>nuclear lumen	0.000
		>>>>>nucleobase-containing compound metabolic process	0.000	>>>>>transferase activity	0.010	>>>intracellular organelle lumen	0.000
		>>>>>organic cyclic compound metabolic process	0.000	>>S-adenosylmethionine-dependent methyltransferase activity	0.000	>>>>organelle lumen	0.000
		>>>>>>heterocycle metabolic process	0.000	tRNA (adenine-N1-)-methyltransferase activity	0.010	>>>>>membrane-enclosed lumen	0.000
		>>>>>>>cellular metabolic process	0.000	>tRNA (adenine) methyltransferase activity	0.014	>>>nucleus	0.025
		>>>>>>>>cellular process	0.000	>>tRNA methyltransferase activity	0.000	>>>>intracellular membrane-bounded organelle	0.002
		>>>>>>primary metabolic process	0.000	>>>catalytic activity, acting on a tRNA	0.001	>>>>>membrane-bounded organelle	0.015
		>>>>>>cellular aromatic compound metabolic process	0.000	acyl-CoA desaturase activity	0.013	>>intracellular non-membrane-bounded organelle	0.033
		>>>>>>cellular nitrogen compound metabolic process	0.000	>oxidoreductase activity, acting on paired donors, with oxidation of a pair of donors resulting in the reduction of molecular oxygen to two molecules of water	0.009	>>>non-membrane-bounded organelle	0.032
		>>>>>>>nitrogen compound metabolic process	0.000	RNA polymerase III activity	0.000	>90S preribosome	0.001
		>RNA methylation	0.000	>DNA-directed 5'-3' RNA polymerase activity	0.015	>>preribosome	0.000
		>>macromolecule methylation	0.000	>>5'-3' RNA polymerase activity	0.018	>>>ribonucleoprotein complex	0.000
		>>>methylation	0.000	>>>RNA polymerase activity	0.018	RNA polymerase I complex	0.000
		maturation of LSU-rRNA	0.002	RNA polymerase I activity	0.000	box C/D RNP complex	0.020
		>rRNA processing	0.000	C-methyltransferase activity	0.037	>sno(s)RNA-containing ribonucleoprotein complex	0.033
		>>ncRNA processing	0.000	U3 snoRNA binding	0.009	preribosome, large subunit precursor	0.000
		>>>RNA processing	0.000	>snoRNA binding	0.000	RNA polymerase III complex	0.001
		>>>>gene expression	0.000	>>RNA binding	0.000	small-subunit processome	0.000
		>>>ncRNA metabolic process	0.000	>>>nucleic acid binding	0.010	mitochondrion	0.020
		>>rRNA metabolic process	0.000	>>>>heterocyclic compound binding	0.000	>cytoplasm	0.000
		>>ribosome biogenesis	0.000	>>>>>binding	0.039	nucleoplasm	0.000
		>>>ribonucleoprotein complex biogenesis	0.000	>>>>organic cyclic compound binding	0.000	Unclassified	0.000
		>>>>cellular component biogenesis	0.000	tRNA (guanine) methyltransferase activity	0.012		
		>ribosomal large subunit biogenesis	0.000	tRNA binding	0.018		
		tRNA methylation	0.000	N-methyltransferase activity	0.005		
		>tRNA modification	0.001	protein methyltransferase activity	0.011		
		>>tRNA processing	0.002	Unclassified	0.005		
		>>>tRNA metabolic process	0.000				
		maturation of SSU-rRNA from tricistronic rRNA transcript (SSU-rRNA, 5.8S rRNA, LSU-rRNA)	0.001				
		>maturation of SSU-rRNA	0.005				
		>>ribosomal small subunit biogenesis	0.000				
		ribosomal large subunit assembly	0.015				
		>ribosome assembly	0.010				
		transcription by RNA polymerase I	0.005				
		>>>>organic substance biosynthetic process	0.011				
		>>>>>biosynthetic process	0.007				

		>>>>>cellular biosynthetic process	0.002				
		>>>>organic cyclic compound biosynthetic process	0.049				
		cholesterol biosynthetic process	0.007				
		>sterol biosynthetic process	0.015				
		>>>>lipid metabolic process	0.000				
		>>>lipid biosynthetic process	0.004				
		>>>>small molecule metabolic process	0.000				
		>secondary alcohol biosynthetic process	0.007				
		>>>small molecule biosynthetic process	0.000				
		nucleobase metabolic process	0.047				
		maturation of 5.8S rRNA	0.050				
		rRNA modification	0.049				
		ribonucleotide metabolic process	0.044				
		>ribose phosphate metabolic process	0.050				
		organophosphate biosynthetic process	0.050				
		cellular lipid metabolic process	0.004				
		oxoacid metabolic process	0.038				
		Unclassified	0.022				
dmrt1L males	5	NS	–	NS	–	NS	–
dmrt1S females	20	NS	–	NS	–	NS	–
dmrt1S males	1251	gamma-aminobutyric acid biosynthetic process	0.013	carbon-sulfur lyase activity	0.035	external side of apical plasma membrane	0.026
		>amino acid biosynthetic process	0.016	>>catalytic activity	0.000	>apical plasma membrane	0.022
		>>carboxylic acid biosynthetic process	0.000	L-amino acid transmembrane transporter activity	0.002	>>plasma membrane region	0.000
		>>>carboxylic acid metabolic process	0.000	>amino acid transmembrane transporter activity	0.000	>>>membrane	0.006
		>>>>oxoacid metabolic process	0.000	>>carboxylic acid transmembrane transporter activity	0.000	>>>>cellular anatomical entity	0.000
		>>>>>organic acid metabolic process	0.000	>>>organic acid transmembrane transporter activity	0.000	cytosolic small ribosomal subunit	0.017
		>>>>>>cellular metabolic process	0.000	>>>>transmembrane transporter activity	0.000	>cytosolic ribosome	0.021
		>>>>>>>metabolic process	0.000	>>>>>transporter activity	0.000	>>ribosome	0.010
		>>>>>>>cellular process	0.000	>>>>organic anion transmembrane transporter activity	0.000	>>>intracellular organelle	0.000
		>>>>>>small molecule metabolic process	0.000	secondary active transmembrane transporter activity	0.000	>>>>intracellular anatomical structure	0.000
		>>>>>>organic substance metabolic process	0.000	>active transmembrane transporter activity	0.000	>>>>organelle	0.000
		>>>organic acid biosynthetic process	0.000	structural constituent of ribosome	0.028	>>cytosol	0.000
		>>>>cellular biosynthetic process	0.000	>structural molecule activity	0.044	>>>cytoplasm	0.000
		>>>>>biosynthetic process	0.000	active monoatomic ion transmembrane transporter activity	0.030	>small ribosomal subunit	0.018
		>>>>organic substance biosynthetic process	0.000	>monoatomic ion transmembrane transporter activity	0.027	>>ribosomal subunit	0.003
		>>>>small molecule biosynthetic process	0.000	salt transmembrane transporter activity	0.008	basolateral plasma membrane	0.001
		>>organonitrogen compound biosynthetic process	0.001	inorganic molecular entity transmembrane transporter activity	0.028	>basal plasma membrane	0.003
		>>>organonitrogen compound metabolic process	0.000	oxidoreductase activity	0.028	>>basal part of cell	0.004
		>>>>nitrogen compound metabolic process	0.000	identical protein binding	0.003	extracellular matrix	0.022
		>>amino acid metabolic process	0.004	>protein binding	0.000	>external encapsulating structure	0.021
		>>>primary metabolic process	0.000	>>binding	0.000	extracellular exosome	0.000
		>gamma-aminobutyric acid metabolic process	0.027	transferase activity	0.050	>extracellular vesicle	0.000
		>>monocarboxylic acid metabolic process	0.003	Unclassified	0.000	>>extracellular membrane-bounded organelle	0.000
		liver regeneration	0.037	olfactory receptor activity	0.000	>>>membrane-bounded organelle	0.000
		>liver development	0.018			>>>extracellular organelle	0.000
		>>>animal organ development	0.049			>>>>extracellular region	0.001
		>>>>anatomical structure development	0.005			>>vesicle	0.000
		>>>>>developmental process	0.018			>extracellular space	0.000
		>>hepaticobiliary system development	0.021			mitochondrial membrane	0.040
		>>>system development	0.016			>mitochondrial envelope	0.033
		>>>>multicellular organism development	0.002			>>mitochondrion	0.016
		>>>>>multicellular organismal process	0.023			>>>intracellular membrane-bounded organelle	0.000
		neutral amino acid transport	0.018			>organelle membrane	0.004

		>amino acid transport	0.001			endoplasmic reticulum	0.002
		>>nitrogen compound transport	0.009			>endomembrane system	0.034
		>>>transport	0.000			cell junction	0.012
		>>>>establishment of localization	0.000			intracellular organelle lumen	0.016
		>>>>>localization	0.008			>organelle lumen	0.017
		>>carboxylic acid transport	0.000			>>membrane-enclosed lumen	0.015
		>>>organic acid transport	0.000			Unclassified	0.000
		>>>>organic substance transport	0.002				
		>>>>>organic anion transport	0.000				
		>>>>sulfur compound transport	0.044				
		L-alpha-amino acid transmembrane transport	0.039				
		>amino acid transmembrane transport	0.000				
		>>carboxylic acid transmembrane transport	0.000				
		>>>organic acid transmembrane transport	0.001				
		>>>>transmembrane transport	0.001				
		>L-amino acid transport	0.043				
		response to osmotic stress	0.019				
		cytoplasmic translation	0.045				
		>>>>amide metabolic process	0.003				
		>>>amide biosynthetic process	0.044				
		>>>>cellular nitrogen compound biosynthetic process	0.043				
		alpha-amino acid metabolic process	0.007				
		cell fate commitment	0.044				
		response to inorganic substance	0.019				
		response to organonitrogen compound	0.004				
		>response to organic substance	0.003				
		>response to nitrogen compound	0.004				
		response to organic cyclic compound	0.033				
		monoatomic ion transport	0.019				
		tube development	0.049				
		response to oxygen-containing compound	0.001				
		response to endogenous stimulus	0.012				
		cellular response to chemical stimulus	0.002				
		catabolic process	0.044				
		regulation of biological quality	0.002				
		anatomical structure morphogenesis	0.043				
		negative regulation of biological process	0.014				
		positive regulation of biological process	0.014				
		Unclassified	0.000				
		detection of chemical stimulus involved in sensory perception of smell	0.000				
		>detection of chemical stimulus involved in sensory perception	0.000				
		>>detection of stimulus involved in sensory perception	0.002				
		>>>detection of stimulus	0.005				
		>>detection of chemical stimulus	0.000				
		>>sensory perception of chemical stimulus	0.001				
		>sensory perception of smell	0.002				
MF1	3	NS	–	NS	–	NS	–
MF2	32	NS	–	monooxygenase activity	0.027	NS	–
MF3	105	NS	–	haptoglobin binding	0.021	hemoglobin complex	0.000
				oxygen carrier activity	0.026	haptoglobin-hemoglobin complex	0.005
				sulfotransferase activity	0.029		

S6. Paper entitled “Functional dissection and assembly of a small, newly evolved, female-specific genomic region of the W chromosome of the African clawed frog *Xenopus laevis*” by Cauret et al. submitted to PLOS Genetics on July 19th, 2023. I am identified as a coauthor of this paper due to contributions to the histological examination of *X. laevis dm-w* null individuals.

Functional dissection and assembly of a small, newly evolved, female-specific genomic region of the W chromosome of the African clawed frog *Xenopus laevis*

Caroline M. S. Cauret[1,2], Danielle C. Jordan[3,4], Lindsey M. Kukoly[1], Sarah R. Burton[3], Emmanuela U. Anele[1,5], Jacek M. Kwiecien[6], Marie-Theres Gansauge[7], Sinthu Senthillmohan[1], Eli Greenbaum[8], Matthias Meyer[7], Marko E. Horb[3], Ben J. Evans[1]*

[1]Biology Department, Life Sciences Building Room 328, McMaster University, 1280 Main Street West, Hamilton, ON L8S4K1, Canada

[2] Department of Botany and Plant Pathology, Oregon State University, Corvallis, OR 97331, USA

[3] Eugene Bell Center for Regenerative Biology and Tissue Engineering and National Xenopus Resource, Marine Biological Laboratory, 7 MBL St, Woods Hole, MA 02543 USA

[4] The School of Biological Sciences, University of Aberdeen, Aberdeen, United Kingdom

[5] Department Zoology, Ahmadu Bello University, Zaria, Nigeria

[6] Department of Pathology and Molecular Medicine, McMaster University, 1280 Main Street West, Hamilton, ON L8S4K1, Canada

[7] Department of Evolutionary Genetics, Max Planck Institute for Evolutionary Anthropology, Leipzig, Germany

[8] Department of Biological Sciences, The University of Texas at El Paso, El Paso, TX 79968, USA

Correspondence: evansb@mcmaster.ca

Abstract

Genetic triggers for sex determination are frequently co-inherited with other linked genes that may also influence one or more sex-specific phenotypes. To better understand how sex-limited regions evolve and function, we studied a small female-specific region of the frog *Xenopus laevis* that drives female differentiation. Using gene editing, we found that the sex-determining function of this region requires a gene called *dm-w* and that the two other female-specific loci (*scan-w* and *ccdc69-w*) are not essential for viability, female development, or fertility. Analysis of mesonephros/gonad transcriptomes during sexual differentiation illustrates masculinization of the *dm-w* knockout transcriptome and identifies mostly non-overlapping sets of differentially expressed genes in three knockout lines (*dm-w*, *scan-w*, *ccdc69-w*) compared to wildtype sisters. Capture sequencing of almost all *Xenopus* species and PCR surveys indicate that the female-determining function of *dm-w* is present in only a subset of species that carry this gene. These findings map out a dynamic evolutionary history of a newly evolved but functionally fragile female-specific genomic region, whose components have distinctive functions that frequently degraded during *Xenopus* diversification, and evidence the evolutionary consequences of recombination suppression.

Introduction

Proteins with functional associations are sometimes encoded by genes that are genetically linked in the genome [1] or in the same physical space in the nucleus [2], which may promote their co-regulation. Supergenes are physically linked sets of genes that together orchestrate ecologically relevant and

potentially complex phenotypes [3] such as behaviour [4], mimicry [5], color [6], heterostyly [7], male reproductive behaviour [8], offspring sex ratio [9], and (perhaps most notably) sexual differentiation [10].

Genetic associations between alleles of different loci can be favored under several scenarios such as heterogeneity of environmental conditions (if certain combinations of alleles are beneficial in some habitats but not others) or negative epistasis [if certain combinations of alleles are deleterious; 11]. Recombination arrest could be favored by natural selection in order to maintain advantageous combinations of alleles across multiple genes [12-16] and mechanistically could be achieved by genomic changes such as inversions or allelic divergence. Expansion of recombination suppression could be triggered by regulatory changes [17, 18], sexual antagonism [15, 19], heterozygote advantage and balancing selection [20, 21], meiotic drive [19], and neutral processes [22, 23].

Because recombination suppression causes co-inheritance of genes that are physically linked to the sex-determining locus, sex-specific portions of sex chromosomes may act as supergenes by working together to sculpt sex-specific phenotypes [10]. However, in some cases, sex-linked genes encode diverse phenotypes, including some that are not directly related to sex determination. For example, the male-specific portion of the human Y-chromosome encodes a protein (*Sry*) that triggers male primary gonadal differentiation, and also several other genes that function long after primary sexual differentiation has been achieved [albeit related to male fertility; 24].

In principle, different genes in a supergene could have epistatic interactions that influence one phenotype [25]. If this were the case, each gene would be necessary but not individually sufficient to produce the phenotype that is controlled by the supergene, or multiple supergene components could have modifier effects on this phenotype. In the case of a sex-determining supergene, for example, sexual differentiation might require a functional version of all genes in the supergene. In some plants, for example, male differentiation is orchestrated by two genes; natural selection may have favoured the co-localization of both on a male-specific supergene in kiwis [26, 27]. At the other extreme is the possibility that individual genes on a sex-determining region lack strong epistatic interactions, with each locus influencing a different phenotype. For example, one locus could influence primary (gonadal) sexual differentiation and another could influence secondary (non-gonadal) differentiation, or even a non-essential or subtle trait. Because they occur in only one sex, each gene in a sex-specific genomic region necessarily must have sex-specific phenotypic influences. Clearly, however, not all loci on a sex-specific region are necessarily required for the most fundamental aspects of sexual differentiation, which are viability and reproduction.

A small female-specific genomic region in the African clawed frog (*Xenopus laevis*)

To explore how sex-limited genomic regions arise, function, and change over time, we studied a small female-determining genomic region on the W chromosome of the African clawed frog, *Xenopus laevis*. This region is ~278 kilobases (kb) long, located on chromosome 2L, and contains only three female-specific genes [28]: *dm-w*, *scan-w*, and *ccdc69-w*. No gametolog of these three female-specific genes is known to be present on the Z chromosome, and low sequence homology between the female-specific portion of the W chromosome and the Z chromosome [apart from repetitive elements; 28] presumably contributes to recombination suppression in this female-specific region. One of these genes – *dm-w* – is thought to be the main trigger for primary (gonadal) sexual differentiation of female *X. laevis* [29, 30].

There are strong reasons to suspect that sex determination in *X. laevis* is triggered by the presence or absence of this female-specific genomic region, as opposed to environmental factors, or a polygenic trigger that involves genes outside of this female-specific region (such as the male related genes *dmrt1L* and *dmrt1S* which reside on chromosomes 1L and 1S, respectively). In a survey of 24 females and 12 males in nature, all females and no males carried *dm-w* [31]. In a laboratory-reared family that included 17 daughters and 20 sons, reduced representation genome sequencing recovered a strong association with phenotypic sex exclusively on the region of Chromosome 2L that contains the female-specific region

[32]. In three of nine or three of seven transgenic (ZZ) males (depending on the construct used), insertion of *dm-w* by restriction enzyme-mediated integration resulted in the development of ovotestes, which contain both ovarian and testicular structures [29]. In the transgenic males that did not develop ovotestis, the *dm-w* transgene was generally lowly expressed [29]. In three of 11 (ZW) female tadpoles and 10 of 38 female adults that carried an RNA interference transgene against *dm-w*, abnormal gonads developed that were partially sex-reversed [29, 30] and gonads of two of 38 transgenic female adults were fully sex reversed [30]. The variable effects of *dm-w* transgenes and inactivation could indicate that dosages of other W-linked genes or Z-linked loci also influence sexual differentiation, or alternatively this could have a methodological basis (e.g., positional effects of the *dm-w* transgene or incomplete inactivation of *dm-w* by RNA interference).

In adult *X. laevis*, the other two female-specific genes in *X. laevis* – *scan-w* and *ccdc69-w* – are have substantial expression levels in either the brain and stomach or the gonads and brain respectively [28]. In tadpoles, *scan-w* and *ccdc69-w* are both expressed in the developing gonads during and after sexual differentiation [28]. The scan domain, which is present in *scan-w* [28], is a highly conserved motif that facilitates dimerization and is typically found near the N-terminus of vertebrate C_2H_2 zinc-finger proteins, but most of these proteins have unknown function [33]. The *ccdc69* protein, which is paralogous to *ccdc69-w*, is involved with microtubule binding activity and spindle formation during cytokinesis [34].

These three W-linked loci in *X. laevis* each became W-linked due to independent duplication events because their closest paralogs in the autosomes are not tightly linked [28, 29, 35-37]. These duplication events are separate from and subsequent to those associated with allotetraploidization in *Xenopus* (which occurred at least two separate times to generate the ancestors of extant allotetraploid species) [38, 39]. These allotetraploid species (ancestral and extant) have two subgenomes that are respectively derived from two different diploid ancestors. The subgenomes of the most recent common allotetraploid ancestor of *X. laevis* and *X. clivii* are denoted "L" and "S" [40] and homeologous genes in each subgenome generally include these letters as a suffix (e.g., *dmrt1L* and *dmrt1S* are homeologs that by definition are duplicated genes that arose from genome duplication). Strikingly, *dm-w* appears to be a chimerical gene, whose components are derived from as many as three different sources including: (i) the second and third exons and flanking regions, which formed from gene duplication of *dmrt1S* [28, 35, 36], (ii) the fourth exon and flanking regions, which arose from a noncoding DNA transposon called hAT-10 [36], and (iii) the first exon and flanking regions, which does not have discernible homology to *dmrt1S*, is rich in transposable elements, and has unclear origins [41]. A recent genome assembly for *X. laevis* (version 10.1) suggests that the transcribed regions of *dm-w* and *scan-w* overlap because exons 4-6 of *scan-w* are located in the first intron of *dm-w*. All three of these genes are transcribed in the same direction, which is in the reverse orientation of the coordinates for chromosome 2L in the *X. laevis* genome assembly. Combined with the differing genomic locations of paralogous genes [28], the overlapping transcribed regions of *dm-w* and *scan-w* is consistent with a chimerical origin of *dm-w* wherein exons 2 and 3 originated via separate duplication/translocation events from exon 1 and exon 4 [29, 36, 41].

We set out to better understand evolution and function of the W-linked sex-linked genomic region of *X. laevis*. We explored function of each of the three genes in this region by independently inactivating each one of them using CRISPR/Cas9 gene editing, and we then explored their mutant phenotypes in terms of sex-determination, fertility, and gonadal transcriptomics. We also investigated the evolutionary histories of each of these three genes using targeted capture sequencing across almost all *Xenopus* species and PCR assays, with interpretations in a phylogenetic context. These efforts provide comprehensive insights into functional evolution and assembly of a small female-specific sex-determining region, demonstrate non-overlapping and partially non-essential activities of its components, and evidence functional degeneration of each component – findings that are in step with the expectation that the efficacy of natural selection is reduced in genomic regions lacking recombination [42, 43].

Results

Female differentiation of *X. laevis* is triggered by *dm-w*, but not *scan-w* or *ccdc69-w*

To further characterize their functional roles, we created a knockout line for each of three genes: *dm-w*, *scan-w* and *ccdc69-w* in *X. laevis* using CRISPR/Cas9 (Supplementary Information; Fig. S1). F0 mosaic individuals were crossed with wildtype individuals to generate non-mosaic (i.e., containing only the mutant allele in all cells) F1 individuals. For each knockout line, viable F1 individuals were recovered, which demonstrates non-essentiality for each of these genes for viability of genetic females. Fertility of F1 knockout individuals was assessed by crossing them to wildtype individuals with the opposite sex phenotype; gonadal gross anatomy and histology of F1 individuals were then characterized after euthanasia.

In the F0 and F1 generations, genetic females carrying the *dm-w* knockout mutation (a 10 bp deletion that was confirmed by Sanger sequencing; Fig. S1) developed into phenotypic males. When F0 individuals were crossed with wildtype (ZW) females, viable F1 offspring were produced, which demonstrates that the sex reversed F0 females developed into phenotypically fertile males. In the F1 generation, a wildtype (ZW) female and a phenotypically male (ZW*) mutant female (where W* indicates the W chromosome carrying an inactivated copy of *dm-w* that was confirmed by Sanger sequencing) were crossed to produce offspring with four different sex chromosome phenotypes: W*Z (n = 6), W*W (n = 8), WZ (n = 5), and ZZ (n = 6). All W*Z individuals developed into phenotypic males and all W*W individuals developed into phenotypic females; wildtype offspring matched their expected sexes with WZ individuals developing into phenotypic females and ZZ individuals developing into phenotypic males. Fertility of a W*W female was confirmed by a cross to a phenotypically male (ZW*) mutant female. This cross produced offspring that were WZ (n = 8), W*W (n = 16), and W*Z or W*W* (n = 19 in total for these two offspring genotypes; we did not distinguish them because their *dm-w* sequences are identical for the hemizygous mutant allele and the homozygous mutant allele). As expected, the W*Z or W*W* offspring were phenotypically male and the W*W and WZ offspring were phenotypically female. Histological analysis of testis tissue from four F2 sex-reversed *dm-w* mutant females (W*Z) is consistent with complete sex reversal, including normal sperm development (Figs. 1, S2). We also were able to obtain offspring from a sex-reversed genetic female and a wildtype female using natural mating after both individuals were injected with human chorionic gonadotropin (which is generally required to elicit sexual behavior in captive *Xenopus*). This indicates that, in addition to producing normal sperm and being fertile, sex-revered genetic females also exhibit sexual behaviour of phenotypic males (amplexus).

Together these results indicate in *X. laevis* that (i) loss of function mutation in *dm-w* causes complete sex reversal of a genetic female to a fertile male, (ii) *dm-w* is not necessary for viability of genetic females which develop into phenotypic males, and (iii) having a functional copy of *scan-w* and *ccdc69-w* does not prevent development of the male phenotype by genetic females that carry a knockout mutation for *dm-w*.

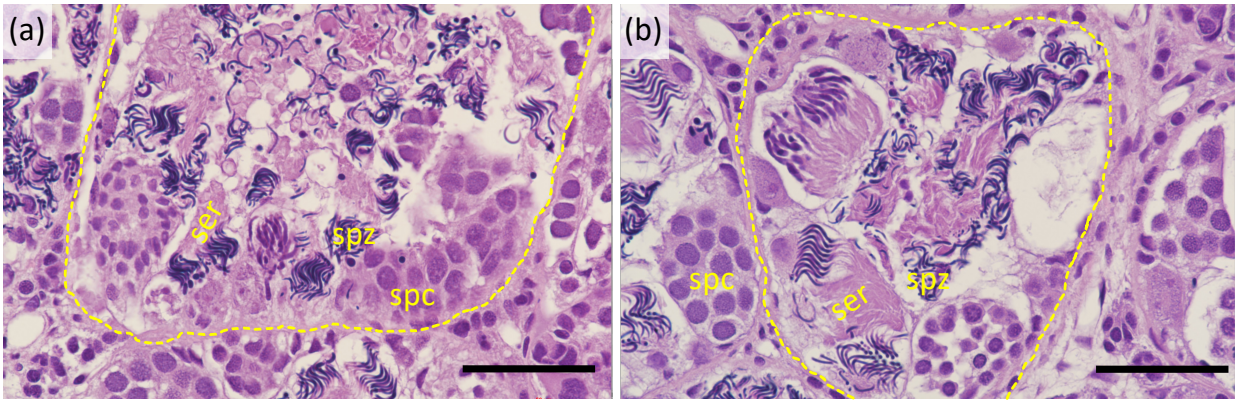

Fig. 1. Testis histology of (a) a wildtype male and (b) a sex reversed F1 female carrying a *dm-w* knockout mutation. Black bars are 50 μm; individuals' identification numbers are (a) 17FO and (b) 1847. Dotted circles indicate the margins of seminiferous tubules, and Sertoli cells (ser), spermatocytes (spc) and spermatozoa (spz) are labeled.

All F1 *scan-w* knockout individuals (n = 10 individuals with 20 bp deletion that creates a premature stop codon; Fig. S1) and all *ccdc69-w* knockout individuals (n = 9 individuals in total including two with a 22 bp deletion creates a premature strop codon, Fig. S1, and seven with a 214 bp deletion associated with a 12 bp insertion that also creates a premature strop codon) developed into phenotypically normal (and gravid) adult females. These observations demonstrate that neither *scan-w* nor *ccdc69-w* are both not required for female differentiation. When crossed to wildtype males, *scan-w* and *ccdc69-w* knockout lines each produced viable F2 individuals, demonstrating that *scan-w* and *ccdc69-w* are not required for female fertility.

Variable transcriptomic responses to knockout of different W-specific genes

In females, *dm-w* is expressed in the developing gonad during sexual differentiation, and in adult ovary and liver [28, 44]. Using RNAseq data, we confirmed female-specificity of *dm-w* in the developing mesonephros/gonad (Fig. S3). Because *scan-w* and *ccdc69-w* were not present in the most recent reference transcriptome (version 10), in order to evaluate expression of these loci we added previously reported transcripts from [28] to this reference transcriptome and performed a separate quantification and normalization. Both genes were found to have zero or almost zero expression in the tadpole stage 50 mesonephros/gonad of all individuals, whether male or female, knockout or wildtype. While this does not rule out expression in other tissues or developmental stages, it is at odds with real-time PCR results reported previously that detected expression of these genes in female tadpole stage 50 mesonephros/gonad tissue [28].

We then compared expression of genes in the developing mesonephros/gonad of genetically female knockout and wildtype individuals at tadpole stage 50. Irrespective of the methods for transcript quantification or analysis of differential expression (Methods), the sets of differentially expressed genes for each mutant line (mutant versus wildtype sisters; Table S1) were almost entirely non-overlapping with each other or with three independent analyses of sex-biased expression in wildtype individuals (wildtype brothers versus wildtype sisters; Table S1, Figs. 2, S4-S6). These results may be attributable in part to batch effects discussed below, but are also consistent with the distinctive functions of each of these genes that are evidenced respectively by the adult knockout phenotypes (sex-reversal for *dm-w* but not for *scan-w* or *ccdc69-w*).

Analysis of differential expression of the *dm-w* knockout line compared to wildtype siblings found 8–33 significantly differentially expressed genes depending on the analysis pipeline Table S1, Figs. 2, S4-S6). Gene ontology of differentially expressed genes in the *dm-w* knockout line did not recover significant enrichments in biological process, molecular function, or cellular component in any analysis pipeline (Table S2).

Analysis of differential expression of the *scan-w* knockout line identified between 17 and 34 significantly differentially expressed genes, depending on the analysis pipeline (Table S1, Figs. 2, S4-S6). Gene ontology of differentially expressed genes identified enrichments in cellular components associated with extracellular space for results from some analysis pipelines (Kallisto + DeSeq2, STAR + DeSeq2; Table S2).

Analysis of differential expression of the *ccdc69-w* knockout line identified 17–263 significantly differentially expressed genes, depending on the analysis pipeline (Table S1, Figs. 2, S4-S6). Gene ontology of differentially expressed genes in the *ccdc69-w* knockout line recovered a significant

enrichment of genes involved in biological processes such as oxygen transport, detoxification, molecular functions such as binding of oxygen and heme, and cellular components associated with hemoglobin (Table S2).

We also evaluated sex-biased expression in the developing mesonephros/gonad in wildtype individuals. Here again, significantly differentially expressed genes were generally non-overlapping across these three independent clutches, even though the genotypes in each treatment were the same (i.e., wildtype male versus wildtype female). Gene ontology analysis identified an enrichment in biological processes including oxygen transportation and hydrogen peroxide catabolism, molecular functions such as haptoglobin and iron binding and oxygen carrier activity, and cellular components such as the hemoglobin complex (Table S2).

Overall, we found substantial among-batch variation in the number and identity of transcripts with significant sex-biased expression in three different batches of wildtype female and male gonad/mesonephros transcriptomes (MF1, MF2, MF3; Figs. 2, S4-S6). This variation could be in part due to technical differences, such as among-batch variation in the number of biological replicates and number of reads per individual. It could also stem from among-batch developmental asynchrony in the timing of gonadal differentiation versus the morphological features that demarcate tadpole stage 50. Transcriptomic variation could also stem from among-individual genetic variation (e.g., nucleotide and epigenetic variation, maternal proteins); and variation among batches could be attributable to differences between tanks in temperature and other environmental parameters.

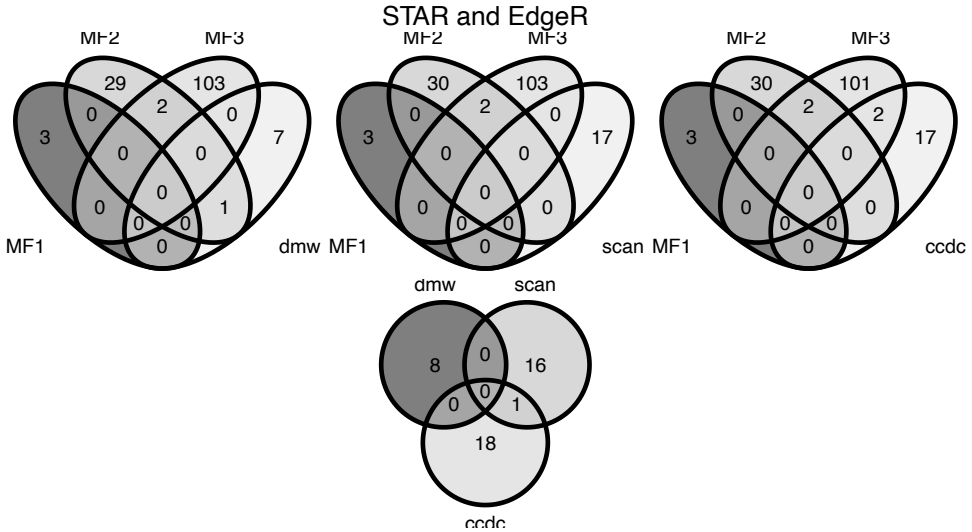

Fig. 2. Venn diagrams showing the numbers of overlapping and batch-specific differentially expressed genes in three batches where sex-specific expression was considered (MF1, MF2, MF3) and knockout to wildtype comparison for each knockout line: *dm-w* (dmw), *scan-w* (scan), and *ccdc69-w* (ccdc). Results are shown for quantification using STAR and analysis of differential expression using edgeR. In the analyses of sex-specific expression, female expression is the reference; in the analysis of knockout expression, wildtype (female) expression is the reference.

Masculinization of the developing gonad transcriptome in the *dm-w* knockout

The comparison between the *dm-w* knockout and wildtype transcriptomes discussed above did not recover a large number of shared significantly differentially expressed transcripts, and those that were recovered did not have a significant enrichment for sex-related functional ontologies. In addition to batch effects and technical variation, the inclusion of mesonephros tissue – which are substantially (>20X) larger than the gonads at tadpole stage 50 – in our transcriptomic analyses may have decreased the signal of sex-biased expression in the gonad transcriptomes.

However, it is still possible that knockout of *dm-w* did lead to masculinization of the transcriptome of the mesonephros/gonad complex at this early stage of sexual differentiation, but that we lacked statistical power to detect this. To explore this possibility, we focused on 74 sex-related genes (Table S3) and tested whether the knockout:wildtype expression ratios of these genes were positively correlated with the wildtype male:female expression ratios of these genes at the same developmental stage and tissue type. For three of four analysis pipelines, there was a significantly positive correlation between the log2 fold changes of the *dm-w* knockout analysis and those of the wildtype male:female MF1 analysis and with the wildtype male:female MF3 analysis (Figs. 3, S7-8). Permutation tests indicated that comparisons between the *dm-w* knockout analysis male:female MF3 analysis were significantly more positive than expected by chance for three of four analysis pipelines (all except Kallisto-EdgeR). Overall, these results indicate that the *dm-w* knockout transcriptomes are masculinized compared to wildtype females.

A few other correlations were significantly positive (e.g., between the *scanw-w* knockout analysis and the MF2 analysis for two of the four pipelines, and between the *ccdc69-w* knockout analysis and the MF1 analysis or the MF1 and MF3 analyses for two pipelines). However, permutation tests indicate that only the first of these comparisons (between the *scanw-w* knockout analysis and the MF2 analysis) is significantly more positive than expected and this was for only one of the analysis pipelines (Kallisto-EdgeR, Fig. S9). We expected expression ratios to generally be positively correlated between the *ccdc69-w* knockout analysis and the MF1 analysis because the wildtype females in these analyses were the same. Taken together, these results indicate that there is no evidence for masculinization of the transcriptomes of the *ccdc69-w* knockout lines, and that evidence for masculinization of the *scan-w* knockout lines is modest.

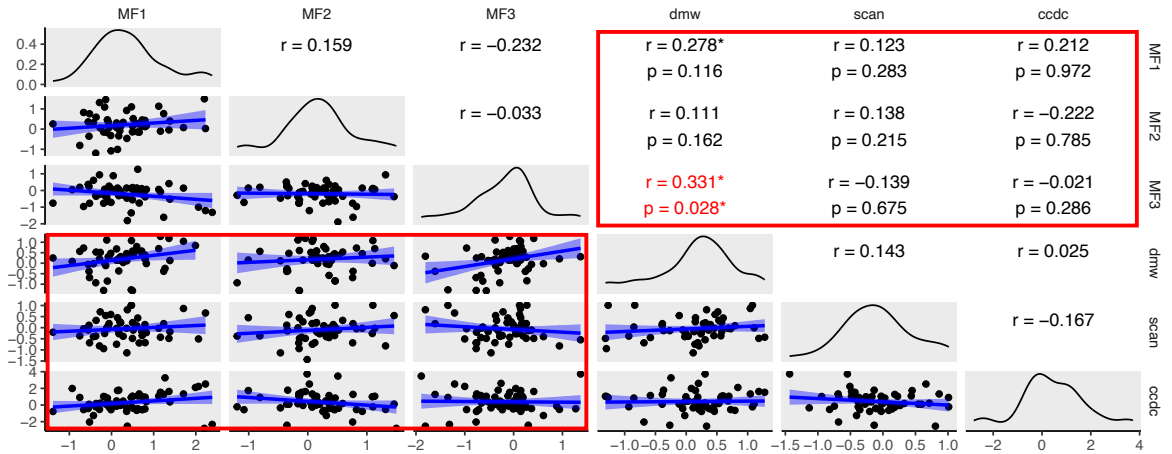

Fig. 3. Analysis of transcriptome masculinization using the STAR-EdgeR pipeline. Pairwise correlations between non-outlier log2 fold changes of sex-related genes are plotted below the diagonal. Pearson's correlation coefficients are plotted above the diagonal with asterisks indicating significantly positive correlation coefficients. The diagonal is a density plot of log2 fold changes for each analysis. For pairwise comparisons between wildtype analyses (MF1, MF2, MF3) and the knockout and wildtype analysis (dmw, scan, ccdc), which are highlighted by red boxes, p-values of permutation tests are reported in the top below each correlation coefficient, with red font and a red asterisk highlighting significantly positive correlations based on permutation tests.

Assembly of the female-specific portion of the *X. laevis* W chromosome

The components of *dm-w* were assembled during diversification of *Xenopus* [35, 36, 41, 45] around 20 million or more years ago [37, 38, 46, 47]. To further explore the origins of genetic components of the

female-specific region of the *X. laevis* W chromosome, we collected capture sequence data for exon 4 of *dm-w*, exons 4 and 5 of *scan-w*, and both exons of *ccdc69-w* in the same sample of *Xenopus* species as previously [Table S4; 45]. This included all *Xenopus* species except *X. fraseri*, and almost all individuals from each species were female. Capture sequencing of *dm-w* exons 2 and 3 were previously reported [45]. Exon 1 of *dm-w* is small and non-coding and was not intentionally targeted for capture sequencing. However, as detailed below, *dm-w* exon 1 was sequenced as "by-catch" of *scan-w* exon 4 in some species. *Scan-w* has six exons but we focused our attention on only exons 4 and 5 because the other exons are highly repetitive based on searches using the *X. laevis* genome sequence version 10.1. *Ccdc69-w* has two exons and we captured both.

Capture sequencing of one individual (usually a female) from almost all *Xenopus* species identified *dm-w* exon 4 in *X. laevis*, *X. victorianus*, *X. poweri*, *X. petersii*, *X. gilli*, *X. pygmaeus*, *X. kobeli*, *X. itombwensis*, *X. andrei*, and *X. largeni*. The top BLAST hit of the *dm-w* exon 4 sequences that were capture sequenced matched the annotated exon 4 of this gene in the *X. laevis* version 10 genome sequence (Table S5), which is consistent with our interpretation that these capture sequences were indeed *dm-w* exon 4. *Xenopus vestitus* and *X. clivii* are the only species in which *dm-w* exons 2 and 3 were previously detected [45] but where capture sequences reported in this study did not detect *dm-w* exon 4. These observations minimally indicate an origin of *dm-w* exon 4 prior to the diversification of the most recent common ancestor species that contain this exon (a blue star Fig. 4). These results further suggest that *dm-w* exon 4 is not present in species that also lack *dm-w* exons 2 and 3 [45] and that *dm-w* exon 4 may have been lost in *X. vestitus* and possibly *X. clivii* (depending on when this exon became linked to *dm-w* exons 2 and 3; discussed further below). *Xenopus petersii, X. itombwensis*, and *X. andrei* had in-frame deletions in the coding region of *dm-w* exon 4, and *X. poweri* had a frameshift deletion near the end of the coding region of this exon (Supplemental Information); we did not attempt to assess the functional effects of these mutations.

Capture sequencing identified *scan-w* exons 4 and 5 in five species (*X. laevis*, *X. petersii*, *X. poweri, X. victorianus,* and *X. gilli*; Fig. 4). We detected *scan-w* exon 4 but not exon 5 in *X. largeni*. Capture sequencing identified *ccdc69-w* exons 1 and 2 in seven species (*X. laevis*, *X. petersii*, *X. poweri, X. victorianus, X. gilli*, *X. largeni*, and *X. andrei*; Fig. 4). BLAST results to the *X. laevis* genome were consistent with our annotations of these sequences (Table S5). Capture sequencing of *scan-w* exon 4 also captured the sequences of the *dm-w* exon 1 (which is non-coding) in each individual for which *scan-w* exon 4 was detected (*X. laevis*, *X. petersii*, *X. poweri*, *X. victorianus*, *X. gilli*, and *X. largeni*; Table S5). This demonstrates that these exons of these genes are physically linked at least in these five species.

Capture sequencing additionally identified non-target sequences that are homologous to some of the targeted exons in various species (Table S5). In *X. laevis*, for example, we identified exons 1 and 2 of *ccdc69.L* but not exons 1 and 2 of *ccdc69.S*, even though the genome assembly evidences both exons for both homeologs. This opens the possibility that the *X. laevis* sample used for capture sequencing lacked the *ccdc69.S* gene, though we cannot rule out the possibility that this is due to failure to capture this sequence (for example due to divergence of *ccdc69.S* from the capture probes).

Scan-w and *ccdc69-w* originated by gene duplication of autosomal loci [28], and we therefore interpret the detection of any portion of these genes as evidence that the entirety of these loci (i.e., all exons that are currently present in *X. laevis*) were present ancestrally. The capture data from *scan-w* and *ccdc69-w* thus indicate that all three of these genes became linked around the same time that *dm-w* exon 4, or even earlier if *scan-w* and *ccdc69-w* were either lost or undetected in *X. clivii* (Fig. 4).

Some of the capture sequences had mutations that interrupted the reading frame (Supplementary Information). Overall, however, these capture results identify uninterrupted coding regions of exons 1 and 2 of *ccdc69-w* and exons 4 and 5 of *scan-w* in five species (*X. laevis*, *X. petersii*, *X. poweri, X.*

victorianus, and *X. gilli*) and a subset of these exons and/or closely related paralogs in *X. largeni* and *X. andrei*.

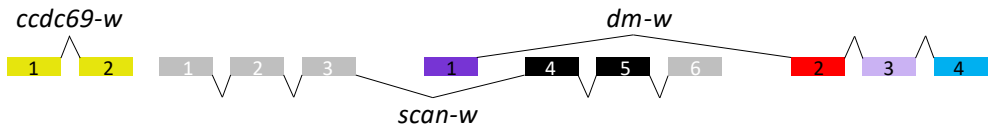

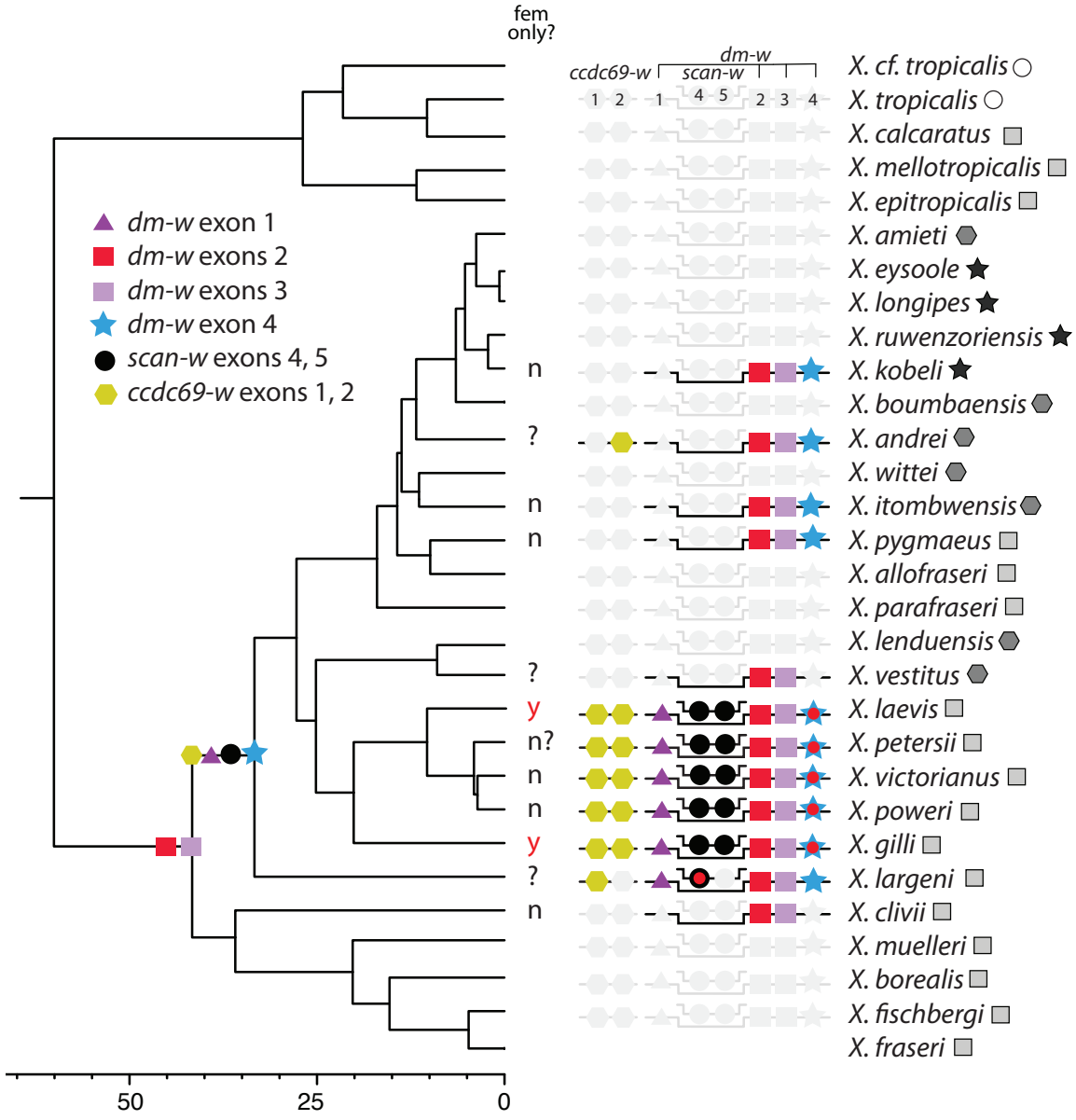

Fig. 4. Targeted capture sequencing reveals evolutionary steps toward the female-determining supergene of *X. laevis*. The genomic orientations of transcribed exons is depicted above a phylogenetic representation of the presence/absence data of capture data from exons 1 and 2 of *ccdc69-w*, exons 4 and 5 of *scan-w* and exons 1, 2, 3, and 4 of *dm-w*. Female specificity of *dm-w* (fem only?) is based on PCR assays [this study; 45] with question marks indicating species where female-specificity of *dm-w* is unknown, including for *X. petersii* where our PCR assay had inconsistent results. *Xenopus fraseri* and *X.*

cf. *tropicalis* were not assayed by the capture sequencing. The order of numbered exons of each gene corresponds to their genomic locations, including overlapping transcribed regions of *scan-w* and *dm-w*; only captured exons are mapped on the phylogeny (limitations of "by-catch" data for *dm-w* exon 1 are discussed in main text). A red dot inside symbols indicates mutations that alter the reading frame as detailed in the supplement. Data are plotted on a Bayesian phylogeny estimated from complete mitochondrial genomes [48] which does not reflect reticulating relationships among species that stem from allopolyploidation [38]. Ploidy level of each species is indicated by a circle (diploids), a square (tetraploids), a hexagon (octoploids), or a star (dodecaploids). Scale bar is in millions of years before the present, and almost all nodes have 100% posterior probability. See Evans et al. [48] for further details on phylogenetic estimation, node confidences, and confidence intervals of divergence estimates.

PCR assay for sex-specificity of *dm-w*

If *dm-w* is the trigger for female differentiation in *Xenopus* species in addition to *X. laevis*, then this gene is expected to be present in all females and no males. However, a previous PCR assay of six *Xenopus* species found *dm-w* to be female specific in *X. laevis* and *X. gilli* but not in *X. itombwensis*, *X. pygmaeus*, *X. clivii*, or *X. victorianus* [45]. We tested the female specificity of *dm-w* with a PCR assay in three additional species beyond those considered by [45]. These assays indicate that *dm-w* is not female-specific in *X. poweri* or *X. kobeli* and possibly not *X. petersii*, though the results in this last species were not conclusive due to inconsistent amplifications Table S6. We also identified additional *X. victorianus* individuals beyond those previously identified [45] in which *dm-w* was not female-specific. With a handful of exceptions, for each individual independent attempts to amplify *dm-w* exons 2, 3, and 4 were generally all successful or all unsuccessful (Table S6). This is consistent with these three exons being genetically linked and co-inherited. Based on these results and the consistent detection of all three exons in one female individual from several other species (Fig. 4), we suspect these exons, when present, are genetically linked in other *Xenopus* species as well.

Results presented here and in [45] – which include capture sequencing of one individual (usually female) of almost all *Xenopus* species and PCR surveys of multiple male and female individuals of several *Xenopus* species – provide context into the evolution of female-specificity of *dm-w* in extant *Xenopus* species (Fig. 4). These results suggest that female-specificity of *dm-w* is positively correlated with (i) the presence of exon 4, (ii) a derived extension of the coding region of *dm-w* exon 4 (due to mutation in an ancestral stop codon that extended the coding region; additional details are provided in the Supplement), and (iii) seemingly intact *scan-w* and *ccdc69-w* (for the exons examined here) on the ancestral genomic region that is female-specific in *X. laevis* (Fig. 4). In *X. victorianus*, *X. poweri*, and possibly *X. petersii* the most parsimonious interpretation is that sex-specificity of *dm-w* was lost recently, presumably at some point after divergence from an ancestor of *X. laevis*.

Discussion

We examined function and assembly of a female-specific genomic region on the W chromosome of the African clawed frog *Xenopus* laevis that includes three W-linked genes (*dm-w*, *scan-w*, *ccdc69-w*). All three of these genes arose *de novo* by one or more independent small scale duplication events during diversification of *Xenopus* [this study; 28, 35, 36].

A striking finding to emerge from this study is that all genes in this female-specific genomic region either are or have been functionally dispensable. Rapid and pervasive degeneration of these genes is consistent with the expectation that the efficacy of natural selection is lower in non-recombining compared to recombining genomic regions [42, 43]. In *X. laevis*, only *dm-w* is required to trigger female development and fertility, but not for viability, and *scan-w* and *ccdc69-w* are not essential for viability or female development and fertility. We note that this study does not demonstrate whether *dm-w* alone is sufficient to trigger female development because another (unidentified) factor could act upstream of *dm-w*. This possibility was tested using transgenic males that ectopically express *dm-w* [29] but, as discussed

previously, sex reversal was observed only in a subset of transgenic males, possibly due to variable levels of transgene expression.

Comparisons across *Xenopus* species evidence dispensability of all three of these genes. Most descendant *Xenopus* species of the ancestor in which *scan-w* and *ccdc69-w* arose now carry truncated and perhaps non-functional versions of these genes, or appear to lack them altogether, and females that carry knockout mutations for *scan-w* or *ccdc69-w* are viable and fertile. Likewise, since its origin, several *Xenopus* species have lost *dm-w*, and several other species appear to retain it in a shorter (*X. clivii*, *X. vestitus*) and/or diminished form (compared to the ortholog in *X. laevis*) in which *dm-w* lacks a completely dominant female-determining function (*X. kobeli*, *X. itombwensis*, *X. pygmaeus*, *X. clivii*, *X. victorianus*, *X. petersii*, *X. poweri*) [this study; 45]. Thus, available information suggests that *dm-w* is the trigger for female differentiation in *X. laevis*, this gene became dispensable over relatively modest stints of evolution, with new mechanisms of sex determination abetting or replacing *dm-w* in several species. Below we discuss these findings in more detail, and their implications for understanding the origin and evolution of supergenes.

Non-overlapping functional components of a sex-specific supergene

In principle, the origin of a supergene may be favored by natural selection if it binds together genetic variation with synergistic benefits. This is perhaps most obvious at the level of an individual gene that triggers sex determination, and where recombination suppression prevents intra-genic disruptions that could lead to neutered, intersex, or infertile offspring. Across multiple linked genes, synergy conceivably could be achieved through biological interactions (epistasis). That *dm-w*, *scan-w,* and *ccdc69-w* are all female-specific in *X. laevis* opens the possibility that a combination of some or all three of these loci are necessary for female differentiation, fertility, or viability. However, we recovered no evidence for strong epistatic effects among these three genes. Sex-specific supergenes also have the potential to resolve sexual antagonism [12, 15]; in this study we did not attempt to evaluate this possibility.

Our knockout lines demonstrate that only *dm-w* is required for female differentiation and fertility in *X. laevis* because genetic females with a non-functional *dm-w* gene develop into fertile sex-reversed phenotypic males. Genetic females that carry non-functional *scan-w* and *ccdc69-w* genes develop into fertile phenotypic females, which demonstrates that these two genes are not required for female differentiation, fertility, or viability. This extends previous work by demonstrating that full knockout of *dm-w* in *X. laevis* causes complete female to male sex reversal in all individuals, and allows us to reject the notion that all three or any two of the female-specific loci on the *X. laevis* W-chromosome are essential for female differentiation or fertility. Our knockout lines thus support previous inferences based on the observation of partial sex reversal elicited by RNA interference of *dm-w* [29, 30].

In fruit flies, 30% of newly evolved genes (which are typically also young) appear to be essential [49], which suggests that essential functions may arise quickly. Though *dm-w* is essential for female development and thus reproduction of *X. laevis*, *scan-w* and *ccdc69-w* are not. In several other *Xenopus* species, *dm-w* was replaced several times by novel but not yet known triggers for sex determination. These findings thus fail to provide support rapid evolution of essentiality in new genes.

Several insights into biological function of these supergene components can be gleaned from comparisons of the transcriptomes in the developing mesonephros/gonads at a crucial developmental junction (at tadpole stage 50) where *dm-w* is thought to initiate sexual differentiation [29]. At this early stage of sexual differentiation, relatively few genes were found to be significantly differentially expressed in the *dm-w* knockout line compared to wildtype sisters, and no significant enrichment of gene ontology was identified in differentially expressed genes in the *dm-w* knockout line (Tables S1, S2). This suggests that pronounced transcriptomic consequences of *dm-w* expression are realized later in development or that subtle (and undetected) changes in the transcriptome at this stage have mushrooming effects later during

development. Consistent with this latter scenario, a focused analysis of differential expression of 74 sex-related genes demonstrates that the gonad/mesonephros transcriptome of the *dm-w* knockout is significantly masculinized at tadpole stage 50 (Figs. 3, S7-8), even though most sex-related transcripts are not individually significantly differentially expressed.

Because they share a DNA binding domain and are co-expressed during development, *dm-w* is proposed to be a transcription factor that competitively binds to regulatory regions that are also recognized by the male-related gene *dmrt1* (from which *dm-w* is partially derived [29]), thereby inhibiting the initiation of male differentiation by *dmrt1* [30]. Antagonistic function analogous to that proposed for *dm-w* also exists in newly evolved partial paralogs of the *srgap2* gene that are involved in human cortical development [50, 51] and in amphioxus where one paralogous estrogen receptor is activated by estrogen while another lost this ancestral function and acts as a repressor of the first [52]. An interesting direction for future work would be to evaluate how knockouts of *dmrt1.L* and *dmrt1.S* affect sexual differentiation and gene expression in *X. laevis* and the diploid species *X. tropicalis*, which could offer insights into whether subfunctionalization or neofunctionalization of these homeologs after allotetraploidization preceded the origin of *dm-w*.

In the mesonephros/gonad at tadpole stage 50, transcriptome masculinization was not observed in the *ccdc69-w* knockout line and there was only a weak signal masculinization in the *scan-w* knockout line. Gene ontology analysis of significantly differentially expressed genes in the *scan-w* and *ccdc69-w* lines suggest distinctive functions with unclear relevance to sexual differentiation (Table S3). This suggests distinctive functional roles of these genes in comparison to *dm-w*. The functions of *scan-w* and *ccdc69-w* presumably overlap to some degree with those of their respective autosomal paralogs, but arguably are both substantially distinct from *dm-w* and from each other, and our findings suggest they minimally impact or are extraneous to female sexual differentiation. Taken together, these results point to distinctive biological functions of each of these supergene loci, with effects of each gene that extend to diverse biological processes, cellular compartments, and developmental stages.

Only one gene – *capn5-z* – is found on the Z chromosome but not the W chromosome of *X. laevis* [28]. Wildtype females have one W and one Z chromosome and therefore have one *capn5-z* allele, whereas wildtype males have two Z chromosomes and two *capn5-z* alleles. This gene is expressed in both sexes in the developing gonads, and also in adult gonads, brain, and spleen, and to a lesser extent in several other tissues [heart, liver, stomach, mesonephros; 28]. That *dm-w* knockout individuals (W*Z individuals) develop into what appear to be phenotypically normal and fertile males, demonstrates that two alleles of *capn5-z* are not required for male development or viability in *X. laevis*. That W*W* knockout individuals also developed into phenotypic males suggests that *capn5-z* may not be required at all for male development; this possibility could be further explored with histology or fertility assays that we did not perform.

Diverse origins and temporarily staggered assembly of a sex-specific genomic region

New genes arise from a variety of mechanisms, including horizontal gene transfer [53], gene duplication [54], exon shuffling [55], replication or modification by transposable elements [56], gene fusion [57] or fission [58], and *de novo* origin from previously non-coding genomic regions [59]. These diverse possible origins raise the question of how the three differently functioned genes on the W chromosome of *X. laevis* arose and become tethered together. As discussed above, the closest paralogs in the autosomes of *dm-w, scan-w,* and *ccdc69-w* are not tightly linked, which suggests that they have independent origins on the female-specific portion of the W chromosome [28, 29, 35-37]. Homeologs of exons 2 and 3 of *dm-w* (*dmrt1.L, dmrt1.S*) are on chr1L and chr1S at positions ~139 and 119 Mb in *X. laevis* genome assembly 10.1, respectively. Another part of the coding region of *dm-w* (in exon 4) arose independently from a non-coding transposon sequence, and homologous sequences of *dm-w* exon 4 are present on chromosomes 2L, 7L, and unplaced scaffolds [36]. Using Blast [60], we identified homeologs of *ccdc69-w* on chr3L

(*ccdc69.L*) and chr3S (*ccdc69.S*) at positions ~21.5 and 7.6 Mb, respectively, and on chr5L (*LOC108716149*) at ~63.5 Mb on the *X. laevis* genome assembly version 10.1. Blast searches identified sequences with homology to *scan-w* in multiple genomic locations, including regions that are annotated as genes and regions that are not annotated. Despite its small size, this scattered genomic distribution of supergene homology underscores remarkably diverse origins of the small female-specific sex determining supergene of *X. laevis*.

Targeted capture sequencing reported here and elsewhere [45] demonstrates that the most recent common ancestor of species that carry *dm-w* exons 2 and 3 is older than the MRCA of species in which *dm-w* exon 4, *scan-w* exons 4 and 5, and *ccdc69-w* exons 1 and 2 were detected (Fig. 4). We note that this inference depends on the phylogenetic placement of *X. clivii*; the placement of *X. clivii* depicted in the mitochondrial phylogeny presented in Fig. 4 is consistent with that recovered from a phylogenetic analysis of over 1,000 expressed transcripts [61]. "By-catch" sequencing of the non-coding *dm-w* exon 1 with probes for *scan-w* exon 4 indicates that *dm-w* exon 1 was present in the most recent common ancestor of *X. laevis* and *X. largeni*, which is consistent with findings from another study [41]. Because we did not attempt to directly capture *dm-w* exon 1, these data do not allow us to determine whether this exon was also present in an even older ancestor. *Dm-w* exon 4 has an independent origin from exons 2 and 3 [36] and has previously been detected in *X. laevis*, *X. largeni*, *X. petersii*, *X. itombwensis*, and *X. pygmaeus* [29, 36, 45]. We extend these findings by identifying *dm-w* exon 4 in several more species (Fig. 4), but notably we do not infer *dm-w* exon 4 to have been present in a more phylogenetically diverged species (such as *X. clivii* which carries *dm-w* exons 2 and 3 but not 4) as compared to previous inferences.

One interpretation of these data is that *dm-w* exons 2 and 3 appeared in the most recent common ancestor of *X. clivii* and *X. laevis*, and that *dm-w* exon 4, *scan-w*, *ccdc69-w*, and possibly *dm-w* exon 1 subsequently arose in the most recent common ancestor of *X. largeni* and *X. laevis*. Another interpretation is that all of these components were present in the most recent common ancestor of *X. clivii* and *X. laevis*, and that *dm-w* exon 4, *scan-w*, *ccdc69-w*, and perhaps *dm-w* exon 1 were later lost in *X. clivii*. This second scenario is less parsimonious than the first because it necessitates two deletions in an ancestor of *X. clivii* (one upstream of *dm-w* exons 2 and 3 to remove *scan-w*, and *ccdc69-w* and one downstream of *dm-w* exons 2 and 3 to remove *dm-w* exon 4). Either way, capture data suggests that subsequent evolution led to the loss of supergene components in various lineages (e.g., *ccdc69-w* exon 1 in *X. andrei*, *scan-w* exon 5 in *X. largeni*, *dm-w* exon 4 in *X. vestitus*).

A caveat to our interpretations of the targeted capture sequences is the possibility of false negatives, where a gene was not detected in some species even though it was present. However, the congruence between the results from different capture data for *dm-w* exons 2 and 3 [45], a PCR survey for these exons [35], and capture data from *dm-w* exon 4 (this study) is very high, with only two biologically plausible discrepancies (a failure to detect exon 4 in two species). For this reason, we suspect that the frequency of false negatives in our capture data is low.

With the exception of the "by capture" of *dm-w* exon 1 by our probes for *scan-w* exon 4, these capture sequences by themselves do not demonstrate that the captured sequences are physically linked on the same chromosome (apart from *X. laevis* where we know they are physically linked based on the genome assembly [28]). However, linkage of these exons in several other *Xenopus* species is supported by a PCR survey [45] that included 2–6 independent amplicons of different regions of *dm-w*, including portions of dm-w exons 2, 3, and 4, a non-transcribed region upstream of *dm-w*, and a portion of the coding region of *scan-w*. Although *dm-w* was found to not be female-specific specific in several species, independent attempts to amplify different portions of this gene in different samples from different species were generally all either successful or all unsuccessful [45], which is consistent with linkage, even in the absence of sex-specificity.

Developmental systems drift

Developmental system drift refers to the origin of diverse genetic underpinnings for conserved traits across different species [62]. In sexual species, developmental pathways linked to sexual differentiation are crucial for reproduction but are orchestrated by diverse genes and genetic interactions, and are thus a prime example of developmental systems drift [62]. Findings discussed here and elsewhere [45] evidence developmental systems drift of sex-determination in *Xenopus* by demonstrating that *dm-w* is not female-specific in almost all species that carry this gene, even though it triggers female differentiation in *X. laevis* and possibly *X. gilli* (Fig. 4). The phylogenetic distribution of female-specificity of *dm-w* suggests that the female determining capacity of *dm-w* was probably in place in the most recent common ancestor of *X. laevis* and *X. gilli*, but then lost by developmental systems drift in several closely related species such as *X. victorianus*. An alternative interpretation is that the female determining capacity of *dm-w* arose independently in *X. laevis* and *X. gilli*.

One or more mutations extended the coding region of *dm-w* exon 4 of *X. laevis*, *X. gilli* and closely related species (Supplementary Information). Exon 4 increases the DNA-binding activity of *dm-w* in *X. laevis* [36] though it is not clear what the functional implications of the ancestral extension of the coding region may be. Even though the coding region of *dm-w* seems intact in *X. victorianus*, *X. poweri*, and *X. petersii* and includes the extended coding region in exon 4, female-specificity of *dm-w* was lost in some or all of these species based on our PCR surveys of several male and female individuals (results were inconclusive for *X. petersii*; Table S6), thereby providing further evidence of developmental systems drift of genetic sex determination.

Outlook

Key unanswered questions raised by these findings ask what the ancestral function of *dm-w* was when it arose, and whether and how *dm-w* influences sex determination in species where this gene is not female-specific (minimally *X. kobeli*, *X. itombwensis*, *X. pygmaeus*, *X. clivii*, *X. victorianus*, *X. poweri*, *X. petersii*). It remains unclear why *dm-w* appears to segregate as a single allele in *X. clivii*, *X. kobeli*, and several other species – which would explain why it is found in some female and male individuals but not others – as opposed to being a "regular" autosomal locus with two alleles in all individuals of both sexes, which is the case in *X. itombwensis* [45]. It is possible that *dm-w* was (and in some species is) an "influencer" of female differentiation in the sense that it tends to be found in females, but this also depends on variation at other loci. Because these downstream genes are autosomal, they also have been duplicated by allopolyploidization, which occurred several times independently in *Xenopus* to generate a diversity of tetraploids, octoploid, and dodecaploids species [47, 63, 64]. Due to differences in ploidy level, copy numbers of autosomal genes that interact with *dm-w* – such as *dmrt1* – vary considerably; barring gene loss and pseudogenization, dodecaploid species such as *X. kobeli* carry six copies of autosomal genes (each with two alleles); octoploid species such as *X. itombwensis* carry four, and tetraploid species have two. Interestingly, pseudogenization of *dmrt1* homeologs has occurred independently multiple times in *Xenopus*, and in a phylogenetically biased fashion with more silencing of genes from one homeologous lineage (*dmrt1S*) than the other (*dmrt1L*) [35]. Clearly, further insights into these questions could be gained with experiments that explore function of homeologs of *dmrt1* and other duplicated sex-related genes in *X. laevis* and of *dm-w* in species where this locus is not female-specific.

Methods

Knockout of *dm-w*, *scan-w*, and *ccdc69-w*

We generated knockout individuals using CRISPR/Cas9 [65]. Single guide RNAs (sgRNAs) were designed to target the beginning of the coding region for *dm-w*, *scan-w*, and *ccdc69-w* using CRISPRdirect (https://crispr.dbcls.jp/) with an aim of maximizing disruption of protein function (Table S7). The specificity of our guides was evaluated using the *X. laevis* genome assembly 9.1. Single stranded

guide RNA (sgRNA) was generated from a DNA template that contained a promoter (SP6 for *dm-w* and T7 for *scan-w* and *ccdc69-w*) and a universal reverse primer for subsequent transcription. The DNA template was then used for sgRNA production using the Megascript SP6 or T7 kit (Invitrogen, Thermo Fisher Scientific).

SgRNAs were injected with the Cas9 protein into one cell embryos from *X. laevis* J-strain individuals. Because cutting generally happens after several rounds of cell division, the resulting F0 embryos are mosaics of wild-type and mutant cells. F0 phenotypic females (in the case of *scan-w* and *ccdc69-w*) or phenotypic males (in the case of *dm-w*) were then back-crossed to wildtype (J strain) males or females respectively. Mutations were confirmed by sequencing and the genetic sex was verified by amplification of other W-specific genes and by surgical inspection of gonads after euthanasia. F1 individuals were also crossed to wild-type individuals to evaluate fertility, with ovulation (phenotypic females) or clasping (phenotypic males) facilitated by injection of human chorionic gonadotropin (Sigma).

For all three genes, sequence chromatograms of F0 individuals had overlapping sequences that begin at the targeted region and that disrupted the putative open reading frame of each gene. Because cutting occurs at a multicell stage of embryogenesis, overlapping sequences were expected due to a mosaic genotype comprising wild-type and mutant sequences. These F0 females were then crossed with wild-type (J-strain) males to generate non-mosaic F1 knockout individuals, which were confirmed by Sanger sequencing (Fig. S1).

Transcriptome analysis of F1 progeny

With an aim of better understanding the functions of *dm-w*, *scan-w,* and *ccdc69-w*, we compared transcriptomes of the developing mesonephros/gonad of knockout individuals to developmental-stage-matched wildtype sisters that were co-reared in the same tank. We focused on tadpole stage 50, which is when gonadal differentiation is thought to be initiated because the gonads are not differentiated at this stage and because an increase in expression of *dm-w* at this stage precedes gonadal differentiation thereafter [29]. Tadpole stage 50 was determined based on morphological attributes including the shape of the head, size of tentacles, and size and shape of rear limb buds [66, 67]. The genotypic sex of the tadpoles was assessed by amplifying the three known W chromosome-specific genes (*dm-w*, *scan-w*, and *ccdc69-w*) with successful amplifications in all three genes used to identify genetic females. Mutant and wildtype individuals were then distinguished by sequencing the mutant gene for each line.

We compared transcriptomes from each knockout line to stage-matched wildtype sisters that were co-reared in the same tank. For the *dm-w*, *scan-w* and *ccdc69-w* knockout lines, mesonephros/gonadal transcriptomes from six, five, and six knockout individuals, and six, four, and two wildtype females were analyzed. To further understand the transcriptomic consequences of our gene knockouts, we established a baseline expectation for sex-biased gene expression using three independent batches of wildtype male and female gonad/mesonephros transcriptomes that were derived from three independent clutches of siblings at tadpole stage 50. The MF1, MF2, and MF3 batches included two, three, or six females and six, five, or six males, respectively. The wildtype females in the MF1 of the sex-biased expression analysis were the same as those in the *ccdc69-w* knockout versus wildtype analysis; data from the MF2 and MF3 batches were from different clutches from each other and from all other analyses. For the *dmw* dataset, four wildtype females were run on a different lane from the other samples. For the *ccdc69-w* and MF2 datasets, three wildtype males from each dataset were run on a different lane from the other samples. For the MF3 dataset, three wildtype females and three wildtype males were run on a different lane from the other samples. Because of this sampling distribution, we were only able to control for possible lane effects in the design of the MF3 analysis.

RNA quality was assessed for each sample using an Agilent Bioanalyzer; we selected samples with an RNA integrity number [68] of at least 8.5 out of 10 for analysis (median = 9.6). RNAseq libraries were

generated using Clontech/Takara SMARTer v4 cDNA conversion kit followed by the Illumina Nextera XT library preparation. Paired-end sequencing (150 bp) was performed on portions of three lanes of an Illumina Novaseq 6000 machine. Adapters and reads of poor quality and short length were removed using Trimmomatic v. 0.39 [69] with settings that retained reads of at least 36 bp and with an average quality per base higher than 15 on a sliding window of 4 bp; bases of poor quality (below 3) at the start and end of a read were also removed. After trimming this resulted in an average of 46.9 million (*dm-w*), 45.6 million (*scan-w*), and 54.6 million (*ccdc69-w*) paired-end reads per sample. These data have been deposited in the NCBI SRA (BioProject PRJNA989530).

For each analysis of differential expression, we quantified transcript abundance in the *X. laevis* transcriptome reference version 10.1 using a mapping method: STAR version 2.7.9a [70], and a pseudocount method: Kallisto version 0.46.1 [71]. Counts from each method were processed with edgeR version 3.16 [72] and DeSeq2 version 1.34.0 [73] to perform the analysis of differential expression. Prior to analysis of differential expression, genes with an average of less than two reads per individual were removed. Transcripts and genes were considered differentially expressed if the false detection rate adjusted p-value was less than 0.10.

We then performed a gene ontology analysis on each set of differentially expressed genes. Unfortunately, the annotations for the latest version of the *X. laevis* transcriptome are incomplete with many of the differentially expressed genes lacking a functional annotation and instead having unknown annotations that begin with "LOC" (Table S2). Thus, for each quantification method and analysis of differential expression, we extracted the sequence of each differentially expressed gene and used the discontiguous blast algorithm [60] to identify putative orthologs (based on the best bit score) in a human transcriptome GRCh38.p13 release 42 [74]. This approach increased the number of annotated transcripts and the annotations of putative human orthologs generally matched the available annotations of *X. laevis* transcripts (Table S2). We then used the gene ontology resource (http://geneontology.org/) to perform gene ontology analyses of biological function, molecular function, and cellular component, with significant enrichment based on Fisher's exact test with a false discovery rate of 0.05.

Sex related genes and transcriptome masculinization

To further evaluate whether and to what degree each knockout line (each of which are genetically female) has signatures of transcriptome masculinization, we examined correlations between the log2 fold change of 74 sex-related genes [Table S3; 44] between each pairwise comparison between six analyses of differential expression (i.e., three comparisons between male and female wildtype transcriptomes and three comparisons between knockout and wildtype female transcriptomes). The expression data for these 74 sex related genes was obtained from the transcriptomic/RNAseq data. These correlations were calculated for each of the four RNAseq analysis pipelines that we performed (Kallisto + edgeR, Salmon + edgeR, Salmon + DeSeq2, and Kallisto + DeSeq2). For this analysis, no filtering was performed based on transcript abundance; instead we excluded outliers, defined as 1.5 times the interquartile range above or below the upper or lower quartile. Spearman's correlation was calculated between the non-outlier log2 fold changes for each pairwise comparison and a *p*-value for this coefficient was calculated using the cor() function in R, which assumes the samples follow independent normal distributions.

If a knockout mutation (*dm-w*, *scan-w*, or *ccdc69-w*) led to masculinization of the mesonephros/gonad transcriptome, we expected a higher correlation between the log2 fold changes from the knockout analyses and one or more of the analyses of sex-biased expression in the wildtype transcriptomes. To test this, 1000 permutations were performed where the correlation between the non-outlier log2 fold changes of 74 randomly selected genes was calculated and compared to the observed. A *p*-value was calculated as 1 minus the rank of the observed correlation in the permutated correlations, divided by 1001.

Phenotyping of knockout progeny

The phenotype of each knockout line was ascertained with respect to (1) phenotypic sex, (2) fertility, and (3) testis histology (if present). Phenotypic sex was assessed either surgically by inspecting gonads after euthanasia or based on ability to lay eggs after injection with 400 international units of human chorionic gonadotropin. Fertility was assessed by crossing mutant individuals with wildtype individuals of the opposite phenotypic sex and examining whether embryos were produced. Crosses were achieved by injection of 400 or 300 international units of human chorionic gonadotropin in phenotypic female or male individuals, respectively. Testis histology was examined using 4 μm sections of formalin-fixed paraffin-embedded tissues that were stained with a Leica Autostainer XL using Hematoxylin 560MX and Eosin 515LT SelecTech stains (Leica).

Targeted next-generation sequencing and Sanger sequencing of W-specific and autosomal loci

We used targeted next-generation sequencing to assess presence, absence, and sequence variation of *dm-w* exon 4, *scan-w* exons 4 and 5, and both exons of *ccdc69-w* in 28 of 29 *Xenopus* species using the same panel of individuals and genomic DNA libraries as detailed previously [45]. To enrich the genomic libraries, we used 82 bp probes that overlap with 2 bp tiling (GenScript) that were designed based on exons of interest in *X. laevis*. Universal flanking sequences were added to each probe [75] and the probes synthesized on a 12k oligonucleotide array (GenScript). The oligonucleotide pool was then amplified by PCR and converted into single-stranded biotinylated DNA probes for in-solution hybridization capture using the method of [75]. The libraries were multiplexed, and paired end sequencing was performed on a portion of one lane of an Illumina HiSeq 2500 machine, with 125 bp paired-end reads. Sequences from each species were demultiplexed, assembled using Trinity 2.5.1 [76], and captured exons were identified using blastn [60]. Due to repetitive regions in *scan-w*, a 300 bp cutoff on all blast hits was applied. Sequences from each exon were aligned using MAFFT version 7.271 [77], adjusted manually, and manually inspected for putatively chimerical sequences. Our alignment included reference sequences from the *X. tropicalis* genome assembly 10.1 and *X. laevis* genome assembly 9.2 for each exon plus 200 bp upstream and downstream. Assembled capture sequences are deposited in GenBank (accession numbers XXX-XXX).

PCR assay and Sanger sequencing were also performed to evaluate the female-specificity of *dm-w* in three additional species beyond those evaluated previously [45]: *X. kobeli*, *X. petersii*, and *X. poweri* and additional *X. victorianus* individuals from two geographical areas. Amplification of a portion of the mitochondrial 16S ribosomal RNA gene was used as a positive control for each DNA extraction using primers 16Sc-L and 16Sd-H [78] and negative (no DNA) controls were performed for all amplifications. The phenotypic sex of each specimen of each species was determined surgically by inspecting gonads after euthanasia. For each individual, independent amplifications of *dm-w* exons 2, 3, and 4 were attempted and in individuals with unexpected amplifications (positive amplifications in males, negative amplifications in females) multiple independent amplifications were attempted.

Acknowledgements

We thank the National Xenopus Resource for maintaining the knockout lines and hosting the *Xenopus* Gene Editing Workshop at the Marine Biological Laboratory, and Takuya Nakayama for assistance with sgRNA design. We thank Svante Pääbo and Max Planck Institute for Evolutionary Anthropology for hosting B.J.E. on a sabbatical in Leipzig, Germany, and Birgit Nickel for performing library capture. We thank staff at the Central Animal Facility at McMaster University for assistance with animal care and Ian Dworkin for discussions about RNAseq analysis. We also thank two anonymous reviewers for constructive feedback on an earlier draft of this manuscript.

Funding

This work was supported by the Natural Science and Engineering Research Council of Canada (RGPIN-2017-05770), Resource Allocation Competition awards from Compute Canada, the Whitman Center Fellowship Program at the Marine Biological Laboratory, the Max Planck Institute for Evolutionary

Anthropology, the National Xenopus Resource, and National Institutes of Health grants R01-HD084409 and P40-OD010997.

References

1. Ogata H, Fujibuchi W, Goto S, Kanehisa M. A heuristic graph comparison algorithm and its application to detect functionally related enzyme clusters. Nucleic Acids Research. 2000;28(20):4021-8. doi: 10.1093/nar/28.20.4021. PubMed PMID: BIOSIS:PREV200100017132.
2. Thevenin A, Ein-Dor L, Ozery-Flato M, Shamir R. Functional gene groups are concentrated within chromosomes, among chromosomes and in the nuclear space of the human genome. Nucleic Acids Research. 2014;42(15):9854-61. doi: 10.1093/nar/gku667. PubMed PMID: BIOSIS:PREV201400791717.
3. Schwander T, Libbrecht R, Keller L. Supergenes and Complex Phenotypes. Current Biology. 2014;24(7):R288-R94. doi: 10.1016/j.cub.2014.01.056. PubMed PMID: BIOSIS:PREV201400369051.
4. Wang J, Wurm Y, Nipitwattanaphon M, Riba-Grognuz O, Huang Y-C, Shoemaker D, et al. A Y-like social chromosome causes alternative colony organization in fire ants. Nature. 2013;493(7434):664-8.
5. Joron M, Papa R, Beltran M, Chamberlain N, Mavarez J, Baxter S, et al. A conserved supergene locus controls colour pattern diversity in *Heliconius* butterflies. PLoS Biology. 2006;4(10):1831-40. doi: 10.1371/journal.pbio.0040303. PubMed PMID: BIOSIS:PREV200700053212.
6. Funk ER, Mason NA, Palsson S, Albrecht T, Johnson JA, Taylor SA. A supergene underlies linked variation in color and morphology in a Holarctic songbird. Nature Communications. 2021;12(1):Article No.: 6833. doi: 10.1038/s41467-021-27173-z. PubMed PMID: BIOSIS:PREV202200081833.
7. Labonne JDJ, Tamari F, Shore JS. Characterization of X-ray-generated floral mutants carrying deletions at the S-locus of distylous *Turnera subulata*. Heredity. 2010;105(2):235-43. doi: 10.1038/hdy.2010.39. PubMed PMID: BIOSIS:PREV201000464996.
8. Kuepper C, Stocks M, Risse JE, dos Remedios N, Farrell LL, Mcrae SB, et al. A supergene determines highly divergent male reproductive morphs in the ruff. Nature Genetics. 2016;48(1):79-83. doi: 10.1038/ng.3443. PubMed PMID: BIOSIS:PREV201600151866.
9. Lagunas-Robles G, Purcell J, Brelsford A. Linked supergenes underlie split sex ratio and social organization in an ant. Proceedings of the National Academy of Sciences of the United States of America. 2021;118(46):Article No.: e2101427118. doi: 10.1073/pnas.2101427118j1of9. PubMed PMID: BIOSIS:PREV202200071151.
10. Charlesworth D. The status of supergenes in the 21st century: recombination suppression in Batesian mimicry and sex chromosomes and other complex adaptations. Evolutionary Applications. 2016;9(1, Sp. Iss. SI):74-90. doi: 10.1111/eva.12291. PubMed PMID: BIOSIS:PREV201600192110.
11. Otto SP, Lenormand T. Resolving the paradox of sex and recombination. Nature Reviews Genetics. 2002;3:252–61.
12. Fisher RA. The evolution of dominance. Biological Reviews. 1931;6:345–68.
13. Charlesworth D, Charlesworth B. Sex differences in fitness and selection for centric fusions between sex chromosomes and autosomes. Genetical Research. 1980;35(2):205-14. doi: 10.1017/S0016672300014051. PubMed PMID: BIOSIS:PREV198070057440.
14. Rice WR. Sex chromosomes and the evolution of sexual dimorphism. Evolution. 1984;38:735–42.
15. Rice WR. The accumulation of sexually antagonistic genes as a selective agent promoting the evolution of reduced recombination between primitive sex chromosomes. Evolution. 1987;41:911–4.
16. van Doorn GS, Kirkpatrick M. Turnover of sex chromosomes induced by sexual conflict. Nature. 2007;449:909–12.
17. Lenormand T, Fyon F, Sun E, Roze D. Sex chromosome degeneration by regulatory evolution. Current Biology. 2020;30(15):3001–6.
18. Lenormand T, Roze D. Y recombination arrest and degeneration in the absence of sexual dimorphism. Science. 2022;375(6581):663–6.

19. Ponnikas S, Sigeman H, Abbott JK, Hansson B. Why Do Sex Chromosomes Stop Recombining? Trends in Genetics. 2018;34(7):492-503. doi: 10.1016/j.tig.2018.04.001. PubMed PMID: BIOSIS:PREV201800572395.
20. Charlesworth B, Wall JD. Inbreeding, heterozygote advantage and the evolution of neo-X and neo-Y sex chromosomes. Proceedings of the Royal Society Biological Sciences Series B. 1999;266(1414):51-6. doi: 10.1098/rspb.1999.0603. PubMed PMID: BIOSIS:PREV199900220530.
21. Jay P, Chouteau M, Whibley A, Bastide H, Parrinello H, Llaurens V, et al. Mutation load at a mimicry supergene sheds new light on the evolution of inversion polymorphisms. Nature Genetics. 2021;53(3):288-93. doi: 10.1038/s41588-020-00771-1. PubMed PMID: BIOSIS:PREV202100413439.
22. Jeffries DL, Gerchen JF, Scharmann M, Pannell JR. A neutral model for the loss of recombination on sex chromosomes. Philosophical Transactions of the Royal Society B. 2021;376(1832):20200096.
23. Bull JJ. Evolution of sex determining mechanisms. Menlo Park: Benjamin Cummings; 1983.
24. Skaletsky H, Kuroda-Kawaguchi T, Minx PJ, Cordum HS, Hillier L, Brown LG, et al. The male-specific region of the human Y chromosome is a mosaic of discrete sequence classes. Nature. 2003;423:825–37.
25. Komata S, Kajitani R, Itoh T, Fujiwara H. Genomic architecture and functional unit of mimicry supergene in female limited Batesian mimic *Papilio* butterflies. Philosophical Transactions of the Royal Society of London B Biological Sciences. 2022;377(1856):Article No.: 20210198. doi: 10.1098/rstb.2021.0198. PubMed PMID: BIOSIS:PREV202200561162.
26. Akagi T, Varkonyi-Gasic E, Shirasawa K, Catanach A, Henry IM, Mertten D, et al. Recurrent neo-sex chromosome evolution in kiwifruit. Nature Plants. 2023;https://doi.org/10.1038/s41477-023-01361-9.
27. Charlesworth B, Charlesworth D. Model for Evolution of Dioecy and Gynodioecy. American Naturalist. 1978;112(988):975-97. doi: Doi 10.1086/283342. PubMed PMID: WOS:A1978FX45000001.
28. Mawaribuchi S, Takahashi S, Wada M, Uno Y, Matsuda Y, Kondo M, et al. Sex chromosome differentiation and the W- and Z-specific loci in *Xenopus laevis*. Developmental Biology. 2017;426:393–400.
29. Yoshimoto S, Okada E, Umemoto H, Tamura K, Uno Y, Nishida-Umehara C, et al. A W-linked DM-domain gene, DM-W, participates in primary ovary development in *Xenopus laevis*. Proceedings of the National Academy of Sciences. 2008;105(7):2469–74.
30. Yoshimoto S, Ikeda K, Izutsu Y, Shiba T, Takamatsu N, Ito M. Opposite roles of DMRT1 and its W-linked paralog, DM-W, in sexual dimorphism of *Xenopus laevis*: implications of a ZZ/ZW-type sex-determining system. Development. 2010;137:2519–26.
31. Cauret CMS, Jordan DC, Kukoly L, Burton S, Anele EU, Kwiecien JM, et al. Functional dissection and assembly of a small, newly evolved, sex-determining supergene in the African clawed frog *Xenopus laevis*. Plos Genetics. 2023:In review.
32. Furman BLS, Evans BJ. Divergent evolutionary trajectories of two young, homomorphic, and closely related sex chromosome systems. Genome Biol Evol. 2018;10(3):742-55. doi: 10.1093/gbe/evy045. PubMed PMID: 29608717; PubMed Central PMCID: PMCPMC5841384.
33. Sander T, Stringer K, Maki J, Szauter P, Stone J, Collins T. The SCAN domain defines a large family of zinc finger transcription factors. Gene. 2003;310:29-38. doi: 10.1016/S0378-1119(03)00509-2. PubMed PMID: WOS:000183677900003.
34. Pal D, Wu D, Haruta A, Matsumura F, Wei Q. Role of a novel coiled-coil domain-containing protein CCDC69 in regulating central spindle assembly. Cell cycle. 2010;9(20):4117–29.
35. Bewick AJ, Anderson DW, Evans BJ. Evolution of the closely related, sex-related genes DM-W and DMRT1 in African clawed frogs (*Xenopus*). Evolution. 2011;65(3):698–712.
36. Hayashi S, Suda K, Fujimura F, Fujikawa M, Tamura K, Tsukamoto D, et al. Neofunctionalization of a noncoding portion of a DNA transposon in the coding region of the chimerical sex-determining gene dm-W in *Xenopus* frogs. Molecular Biology and Evolution. 2022;39(7):msac138.

887 37. Session AM, Uno Y, Kwon T, Chapman JA, Toyoda A, Takahashi S, et al. Genome evolution in
888 the allotetraploid frog *Xenopus laevis*. Nature. 2016;538(7625):336-43. doi: 10.1038/nature19840.
889 PubMed PMID: 27762356; PubMed Central PMCID: PMCPMC5313049.
890 38. Evans BJ, Carter TF, Greenbaum E, Gvoždík V, Kelley DB, McLaughlin PJ, et al. Genetics,
891 morphology, adverstisement calls, and historical records distinguish six new polyploid species of African
892 clawed frog (*Xenopus*, Pipidae) from West and Central Africa. PLoS One. 2015;10(12):e0142823 (51
893 pages).
894 39. Evans BJ, Kelley DB, Melnick DJ, Cannatella DC. Evolution of RAG-1 in polyploid clawed
895 frogs. Molecular Biology and Evolution. 2005;22(5):1193–207.
896 40. Matsuda Y, Uno Y, Kondo M, Gilchrist MJ, Zorn AM, Rokhsar DS, et al. A new nomenclature of
897 *Xenopus laevis* chromosomes based on the phylogenetic relationship to *Silurana/Xenopus tropicalis*.
898 Cytogenetic and Genome Research. 2015;145(3-4):187-91.
899 41. Hayashi S, Tamura K, Tsukamoto D, Ogita Y, Takamatsu N, Ito M. Promoter generation for the
900 chimeric sex-determining gene dm-W in Xenopus frogs. Genes & Genetic Systems. 2023:22-00137.
901 42. Hill WG, Robertson A. The effect of linkage on limits to artificial selection. Genetics Research.
902 1966;8:269–94.
903 43. Muller HJ. Some genetic aspects of sex. American Naturalist. 1932;66(703):118–38.
904 44. Piprek RP, Damulewicz M, Kloc M, Kubiak JZ. Transcriptome analysis identifies genes involved
905 in sex determination and development of *Xenopus laevis* gonads. Differentiation. 2018;100:46-56. doi:
906 10.1016/j.diff.2018.02.004. PubMed PMID: 29518581.
907 45. Cauret CM, Gansauge M-TT, Tupper A, Furman BLS, Knytl M, Song X, et al. Developmental
908 systems drift and the drivers of sex chromosome evolution. Molecular Biology and Evolution.
909 2020;37:799–810.
910 46. Chain FJJ, Evans BJ. Multiple mechanisms promote the retained expression of gene duplicates in
911 the tetraploid frog *Xenopus laevis*. PLoS Genetics. 2006;2(4):e56.
912 47. Evans BJ, Kelley DB, Tinsley RC, Melnick DJ, Cannatella DC. A mitochondrial DNA phylogeny
913 of clawed frogs: Phylogeography on sub-Saharan Africa and implications for polyploid evolution.
914 Molecular Phylogenetics and Evolution. 2004;33:197–213.
915 48. Evans BJ, Gansauge MT, Stanley EL, Furman BLS, Cauret CMS, Ofori-Boateng C, et al.
916 *Xenopus fraseri*: Mr. Fraser, where did your frog come from? PLoS One. 2019;14(9):e0220892 (14
917 pages). Epub 2019/09/12. doi: 10.1371/journal.pone.0220892. PubMed PMID: 31509539; PubMed
918 Central PMCID: PMCPMC6738922.
919 49. Chen S, Zhang YE, Long M. New Genes in *Drosophila* Quickly Become Essential. Science
920 (Washington D C). 2010;330(6011):1682-5. doi: 10.1126/science.1196380. PubMed PMID:
921 BIOSIS:PREV201100072388.
922 50. Dennis MY, Nuttle X, Sudmant PH, Antonacci F, Graves TA, Nefedov M, et al. Evolution of
923 human-specific neural SRGAP2 genes by incomplete segmental duplication. Cell. 2012;149(4). doi:
924 10.1016/j.cell.2012.03.033. PubMed PMID: BIOSIS:PREV201200430842.
925 51. Charrier C, Joshi K, Coutinho-Budd J, Kim JE, Lambert N, De Marchena J, et al. Inhibition of
926 SRGAP2 function by its human-specific paralogs induces neoteny during spine maturation. Cell.
927 2012;149(4):923–35.
928 52. Bridgham JT, Brown JE, Rodriguez-Mari A, Catchen JM, Thornton JW. Evolution of a new
929 function by degenerative mutation in Cephalochordate steroid receptors. PLoS Genetics.
930 2008;4(9):Article No.: e1000191. doi: 10.1371/journal.pgen.1000191. PubMed PMID:
931 BIOSIS:PREV200800702313.
932 53. Husnik F, McCutcheon JP. Functional horizontal gene transfer from bacteria to eukaryotes.
933 Nature Reviews Microbiology. 2018;16(2):67-79. doi: 10.1038/nrmicro.2017.137. PubMed PMID:
934 BIOSIS:PREV201800212510.
935 54. Tocchini-Valentini GD, Fruscoloni P, Tocchini-Valentini GP. Structure, function, and evolution
936 of the tRNA endonucleases of Archaea: An example of subfunctionalization. Proceedings of the National

Academy of Sciences of the United States of America. 2005;102(25):8933-8. doi: 10.1073/pnas.0502350102. PubMed PMID: BIOSIS:PREV200510191802.
55. Wang W, Zhang J, Alvarez C, Llopart A, Long M. The origin of the Jingwei gene and the complex modular structure of its parental gene, yellow emperor, in *Drosophila melanogaster*. Molecular Biology and Evolution. 2000;17(9):1294-301. doi: 10.1093/oxfordjournals.molbev.a026413. PubMed PMID: BIOSIS:PREV200000441396.
56. Velanis CN, Perera P, Thomson B, de Leau E, Liang SC, Hartwig B, et al. The domesticated transposase ALP2 mediates formation of a novel Polycomb protein complex by direct interaction with MSI1, a core subunit of Polycomb Repressive Complex 2 (PRC2). PLoS Genetics. 2020;16(5):Article No.: e1008681. doi: 10.1371/journal.pgen.1008681. PubMed PMID: BIOSIS:PREV202000575323.
57. Thomson TM, Lozano JJ, Loukili N, Carrio R, Serras F, Cormand B, et al. Fusion of the human gene for the polyubiquitination coeffector UEV1 with Kua, a newly identified gene. Genome Research. 2000;10(11):1743-56. doi: 10.1101/gr.GR-1405R. PubMed PMID: BIOSIS:PREV200100427725.
58. Wang W, Yu H, Long M. Duplication-degeneration as a mechanism of gene fission and the origin of new genes in *Drosophila* species. Nature Genetics. 2004;36(5):523-7. doi: 10.1038/ng1338. PubMed PMID: BIOSIS:PREV200400297756.
59. Cai J, Zhao R, Jiang H, Wang W. De novo origination of a new protein-coding gene in *Saccharomyces cerevisiae*. Genetics. 2008;179(1):487-96. doi: 10.1534/genetics.107.084491. PubMed PMID: BIOSIS:PREV200800476176.
60. Altschul SF, Madden TL, Schaffer AA, Zhang J, Zhang Z, Miller W, et al. Gapped BLAST and PSI-BLAST: A new generation of protein database search programs. Nucleic Acids Res. 1997;25(17):3389–402.
61. Furman BLS, Dang UJ, Evans BJ, Golding GB. Divergent subgenome evolution after allopolyploidization in African clawed frogs (*Xenopus*). J Evol Biol. 2018;31(12):1945-58. doi: 10.1111/jeb.13391. PubMed PMID: 30341989.
62. True JR, Haag ES. Developmental system drift and flexibility in evolutionary trajectories. Evolution and Development. 2001;3:109–19.
63. Evans BJ. Genome evolution and speciation genetics of allopolyploid clawed frogs (*Xenopus* and *Silurana*). Frontiers in Bioscience. 2008;13:4687–706.
64. Evans BJ, Greenbaum E, Kusamba C, Carter TF, Tobias ML, Mendel SA, et al. Description of a new octoploid frog species (Anura: Pipidae: *Xenopus*) from the Democratic Republic of the Congo, with a discussion of the biogeography of African clawed frogs in the Albertine Rift. Journal of Zoology, London. 2011;283:276–90.
65. Nakayama T, Fish MB, Fisher M, Oomen-Hajagos J, Thomsen GH, Grainger RM. Simple and efficient CRISPR/Cas9-mediated targeted mutagenesis in *Xenopus tropicalis*. Genesis: The Journal of Genetics and Development. 2013;51(12):835–43.
66. Zahn N, Levin M, Adams DS. The Zahn drawings: new illustrations of *Xenopus* embryo and tadpole stages for studies of craniofacial development. Development (Cambridge). 2017;144(15):2708-13. doi: 10.1242/dev.151308. PubMed PMID: BIOSIS:PREV201700805866.
67. Nieuwkoop PD, Faber J. Normal table of *Xenopus laevis* (Daudin). New York: Garland Publishing, Inc.; 1994. 252 p.
68. Lightfoot SJ, Mueller O. Quantitation comparison of total RNA using the Agilent 2100 bioanalyzer, Ribogreen analysis and UV spectrometry. Proceedings of the American Association for Cancer Research Annual Meeting. 2003;44:910. PubMed PMID: BIOSIS:PREV200300475698.
69. Bolger AM, Lohse M, Usadel B. Trimmomatic: a flexible trimmer for Illumina sequence data. Bioinformatics. 2014;30(15):2114-20.
70. Dobin A, Davis CA, Schlesinger F, Drenkow J, Zaleski C, Jha S, et al. STAR: ultrafast universal RNA-seq aligner. Bioinformatics (Oxford). 2013;29(1):15-21. doi: 10.1093/bioinformatics/bts635. PubMed PMID: BIOSIS:PREV201300134470.
71. Bray NL, Pimentel HMP, Pachter L. Near-optimal probabilistic RNA-seq quantification. Nature Biotechnology. 2016;34(5):525-7. doi: 10.1038/nbt.3519.

72. Robinson MD, McCarthy DJ, Smyth GK. EdgeR: A Bioconductor package for differential expression analysis of digital gene expression data. Bioinformatics. 2010;26(1):139-40. doi: 10.1093/bioinformatics/btp616.
73. Love MI, Huber W, Anders S. Moderated estimation of fold change and dispersion for RNA-seq data with DESeq2. Genome Biology. 2014;15(12):550. doi: 10.1186/s13059-014-0550-8.
74. Frankish A, Diekhans M, Jungreis I, Lagarde J, Loveland JE, Mudge JM, et al. Gencode 2021. Nucleic Acids Research. 2021;49(D1):D916–D23.
75. Fu Q, Meyer M, Gao X, Stenzel U, Burbano HA, Kelso J, et al. DNA analysis of an early modern human from Tianyuan Cave, China. Proceedings of National Academy of Sciences. 2013;110(6):2223-7. doi: 10.1073/pnas.1221359110. PubMed PMID: 23341637; PubMed Central PMCID: PMCPMC3568306.
76. Grabherr MG, Haas BJ, Yassour M, Levin JZ, Thompson DA, Amit I, et al. Full-length transcriptome assembly from RNA-Seq data without a reference genome. Nat Biotechnol. 2011;29(7):644-52. doi: 10.1038/nbt.1883. PubMed PMID: 21572440; PubMed Central PMCID: PMCPMC3571712.
77. Katoh K, Standley SM. MAFFT multiple sequence alignment software version 7: improvements in performance and usability. Molecular Biology and Evolution. 2013;30:772–80.
78. Evans BJ, Brown RM, McGuire JA, Supriatna J, Andayani N, Diesmos A, et al. Phylogenetics of Fanged Frogs (Anura; Ranidae; *Limnonectes*): Testing biogeographical hypotheses at the Asian-Australian faunal zone interface. Systematic Biology. 2003;52(6):794–819.

S7. Additional work has been completed alongside of Dr. Martin Knytl investigating *X. laevis* with knockouts of the androgen-receptor for further understanding of the factors influencing sex determination in *Xenopus* species.

Bibliography

Alam, S., Sarre, S., Gleeson, D., Georges, A., & Ezaz, T. (2018). Did Lizards Follow Unique Pathways in Sex Chromosome Evolution? *Genes*, *9*(5), 239. https://doi.org/10.3390/genes9050239

Altschul SF, Madden TL, Schaffer AA, Zhang J, Zhang Z, Miller W, et al. Gapped BLAST and PSI-BLAST: A new generation of protein database search programs. Nucleic Acids Res. 1997;25(17):3389–402.

Arandjelovic, S., & Ravichandran, K. S. (2015). Phagocytosis of apoptotic cells in homeostasis. *Nature Immunology*, *16*(9), 907–917. https://doi.org/10.1038/ni.3253

Audacity® software is copyright © 1999-2021 Audacity Team. Web site: https://audacityteam.org/. It is free software distributed under the terms of the GNU General Public License. The name Audacity® is a registered trademark.

Bewick, A. J., Anderson, D. W., & Evans, B. J. (2011). EVOLUTION OF THE CLOSELY RELATED, SEX-RELATED GENES DM-W AND DMRT1 IN AFRICAN CLAWED FROGS (XENOPUS): SEX DETERMINATION IN AFRICAN CLAWED FROGS (XENOPUS). *Evolution*, *65*(3), 698–712. https://doi.org/10.1111/j.1558-5646.2010.01163.x

Birchler, J. A., & Yang, H. (2022). The multiple fates of gene duplications: Deletion, hypofunctionalization, subfunctionalization, neofunctionalization, dosage balance constraints, and neutral variation. *The Plant Cell*, *34*(7), 2466–2474. https://doi.org/10.1093/plcell/koac076

Cauret, C. M. S., Gansauge, M.-T., Tupper, A. S., Furman, B. L. S., Knytl, M., Song, X.-Y., Greenbaum, E., Meyer, M., & Evans, B. J. (2020). Developmental Systems Drift and the Drivers of Sex Chromosome Evolution. *Molecular Biology and Evolution*, *37*(3), 799–810. https://doi.org/10.1093/molbev/msz268

Cauret, C. M. S., Jordan, D. C., Kukoly, L. M., Burton, S. R., Anele, E. A., Kwiecien, J. M., Gansauge, M. -T., Senthillmohan, S., Greenbaum, E., Meyer, M., Horb, M. E., & Evans, B. J. (submitted for review July 19, 2023). *PLOS Genetics*.

Chang, C. Y., & Witschi, E. (1956). Genic Control and Hormonal Reversal of Sex Differentiation in Xenopus. *Experimental Biology and Medicine*, *93*(1), 140–144. https://doi.org/10.3181/00379727-93-22688

Chen, Y., Lun, A.A.T. and Smyth, G.K. (2016). From reads to genes to pathways: differential expression analysis of RNA-Seq experiments using Rsubread and the edgeR quasi-likelihood pipeline. F1000Research. 5: 1438. doi: 10.12688/f1000research.8987.2.

Da Silva, S. M., Hacker, A., Harley, V., Goodfellow, P., Swain, A., & Lovell-Badge, R. (1996). Sox9 expression during gonadal development implies a conserved role for the gene in testis differentiation in mammals and birds. *Nature Genetics*, *14*(1), 62–68. https://doi.org/10.1038/ng0996-62

Dai, S., Qi, S., Wei, X., Liu, X., Li, Y., Zhou, X., Xiao, H., Lu, B., Wang, D., & Li, M. (2021). Germline sexual fate is determined by the antagonistic action of *dmrt1* and *foxl3/foxl2* in tilapia. *Development*, *148*(8), dev199380. https://doi.org/10.1242/dev.199380

Dobin, A., Davis, C. A., Schlesinger, F., Drenkow, J., Zaleski, C., Jha, S., Batut, P., Chaisson, M., & Gingeras, T. R. (2013). STAR: Ultrafast universal RNA-seq aligner. *Bioinformatics*, *29*(1), 15–21. https://doi.org/10.1093/bioinformatics/bts635

El-Mogharbel, N., Wakefield, M., Deakin, J. E., Tsend-Ayush, E., Grützner, F., Alsop, A., Ezaz, T., & Marshall Graves, J. A. (2007). DMRT gene cluster analysis in the platypus: New insights into genomic organization and regulatory regions. *Genomics*, *89*(1), 10–21. https://doi.org/10.1016/j.ygeno.2006.07.017

Evans, B. J., Carter, T. F., Greenbaum, E., Gvoždík, V., Kelley, D. B., McLaughlin, P. J., Pauwels, O. S. G., Portik, D. M., Stanley, E. L., Tinsley, R. C., Tobias, M. L., & Blackburn, D. C. (2015). Genetics, Morphology, Advertisement Calls, and Historical Records Distinguish Six New Polyploid Species of African Clawed Frog (Xenopus, Pipidae) from West and Central Africa. *PLOS ONE*, *10*(12), e0142823. https://doi.org/10.1371/journal.pone.0142823

Evans, B. J., Mudd, A. B., Bredeson, J. V., Furman, B. L. S., Wasonga, D. V., Lyons, J. B., Harland, R. M., & Rokhsar, D. S. (2022). New insights into *Xenopus* sex chromosome genomics from the Marsabit clawed frog *X. borealis*. *Journal of Evolutionary Biology*, *35*(12), 1777–1790. https://doi.org/10.1111/jeb.14078

Fisher, M., James-Zorn, C., Ponferrada, V., Bell, A. J., Sundararaj, N., Segerdell, E., Chaturvedi, P., Bayyari, N., Chu, S., Pells, T., Lotay, V., Agalakov, S., Wang, D. Z., Arshinoff, B. I., Foley, S., Karimi, K., Vize, P. D., & Zorn, A. M. (2023). Xenbase: Key features and resources of the *Xenopus* model organism knowledgebase. *GENETICS*, *224*(1), iyad018. https://doi.org/10.1093/genetics/iyad018

Frankish A, Diekhans M, Jungreis I, Lagarde J, Loveland JE, Mudge JM, et al. Gencode 2021. Nucleic Acids Research. 2021;49(D1):D916–D23.

Furman, B. L. S., Cauret, C. M. S., Knytl, M., Song, X.-Y., Premachandra, T., Ofori-Boateng, C., Jordan, D. C., Horb, M. E., & Evans, B. J. (2020). A frog with three sex chromosomes that co-mingle together in nature: Xenopus tropicalis has a degenerate W and a Y that evolved from a Z chromosome. *PLOS Genetics*, *16*(11), e1009121. https://doi.org/10.1371/journal.pgen.1009121

Furman, B. L. S., Dang, U. J., Evans, B. J., & Golding, G. B. (2018). Divergent subgenome evolution after allopolyploidization in African clawed frogs (*Xenopus*). *Journal of Evolutionary Biology*, *31*(12), 1945–1958. https://doi.org/10.1111/jeb.13391

Furman, B. L. S., & Evans, B. J. (2016). Sequential Turnovers of Sex Chromosomes in African Clawed Frogs (*Xenopus*) Suggest Some Genomic Regions Are Good at Sex Determination. *G3 Genes|Genomes|Genetics*, *6*(11), 3625–3633. https://doi.org/10.1534/g3.116.033423

Hayes, T. B., Khoury, V., Narayan, A., Nazir, M., Park, A., Brown, T., Adame, L., Chan, E., Buchholz, D., Stueve, T., & Gallipeau, S. (2010). Atrazine induces complete feminization and chemical castration in male African clawed frogs (*Xenopus laevis*). *Proceedings of the National Academy of Sciences*, *107*(10), 4612–4617. https://doi.org/10.1073/pnas.0909519107

Herpin, A., & Schartl, M. (2011). *Dmrt1* genes at the crossroads: A widespread and central class of sexual development factors in fish: Sexual development factors in fish. *FEBS Journal*, *278*(7), 1010–1019. https://doi.org/10.1111/j.1742-4658.2011.08030.x

Inui, M., Tamano, M., Kato, T., & Takada, S. (2017). CRISPR/Cas9-mediated simultaneous knockout of Dmrt1 and Dmrt3 does not recapitulate the 46,XY gonadal dysgenesis observed in 9p24.3 deletion patients. *Biochemistry and Biophysics Reports*, *9*, 238–244. https://doi.org/10.1016/j.bbrep.2017.01.001

Ioannidis, J., Taylor, G., Zhao, D., Liu, L., Idoko-Akoh, A., Gong, D., Lovell-Badge, R., Guioli, S., McGrew, M. J., & Clinton, M. (2021). Primary sex determination in birds depends on DMRT1 dosage, but gonadal sex does not determine adult secondary sex characteristics. *Proceedings of the National Academy of Sciences*, *118*(10), e2020909118. https://doi.org/10.1073/pnas.2020909118

Kubiak J. Z., Malgorzata Kloc, & Rafal P Piprek. (2020). History of The Research on Sex Determination. *Biomedical Journal of Scientific & Technical Research*, *25*(3). https://doi.org/10.26717/BJSTR.2020.25.004194

Jeng, S.-R., Wu, G.-C., Yueh, W.-S., Kuo, S.-F., Dufour, S., & Chang, C.-F. (2019). Dmrt1 (doublesex and mab-3-related transcription factor 1) expression during gonadal development and spermatogenesis in the Japanese eel. *General and Comparative Endocrinology*, *279*, 154–163. https://doi.org/10.1016/j.ygcen.2019.03.012

Johnsen, H., Seppola, M., Torgersen, J. S., Delghandi, M., & Andersen, Ø. (2010). Sexually dimorphic expression of dmrt1 in immature and mature Atlantic cod (Gadus morhua L.). *Comparative Biochemistry and Physiology Part B: Biochemistry and Molecular Biology*, *156*(3), 197–205. https://doi.org/10.1016/j.cbpb.2010.03.009

Josso, N., Di Clemente, N., & Gouédard, L. (2001). Anti-Müllerian hormone and its receptors. *Molecular and Cellular Endocrinology*, *179*(1–2), 25–32. https://doi.org/10.1016/S0303-7207(01)00467-1

Kelley, D. B., Ballagh, I. H., Barkan, C. L., Bendesky, A., Elliott, T. M., Evans, B. J., Hall, I. C., Kwon, Y. M., Kwong-Brown, U., Leininger, E. C., Perez, E. C., Rhodes, H. J., Villain, A., Yamaguchi, A., & Zornik, E. (2020). Generation, Coordination, and Evolution of Neural Circuits for Vocal Communication. *The Journal of Neuroscience*, *40*(1), 22–36. https://doi.org/10.1523/JNEUROSCI.0736-19.2019

Kelley, D. B., Elliott, T. M., Evans, B. J., Hall, I. C., Leininger, E. C., Rhodes, H. J., Yamaguchi, A., & Zornik, E. (2017). Probing forebrain to hindbrain circuit functions in *Xenopus*: KELLEY et al. *Genesis*, *55*(1–2), e22999. https://doi.org/10.1002/dvg.22999

Kim, S., Bardwell, V. J., & Zarkower, D. (2007). Cell type-autonomous and non-autonomous requirements for Dmrt1 in postnatal testis differentiation. *Developmental Biology*, *307*(2), 314–327. https://doi.org/10.1016/j.ydbio.2007.04.046

Koopman, P., Gubbay, J., Vivian, N., Goodfellow, P., & Lovell-Badge, R. (1991). Male development of chromosomally female mice transgenic for Sry. *Nature*, *351*(6322), 117–121. https://doi.org/10.1038/351117a0

Krentz, A. D., Murphy, M. W., Sarver, A. L., Griswold, M. D., Bardwell, V. J., & Zarkower, D. (2011). DMRT1 promotes oogenesis by transcriptional activation of Stra8 in the mammalian fetal ovary. *Developmental Biology*, *356*(1), 63–70. https://doi.org/10.1016/j.ydbio.2011.05.658

Lenth R. (2023). _emmeans: Estimated Marginal Means, aka Least-Squares Means_. R package version 1.8.5, <https://CRAN.R-project.org/package=emmeans>.

Li, M.-H., Yang, H.-H., Li, M.-R., Sun, Y.-L., Jiang, X.-L., Xie, Q.-P., Wang, T.-R., Shi, H.-J., Sun, L.-N., Zhou, L.-Y., & Wang, D.-S. (2013). Antagonistic Roles of Dmrt1 and Foxl2 in Sex Differentiation via Estrogen Production in Tilapia as Demonstrated by TALENs. *Endocrinology*, *154*(12), 4814–4825. https://doi.org/10.1210/en.2013-1451

Lynch, M., & Conery, J. S. (2000). The Evolutionary Fate and Consequences of Duplicate Genes. *Science*, *290*(5494), 1151–1155. https://doi.org/10.1126/science.290.5494.1151

Maier, M. C., McInerney, M.-R. A., Graves, J. A. M., & Charchar, F. J. (2021). Noncoding Genes on Sex Chromosomes and Their Function in Sex Determination, Dosage Compensation, Male Traits, and Diseases. *Sexual Development*, *15*(5–6), 432–440. https://doi.org/10.1159/000519622

Masuyama, H., Yamada, M., Kamei, Y., Fujiwara-Ishikawa, T., Todo, T., Nagahama, Y., & Matsuda, M. (2012). Dmrt1 mutation causes a male-to-female sex reversal after the sex determination by Dmy in the medaka. *Chromosome Research*, *20*(1), 163–176. https://doi.org/10.1007/s10577-011-9264-x

Matsuda, M., Nagahama, Y., Shinomiya, A., Sato, T., Matsuda, C., Kobayashi, T., Morrey, C. E., Shibata, N., Asakawa, S., Shimizu, N., Hori, H., Hamaguchi, S., & Sakaizumi, M. (2002). DMY is a Y-specific DM-domain gene required for male development in the medaka fish. *Nature*, *417*(6888), 559–563. https://doi.org/10.1038/nature751

Mawaribuchi, S., Musashijima, M., Wada, M., Izutsu, Y., Kurakata, E., Park, M. K., Takamatsu, N., & Ito, M. (2017). Molecular evolution of two distinct *dmrt1* promoters for germ and somatic cells in vertebrate gonads. *Molecular Biology and Evolution*, msw273. https://doi.org/10.1093/molbev/msw273

McCarthy, D.J., Chen, Y. and Smyth, G.K. (2012). Differential expression analysis of multifactor RNA-Seq experiments with respect to biological variation. Nucleic Acids Research. 40(10): 4288-4297. doi: 10.1093/nar/gks042.

Nagahama, Y., Chakraborty, T., Paul-Prasanth, B., Ohta, K., & Nakamura, M. (2021). Sex determination, gonadal sex differentiation, and plasticity in vertebrate species. *Physiological Reviews*, *101*(3), 1237–1308. https://doi.org/10.1152/physrev.00044.2019

Nakada, K., Sato, A., Yoshida, K., Morita, T., Tanaka, H., Inoue, S.-I., Yonekawa, H., & Hayashi, J.-I. (2006). Mitochondria-related male infertility. *Proceedings of the National Academy of Sciences*, *103*(41), 15148–15153. https://doi.org/10.1073/pnas.0604641103

Ni, F.-D., Hao, S.-L., & Yang, W.-X. (2019). Multiple signaling pathways in Sertoli cells: Recent findings in spermatogenesis. *Cell Death & Disease*, *10*(8), 541. https://doi.org/10.1038/s41419-019-1782-z

Otsu, N. (1979). A Threshold Selection Method from Gray-Level Histograms. *IEEE Transactions on Systems, Man, and Cybernetics*, *9*(1), 62–66. https://doi.org/10.1109/TSMC.1979.4310076

Ottolenghi, C., Pelosi, E., Tran, J., Colombino, M., Douglass, E., Nedorezov, T., Cao, A., Forabosco, A., & Schlessinger, D. (2007). Loss of Wnt4 and Foxl2 leads to female-to-male sex reversal extending to germ cells. *Human Molecular Genetics*, *16*(23), 2795–2804. https://doi.org/10.1093/hmg/ddm235

Owens, I. P., & Short, R. V. (1995). Hormonal basis of sexual dimorphism in birds: implication for new theories of sexual selection. *Trends Ecol Evol*. 10(1):44-47.

Park, Y.-J., & Pang, M.-G. (2021). Mitochondrial Functionality in Male Fertility: From Spermatogenesis to Fertilization. *Antioxidants*, *10*(1), 98. https://doi.org/10.3390/antiox10010098

Piprek RP, Damulewicz M, Kloc M, Kubiak JZ. Transcriptome analysis identifies genes involved in sex determination and development of Xenopus laevis gonads. *Differentiation*. 2018;100:46-56. doi:10.1016/j.diff.2018.02.004. PubMed PMID: 29518581.

Pisarska, M. D., Barlow, G., & Kuo, F. (2011). Minireview: Roles of the folkhead transcription factor FOXL2 in Granulosa cell biology and pathology. *Endocrinology.* 152(4): 119-1208. doi: 10.1210/en.2010-1041

Ramalho-Santos, J., Varum, S., Amaral, S., Mota, P. C., Sousa, A. P., & Amaral, A. (2009). Mitochondrial functionality in reproduction: From gonads and gametes to embryos and embryonic stem cells. *Human Reproduction Update*, *15*(5), 553–572. https://doi.org/10.1093/humupd/dmp016

Raymond, C. (1999). A region of human chromosome 9p required for testis development contains two genes related to known sexual regulators. *Human Molecular Genetics*, *8*(6), 989–996. https://doi.org/10.1093/hmg/8.6.989

Raymond, C. S., Kettlewell, J. R., Hirsch, B., Bardwell, V. J., & Zarkower, D. (1999). Expression of Dmrt1 in the Genital Ridge of Mouse and Chicken Embryos Suggests a Role in Vertebrate Sexual Development. *Developmental Biology*, *215*(2), 208–220. https://doi.org/10.1006/dbio.1999.9461

Raymond, C. S., Murphy, M. W., O'Sullivan, M. G., Bardwell, V. J., & Zarkower, D. (2000). *Dmrt1* , a gene related to worm and fly sexual regulators, is required for mammalian testis differentiation. *Genes & Development*, *14*(20), 2587–2595. https://doi.org/10.1101/gad.834100

Reaume, C. J., & Sokolowski, M. B. (2011). Conservation of gene function in behaviour. *Philosophical Transactions of the Royal Society B: Biological Sciences*, *366*(1574), 2100–2110. https://doi.org/10.1098/rstb.2011.0028

Rideout, E. J., Dornan, A. J., Neville, M. C., Eadie, S., & Goodwin, S. F. (2010). Control of sexual differentiation and behavior by the doublesex gene in Drosophila melanogaster. *Nature Neuroscience*, *13*(4), 458–466. https://doi.org/10.1038/nn.2515

Robinson, M.D., McCarthy, D.J. and Smyth, G.K. (2010). EdgeR: a Bioconductor package for differential expression analysis of digital gene expression data. Bioinformatics. 26(1): 139-140. doi: 10.1093/bioinformatics/btp616.

Roco, Á. S., Olmstead, A. W., Degitz, S. J., Amano, T., Zimmerman, L. B., & Bullejos, M. (2015). Coexistence of Y, W, and Z sex chromosomes in *Xenopus tropicalis*. *Proceedings of the National Academy of Sciences*, *112*(34). https://doi.org/10.1073/pnas.1505291112

Roeszler, K. N., Itman, C., Sinclair, A. H., & Smith, C. A. (2012). The long non-coding RNA, MHM, plays a role in chicken embryonic development, including gonadogenesis. *Developmental Biology*, *366*(2), 317–326. https://doi.org/10.1016/j.ydbio.2012.03.025

RStudio Team (2020). RStudio: Integrated Development for R. RStudio, PBC, Boston, MA URL http://www.rstudio.com/.

Sassoon, D., & Kelley, D. B. (1986). The sexually dimorphic larynx ofXenopus laevis: Development and androgen regulation. *American Journal of Anatomy*, *177*(4), 457–472. https://doi.org/10.1002/aja.1001770404

Schindelin, J., Arganda-Carreras, I., Frise, E., Kaynig, V., Longair, M., Pietzsch, T., Preibisch, S., Rueden, C., Saalfeld, S., Schmid, B., Tinevez, J.-Y., White, D. J., Hartenstein, V., Eliceiri, K., Tomancak, P., & Cardona, A. (2012). Fiji: An open-source platform for biological-image analysis. *Nature Methods*, *9*(7), 676–682. https://doi.org/10.1038/nmeth.2019

Sekido, R., & Lovell-Badge, R. (2009). Sex determination and SRY: Down to a wink and a nudge? *Trends in Genetics*, *25*(1), 19–29. https://doi.org/10.1016/j.tig.2008.10.008

Session, A. M., Uno, Y., Kwon, T., Chapman, J. A., Toyoda, A., Takahashi, S., Fukui, A., Hikosaka, A., Suzuki, A., Kondo, M., Van Heeringen, S. J., Quigley, I., Heinz, S., Ogino, H., Ochi, H., Hellsten, U., Lyons, J. B., Simakov, O., Putnam, N., … Rokhsar, D. S. (2016). Genome evolution in the allotetraploid frog Xenopus laevis. *Nature*, *538*(7625), 336–343. https://doi.org/10.1038/nature19840

Shaidani, N.-I., McNamara, S., Wlizla, M., & Horb, M. E. (2021). Obtaining *Xenopus laevis* Embryos. *Cold Spring Harbor Protocols*, *2021*(3), pdb.prot106211. https://doi.org/10.1101/pdb.prot106211

Shen, M. M., & Hodgkin, J. (1988). Mab-3, a gene required for sex-specific yolk protein expression and a male-specific lineage in C. elegans. *Cell*, *54*(7), 1019–1031. https://doi.org/10.1016/0092-8674(88)90117-1

Shi, J., Li, Y., Ren, K., Xie, Y., Yin, W., & Mo, Z. (2017). Characterization of cholesterol metabolism in Sertoli cells and spermatogenesis (Review). *Molecular Medicine Reports*. https://doi.org/10.3892/mmr.2017.8000

Sinclair, A. H., Berta, P., Palmer, M., Hawkins, J. R., Griffiths, B. L., Smith, M. J., Foster, J. W., Frischauf, A.-M., Lovell-Badge, R., & Goodfellow, P. N. (1990). *A gene from the human sex-determining region encodes a protein with homology to a conserved DNA-binding motif*. *346*.

Smith, C. A., Katz, M., & Sinclair, A. H. (2003). DMRT1 Is Upregulated in the Gonads During Female-to-Male Sex Reversal in ZW Chicken Embryos1. *Biology of Reproduction*, *68*(2), 560–570. https://doi.org/10.1095/biolreprod.102.007294

Teshima, K. M., & Innan, H. (2008). Neofunctionalization of Duplicated Genes Under the Pressure of Gene Conversion. *Genetics*, *178*(3), 1385–1398. https://doi.org/10.1534/genetics.107.082933

Titi-Lartey OA, Khan YS. Embryology, Testicle. [Updated 2023 Apr 24]. In: StatPearls [Internet]. Treasure Island (FL): StatPearls Publishing; 2023 Jan-. Available from: https://www.ncbi.nlm.nih.gov/books/NBK557763/

Tobias, M., Evans, B. J., & Kelley, D. B. (2011). Evolution of advertisement calls in African clawed frogs. Behaviour, 148(4), 519–549. https://doi.org/10.1163/000579511X569435

Tobias, M., Korsh, J., & Kelley, D. (2014). Evolution of male and female release calls in African clawed frogs, *Behaviour*, *151*(9), 1313-1334. doi: https://doi.org/10.1163/1568539X-00003186

Vainio, S., Heikkilä, M., Kispert, A., Chin, N., & McMahon, A. P. (1999). Female development in mammals is regulated by Wnt-4 signalling. *Nature*, *397*(6718), 405–409. https://doi.org/10.1038/17068

Veitia, R., Nunes, M., Brauner, R., Doco-Fenzy, M., Joanny-Flinois, O., Jaubert, F., Lortat-Jacob, S., Fellous, M., & McElreavey, K. (1997). Deletions of Distal 9p Associated with 46,XY Male to Female Sex Reversal: Definition of the Breakpoints at 9p23.3–p24.1. *Genomics*, *41*(2), 271–274. https://doi.org/10.1006/geno.1997.4648

Veyrunes, F., Waters, P. D., Miethke, P., Rens, W., McMillan, D., Alsop, A. E., Grützner, F., Deakin, J. E., Whittington, C. M., Schatzkamer, K., Kremitzki, C. L., Graves, T., Ferguson-Smith, M. A., Warren, W., & Marshall Graves, J. A. (2008). Bird-like sex chromosomes of platypus imply recent origin of mammal sex chromosomes. *Genome Research*, *18*(6), 965–973. https://doi.org/10.1101/gr.7101908

Voordeckers, K., & Verstrepen, K. J. (2015). Experimental evolution of the model eukaryote Saccharomyces cerevisiae yields insight into the molecular mechanisms underlying

adaptation. *Current Opinion in Microbiology*, *28*, 1–9. https://doi.org/10.1016/j.mib.2015.06.018

Webster, K. A., Schach, U., Ordaz, A., Steinfeld, J. S., Draper, B. W., & Siegfried, K. R. (2017). Dmrt1 is necessary for male sexual development in zebrafish. *Developmental Biology*, *422*(1), 33–46. https://doi.org/10.1016/j.ydbio.2016.12.008

Wiechmann, A. F., & Wirsig-Wiechmann, C. R. (2003). *Color Atlas of Xenopus laevis Histology*. Springer US. https://doi.org/10.1007/978-1-4419-9286-4

Yano, A., Guyomard, R., Nicol, B., Jouanno, E., Quillet, E., Klopp, C., Cabau, C., Bouchez, O., Fostier, A., & Guiguen, Y. (2012). An Immune-Related Gene Evolved into the Master Sex-Determining Gene in Rainbow Trout, Oncorhynchus mykiss. *Current Biology*, *22*(15), 1423–1428. https://doi.org/10.1016/j.cub.2012.05.045

Zhou, Y., Sun, W., Cai, H., Haisheng Bao, Zhang, Y., Guoying Qian, & Chutian Ge. (2019). *Supplemental Material for Zhou et al., 2019* (p. 1437758 Bytes) [Data set]. GSA Journals. https://doi.org/10.25386/GENETICS.10028399

Yoshimoto, S., Ikeda, N., Izutsu, Y., Shiba, T., Takamatsu, N., & Ito, M. (2010). Opposite roles of *DMRT1* and its W-linked paralogue, *DM-W* , in sexual dimorphism of *Xenopus laevis*: Implications of a ZZ/ZW-type sex-determining system. *Development*, *137*(15), 2519–2526. https://doi.org/10.1242/dev.048751

Yoshimoto, S., Okada, E., Oishi, T., Numagami, R., Umemoto, H., Tamura, K., Kanda, H., Shiba, T., Takamatsu, N., & Ito, M. (2006). Expression and promoter analysis of Xenopus DMRT1 and functional characterization of the transactivation property of its protein. *Development, Growth and Differentiation*, *48*(9), 597–603. https://doi.org/10.1111/j.1440-169X.2006.00894.x

Yoshimoto, S., Okada, E., Umemoto, H., Tamura, K., Uno, Y., Nishida-Umehara, C., Matsuda, Y., Takamatsu, N., Shiba, T., & Ito, M. (2008). A W-linked DM-domain gene, DM-W, participates in primary ovary development in *Xenopus laevis*. *Proceedings of the National Academy of Sciences*, *105*(7), 2469–2474. https://doi.org/10.1073/pnas.0712244105

Zhang, X., Li, J., Chen, S., Yang, N., & Zheng, J. (2023). Overview of Avian Sex Reversal. *International Journal of Molecular Sciences*, *24*(9), 8284. https://doi.org/10.3390/ijms24098284